UNIVERSITY OF OKLAHOMA

GRADUATE COLLEGE

SYNTHESIS, CHARACTERIZATION, ELECTROCHEMISTRY, AND SPECTROELECTROCHEMISTRY OF GROUP 8 METALLOPORPHYRIN COMPLEXES

A DISSERTATION

SUBMITTED TO THE GRADUATE FACULTY

in partial fulfillment of the requirements for the

Degree of

DOCTOR OF PHILOSOPHY

By
ADAM WARHAUSEN
Norman, Oklahoma
2012

SYNTHESIS, CHARACTERIZATION, ELECTROCHEMISTRY, AND SPECTROELECTROCHEMISTRY OF GROUP 8 METALLOPORPHYRIN COMPLEXES

A DISSERTATION APPROVED FOR THE
DEPARTMENT OF CHEMISTRY AND BIOCHEMISTRY

BY

George B. Richter-Addo

Robert P. Houser

David P. Nagle, Jr.

Kenneth M. Nicholas

Paul F. Cook

Acknowledgements

I would like to begin by thanking my advisor, Dr. George Richter-Addo. Without your support and guidance, my years here at OU would not have been possible. Your insight and instruction in my chemical endeavors along with the advice you have provided with respect to handling professional and personal matters were and still are very valued and appreciated. You have no idea how many times I have asked myself, "How would boss handle this?" while working in your lab, handling administrative TA responsibilities or during life's many questions. I'd like to say thank you for providing me the opportunity to learn from you, I hope that the lessons continue for many years. I would also like to thank the rest of my advisory committee, Dr. Robert Houser, Dr. Kenneth Nicholas, Dr. Paul Cook, and Dr. David Nagle for your support during my Ph.D. studies.

A special thanks goes to the members of the GBRA research group both past and present, Dr. Lilian Chooback, Dr. Dan Copeland, Dr. Shawn Carter, Dr. Zaki Zahran, Dr. Nan Xu, Dr. Jun (Eva) Yi, Dr. Myron Jones, Guan Ye, Adam Campbell, Dennis Awasabisah, and Bing Wang. I consider it an honor and privilege to have worked with all of you during my time at OU. By keeping me calm, discussing experiments, giving advice, or just shooting the breeze you have all helped me through the years, thank you.

I would also like to offer sincere gratitude to our research collaborator and my former M.S. advisor Dr. Michael Shaw. The conversations that we have had over the years and the help you have provided to aid in the advancement of my work and development were invaluable. I look forward to continuing our collaborative efforts in

the future. I would also like to thank and acknowledge Dr. Douglas Powell for his help with my crystallographic work for my dissertation research.

Finally, I would like to thank my family for the support and love that they provided during this journey. First to my parents, Jeff and Nancy Warhausen, I want to say thank you for helping me pursue and achieve everything that I have ever wanted. Any compliments or successes that I have or will achieve are directly related to the outstanding job you did raising me. You are the best parents that a kid could ever have and I love you very much. To my Grandma, Emogene Cushman, thank you for all of your love and prayers that you have given me during my entire life. To my brother Eric, thank you for always believing in me and supporting me. To my son Jared, I hope that you become a better person than I am, that you appreciate hard work and the rewards that come from it, and achieve all of your hopes and desires. I would especially like to thank my wife Laura. Thank you for all of your encouragement, love and support that you have given to me. You have taught me the virtue of patience, a lesson that has obviously been used. Anything that I have accomplished is better because I get to share it with you. I am so lucky and grateful that I have you in my life and love you more than you know.

Table of Contents

List of Tables

List of Figures

Abstract

This dissertation describes the investigations of nitric oxide (NO) and possible NO donors with group 8 metalloporphyrins.

Chapter one is written in a manner so that the general public could read and understand the work that has been done for this dissertation.

Chapter two describes the redox properties of (por)Ru(CO)(L) (por = tetraphenylporphyrin (TPP), octaethylporphyrin (OEP); L = pyridine and 1-MeIm) complexes. A new technique utilizing chronoabsorptometry and chronoamperometry for investigating short lived "intermediate" species that are formed on the cyclic voltammetric (CV) time scale is used in order to probe the visible region of the electronic spectra of the redox-generated species. This new technique has provided results that are similar to previous reports but now it can be done with shorter scan times (which can minimize decomposition) and less manual manipulation of the data such as subtractions and smoothing. As a result, more detail in the spectrum is obtained by using this new chronoabsorptometry-chronoamperometry technique. Also, we were able to provide the first difference IR spectra for the products generated from their second oxidations.

Chapter three describes the synthesis of new 6-coordinate ruthenium porphyrin nitrosyl aryloxide ((por)Ru(NO)(OR)) complexes (por = OEP, TPP and R = $-C_6H_5$ (Ph), $-C_6H_4$-2-$NHC(=O)CF_3$ (^1HO_L), $-C_6H_3$-2,6-$(NHC(=O)CF_3)_2$ (^2HO_L), and -NHC(=O)-C_6H_4-*o*-OH (SalHate) that show varying amounts (0,1,2) of internal H-bonding. These complexes appear to be good structural models of the heme active site of catalase,

which has a tyrosinate ligand coordinated to the iron and internal H-bonds in the active site. They were synthesized by the reaction of the (por)Ru(NO)(O-*i*-C_5H_{11}) or (por)Ru(NO)(OEt) precursor with the appropriate alcohol. The complexes were characterized with the use of ^{1}H NMR, IR, mass spectrometry, cyclic voltammetry, IR spectroelectrochemistry, and UV-vis spectroelectrochemistry. The ν_{NO} of 1821 – 1842 cm^{-1} for these complexes is higher than those of known ruthenium porphyrin nitrosyl alkoxide complexes with ν_{NO} ranges of 1790 – 1810 cm^{-1}, most likely due to the conjugation of the phenyl ring found in the aryloxide complexes, which can delocalize electron density. This influences the metal to nitrosyl ligand back-donating ability affecting the N–O bond strength. We also notice a direct correlation of ν_{NO} to the number of internal H-bonds in the complexes. The structural information gathered from these new (por)Ru(NO)(OR) aryloxide complexes shows similar characteristics to known structures of the (por)Ru(NO)(OR) alkoxide complexes. The only major difference lies in the ∠RuOR bond angles. The (OEP)Ru(NO)(OR) (R = ^1HO_L and ^2HO_L) complexes have ∠RuOR bond angles of 122.26(15) and 124.5(3)º respectively, which are smaller than the reported values of 133.853 – 143.8(5)º. The first oxidation potentials also appear to be increasing with increasing number of internal H-bonds. The cyclic voltammetry for these complexes displays an *ECE* mechanism. The complexes appear to decompose during the first oxidations, while the second oxidations appear to be taking place on the porphyrin rings due to the observation of the porphyrin π-cation radical peaks in the difference IR spectra.

Chapter 4 describes the synthesis and characterization of 5-coordinate iron porphyrin complexes, where the 5th coordination site is occupied by a hydroxamate,

acetate, or aryloxide ligand. The (por)Fe(hydroxamate) complexes (POR = (T(*p*-OMe)PP) and OEP, R = salicylhydroxamate) showed very unique coordination. The hydroxamate moiety of the ligand, which is typically thought of as a bidentate ligand with respect to iron coordination, was not involved in binding to the metal center. Instead, salicylhydroxamic acid coordinates to the iron center via the phenyl hydroxyl moiety, as determined with X-ray crystallography. The electrochemical investigations of the (por)Fe(acetate) and (por)Fe(aryloxide) complexes each showed two reversible features during oxidation within the solvent limits of the experiments performed which was consistent with reports of known (por)Fe(OR) complexes. The electrochemical behavior of the (por)Fe(salicylhydroxamate) complexes provided more complicated cyclic voltammograms. This was most likely due to instability of the complexes upon oxidation. Infrared spectroelectrochemical investigations of the (por)Fe(salicylhydroxamate) complexes provided difference spectra which suggest the formation of a cationic $[(por)Fe(NO)]^+$ complex upon oxidation. This was due to the new bands in the IR spectrum at 1839 cm^{-1} and 1855 cm^{-1} for the (T(*p*-OMe)PP)Fe(salicylhydroxamate) and (OEP)Fe(salicylhydroxamate) complexes respectively. This is the first report of a coordinated hydroxamate donating NO. The reactivity of the (por)Fe(OR) complexes with nitrite and NO, which suggest the formation of new $(por)Fe(NO_X)_y$ complexes, are also discussed in this chapter.

Chapter 1. Introduction

Author's Note: In an effort to practice my communication skills with the general public and strive towards the broader impact goals outlined by the NSF that funded a large portion of my research, Dr. Richter-Addo and I decided that the introduction of my dissertation would be written in a very general manner, similar to that of a newspaper article. This way, a non-scientific audience could read and have a better understanding of the type of research that I have performed. There is currently a national and global movement for scientists to communicate more effectively with the general public so they can appreciate and understand the work that scientists carry out.[1] After all, as academic researchers, we utilize funds from government agencies that are funded by the taxpayers and they deserve to know how their money is being used.

1.1 Introduction

The work done in the Richter-Addo research group at the University of Oklahoma has for many years focused around the chemistry of the simple diatomic molecule, nitric oxide (NO). This simple molecule is generated in nature by the combustion of oxygen (O_2) and nitrogen (N_2) in the atmosphere at extreme temperatures during lightning strikes.[2,3] NO can also be formed during high temperature combustion in the presence of N_2 in internal combustion engines. NO was originally recognized as a pollutant in the atmosphere,[4] but since then has gone on to garner great attention for its involvement in several biologically relevant processes, including, but not limited to vascular regulation,[5] in immune defense mechanism,[6] and in the central and peripheral nervous systems.[7] NO was even revered as molecule of the year in 1992 by *Science*.[8]

Many of the roles that NO plays in natural systems stem from its interactions with proteins that contain a heme unit. In fact, the enzyme that produces NO in the body, is called "nitric oxide synthase" (NOS) which also contains a heme moiety.[9] NO biosynthesis is accomplished via a catalytic reaction involving L-arginine (Equation 1.1).

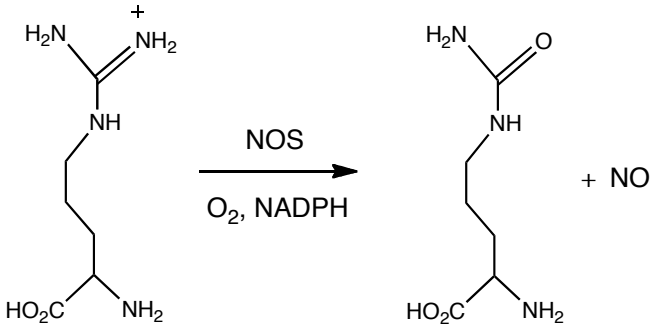

(1.1)

This interaction with heme-containing enzymes is the ground upon which we have built our research.

Heme (heme b) is an important component in biological systems and is commonly referred to as iron protoporphyrin IX (Fe-PPIX).

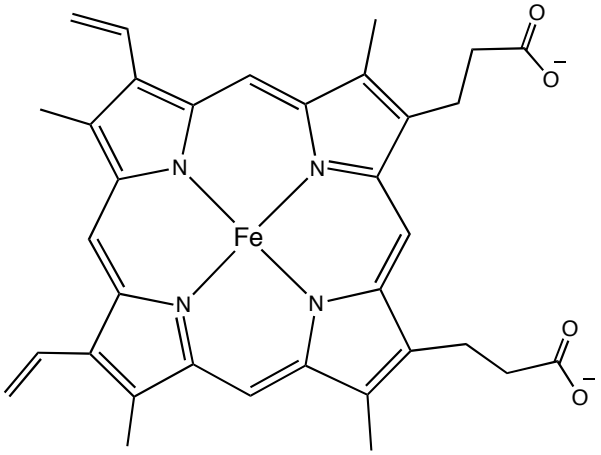

Iron Protoporphyrin IX

Figure 1.1 Drawing of iron protoporphyrin IX

By examining the picture of Fe-PPIX above, it is apparent that the central iron (Fe) is coordinated to four nitrogen (N) atoms of the porphyrin macrocycle. The iron center has two more empty binding sites above and below the porphyrin if we define the plane of the porphyrin to be that of the paper or screen on which this is read. Therefore, the porphyrin unit itself is a four-coordinate ligand to the central metal and iron has the potential to have coordination numbers of 4, 5, or 6.

Several proteins such as the oxygen transporter hemoglobin in blood, and the oxygen storage protein myoglobin in muscles, contain this iron protoporphyrin unit. In these heme-containing proteins, the central Fe atom is where the important chemistry of binding and releasing oxygen (O_2) takes place. In this same manner, the small diatomic molecule nitric oxide (NO) can also bind to the central Fe atom, to enable its physiological functions.

The heme unit is an unsymmetrical porphyrin that can provide some difficulty working with it on the bench. The antisymmetric groups around the porphyrin can provide some complexity in the characterization of these heme compounds. One way that synthetic chemists minimize such complexity is to use symmetrical synthetic porphyrins that have been designed with desired functional groups around the porphyrin. The most common of these synthetic porphyrins are the tetra-*meso*-substituted 5,10,15,20-tetraphenylporphyrin (TPP) (with the potential to vary the phenyl substitutions) and the octa-β-substituted 2,3,7,8,12,13,17,18-octaethylporphyrin (OEP).

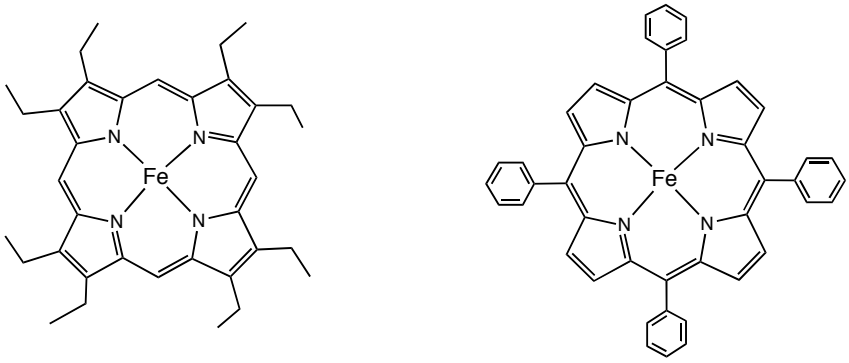

(OEP)Fe (TPP)Fe

Figure 1.2. Synthetic iron porphyrin complexes.

These synthetic porphyrins allow us to prepare compounds that essentially mimic the natural heme system. By synthesizing new synthetic porphyrin complexes, we are able to study the chemistry of these systems without interference from the protein. It may seem odd to study something without all of its components, but it establishes a starting point from which a basic understanding can be established.

An example of the modeling studies that our group has done in the past includes the structural modeling of compounds known as nitrosamines and their interactions with synthetic metalloporphyrins.[10]

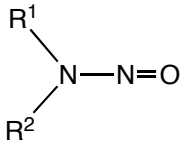

nitrosamine

These nitrosamine compounds are generally thought of as carcinogenic (cancer-causing) compounds. They can be found in beer, rubber, cigarette smoke, and surfaces that have been exposed to cigarette smoke (third hand smoke).[11,12] Their metabolic activation occurs via an interaction with the heme containing enzyme cytochrome P450 commonly found in the lungs and in the liver. The interactions of nitrosamines with the

heme center of cytochrome P450 are believed to proceed in two different ways (Type I and Type II). The Type I interaction involves the nitrosamine binding to the protein pocket near the iron center of the heme unit. The Type II interaction involves direct contact of the nitrosamine to the metal center of the heme unit. Dr. Nan Xu from the Richter-Addo research group was able to synthesize a collection of synthetic iron-porphyrin nitrosamine complexes, which showed Type II interactions for both five- and six-coordinated complexes.

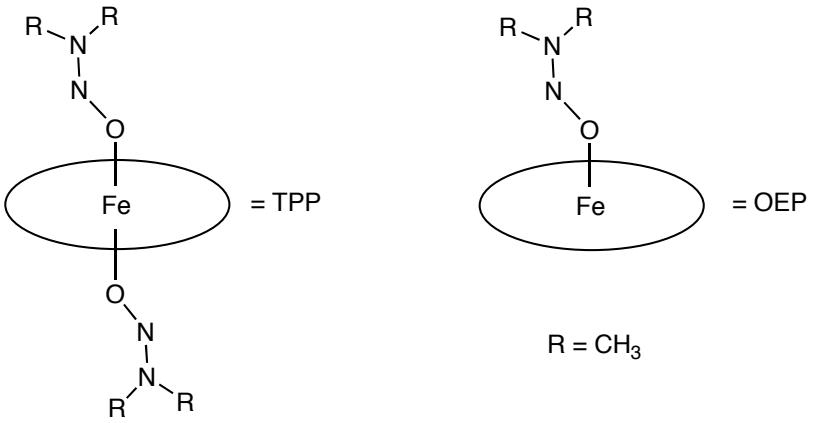

Figure 1.3. Synthetic 6-coordinate and 5-coordinate iron porphyrin nitrosamine compounds.

This allowed for structural comparisons of these complexes, which until this work had been unresolved.

Due to the fact that the metal center of the heme can change oxidation states (gain or lose electrons) during its interactions with molecules, it is important to study the reduction (gain of electron(s)) and/or oxidation (loss of electron(s)) processes (redox) of these systems. For example, the resting state of the heme containing enzyme

catalase has an iron in the +3 oxidation state, however, during its catalytic activity in the conversion of hydrogen peroxide to water and O_2, an intermediate with iron in the +4 oxidation state is believed to occur.[13]

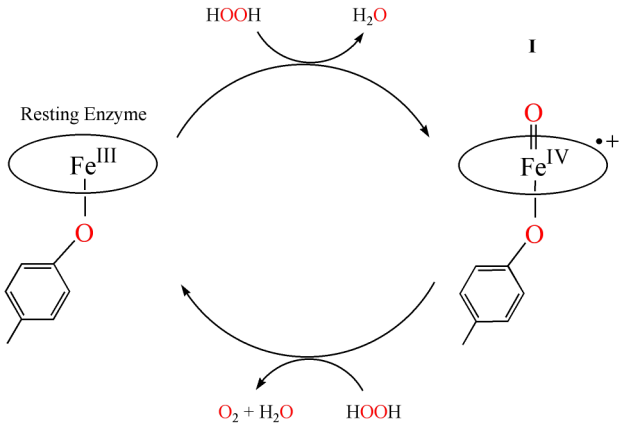

Figure 1.4. Conversion of hydrogen peroxide to water and O_2 by the enzyme catalase.

Cyclic voltammetry is a tool that we use to study the redox properties of synthetic model compounds.[14] This method of analysis not only tells us if the synthetic compounds that we make are redox active, but can give us important information regarding the amount energy (potential in Volts) needed for the process to occur. This provides insight into how the natural system might behave.

The use of cyclic voltammetry is limited in the information that can be obtained about the site of the redox process on the complex and the condition of the complex after the redox process is complete. For example, did the complex survive the redox process; did it decompose, if so, what is the newly generated complex? These are all questions that cannot be answered with cyclic voltammetry alone. Therefore, we pair this electrochemical technique with spectroscopic techniques that can help identify the products formed and the site of the redox process. This pairing of techniques is called

spectroelectrochemistry. One of the pairings that we utilize is with infrared (IR) spectroscopy.[15] As stated before, our group is interested in the interaction of heme systems with small diatomic molecules. One advantage that these molecules give us as researchers is that they have very distinct features in the IR spectrum, very similar to a fingerprint for a human being in that their spectral features are associated only to that particular molecule or part of that molecule. These features are easily monitored in the spectrum and depending on where they are in the IR spectrum, where they move to during a redox process, or even if they disappear, can provide information as to the site of the redox process and the compound that results after the redox process. This information from the synthetic models helps lay the groundwork for other researchers to study the chemistry of the natural systems and form conclusions as to their functions.

1.2 My Dissertation Research

The research that I have done for this dissertation has one centralized theme, but three individual flavors in regards to the research projects. The centralized theme revolves around the synthesis and characterization of synthetic metalloporphyrin compounds of iron and ruthenium.

The first flavor involves the electrochemical and spectroelectrochemical investigations of (por)Ru(CO)(L) (por = TPP and OEP, L = pyridine and 1-methylimidazole) complexes with cyclic voltammetry, IR spectroelectrochemistry, and a newly developed UV-vis spectroelectrochemical technique.[15,16] These studies were performed to help gather information of the product(s) formed during oxidation. The results of the IR spectroelectrochemical investigations provided the first difference IR spectra of the products that result from the second oxidations of these complexes. The

new UV-vis spectroelectrochemical technique has for the first time provided detailed spectra for the products that result from the first oxidations.

The second flavor of research involves the synthesis, characterization, electrochemistry and spectroelectrochemistry of (por)Ru(NO)(OR) (por = TPP, OEP and R = -C_6H_5 (Ph), -C_6H_4-2-NHC(=O)CF_3 (^1HO_L), -C_6H_3-2,6-(NHC(=O)CF_3)$_2$ (^2HO_L), and -NHC(=O)-C_6H_4-*o*-OH (Sal)). We are interested in the synthesis of 6-coordinate

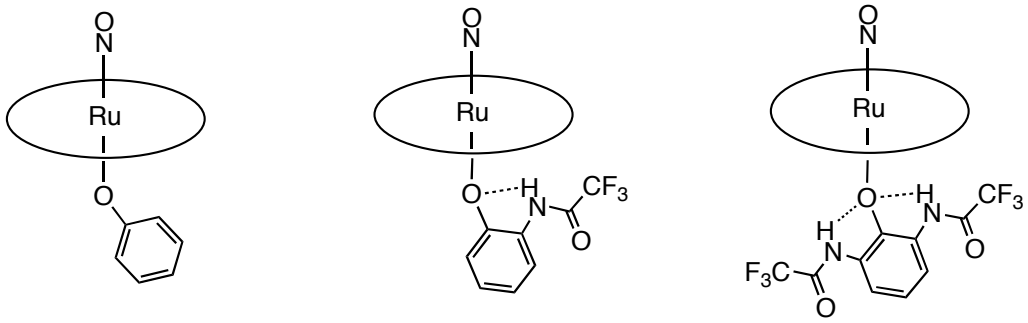

(POR)Ru(^0HO_L) (POR)Ru(^1HO_L) (POR)Ru(^2HO_L)

Figure 1.5. Structural depictions of the (POR)Ru(NO)(OR) (POR = OEP, TPP and represented as a simple oval) complexes.

metalloporphyrin complexes that contain an NO group and some other moiety coordinated to the metal center of the porphyrin as structural models for enzymes that have the amino acid tyrosine coordinated to the heme iron. Our group and others have published works that reported the synthesis and characterization of (por)M(NO)(OR) complexes (M = Ru, Os and R = carbon chain ligands).[17-20] The synthesis of a (por)M(NO)(OR) complex where the R was a cyclic group had yet to be reported. Also, these complexes provide structural models of the enzyme catalase, which has a tyrosinate ligand (OR type ligand) coordinated to the central iron metal of its heme unit and supported by internal hydrogen bonds.[21-24] In 1995, it was reported that catalase activity was inhibited by NO.[25] Until recently, the structure of NO inhibited catalase

was unknown, however, the authors that reported its structure said that the geometry of NO coordination was difficult to assign from the structure that was obtained.[26] Therefore, the synthesis of a new set of (por)Ru(NO)(OR) complexes was attempted and successfully synthesized and characterized in my dissertation work.

Along with the interaction of NO with heme systems, we are interested in organic compounds that can or are suspect of donating NO to the metal center of heme systems. This aspect was also investigated for this dissertation with hydroxamic acids, which are suspected to be NO donors.[27-31]

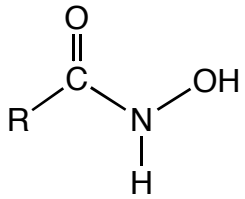

hydroxamic acid

These organic compounds have a well-established chemistry and are known to bind to iron, usually through both of the oxygen atoms in the compound.[32-37] In fact, they have pharmaceutical applications such as chelating drugs for iron overload diseases and anti-tumor activity.[38-41] We had a simple question that we asked ourselves: "If hydroxamic acid compounds bind iron and are used pharmaceutically, how do they interact with iron that is found in a heme containing protein/enzyme?" There is very little information in the literature to answer this question. Therefore, the work presented in my dissertation shows how a particular hydroxamic acid (salicylhydroxamic acid) interacts with synthetic iron porphyrin complexes. Also, the idea that hydroxamic acids can donate NO appears to be valid. In my work I was able to show that once the hydroxamic acid is coordinated to the iron center of a metalloporphyrin, it can donate NO upon

electrochemical oxidation. This appears to be the first time that a hydroxamic acid species that is coordinated to a metal has been shown to generate NO. The other reports of NO donation resulted from the interaction of hydroxamic acids and metal compounds where there was no report of a metal-coordinated hydroxamic acid.

The work done for this dissertation provides information of the interactions of the small diatomic molecule nitric oxide with synthetic heme complexes and organic molecules that can donate NO. The results obtained provide a solid foundation for which other researchers can build upon with respect to new spectroelectrochemical investigations, new (por)M(NO)(OR) (M = metal) complexes, and elucidation of how NO is generated from coordinated hydroxamic acid complexes.

1.3 References

(1) Harpp, D. N.; Fenster, A. E.; Schwarcz, J. A. Chemistry for the Public: Our Challenge, *Journal of Chemical Education* **2011**, *88*, 739.

(2) Hill, R. D. On the Production of Nitric Oxide by Lightning, *Geophysical Research Letters* **1979**, *6*, 945.

(3) Hill, R. D.; Rahmim, I.; Rinker, R. G. Experimental Study of the Production of Nitric Oxide, Nitrous Oxide, and Ozone in a Simulated Atmospheric Corona, *Industrial and Engineering Chemistry Research* **1988**, *27*, 1264.

(4) Ainscough, E. W.; Brodie, A. M. Nitric Oxide-Some Old and New Perspectives, *Journal of Chemical Education* **1995**, *72*, 686.

(5) Radomski, M. W.; Palmer, R. M. J.; Moncada, S. An L-Arginine/Nitric Oxide Pathway Present in Human Platelets Regulates Aggregation, *Proceedings of the Natlional Academy of Science* **1990**, *87*, 5193.

(6) Nathan, C. Nitric Oxide as a Secretory Product of Mammalian Cells, *The Journal of the Federation of American Societies for Experimental Biology* **1992**, *6*, 3051.

(7) Gally, J. A.; Montague, P. R.; Reeke, G. N., Jr.; Edelman, G. M. The Nitric Oxide Hypothesis: Possible Effects of a Short-Lived, Rapidly Diffusible Signal in the Development and Function of the Nervous System, *Proceedings of the Natlional Academy of Science* **1990**, *87*, 3547.

(8) Culotta, E.; Koshland, D. E., Jr. NO News is Good News, *Science* **1992**, *258*, 1862.
(9) Marletta, M. A. Nitric Oxide Synthase Structure and Mechanism, *Journal of Biological Chemistry* **1993**, *268*, 12231.
(10) Xu, N.; Goodrich, L. E.; Lehnert, N.; Powell, D. R.; Richter-Addo, G. B. Five- and Six-Coordinate Adducts of Nitrosamines with Ferric Porphyrins: Structural Models for the Type II Interactions of Nitrosamines with Ferric Cytochrome P450, *Inorganic Chemistry,* **2010**, *49*, 4405.
(11) Sleiman, M.; Gundel, L. A.; Pankow, J. F.; Jacob, P.; Singer, B. C.; Destaillats, H. Formation of Carcinogens Indoors by Surface-Mediated Reactions of Nicotine with Nitrous Acid, Leading to Potential Thirdhand Smoke Hazards, *Proceedings of the National Academy of Science* **2010**, *107*, 6576.
(12) Yang, C. S.; Smith, T. J. Mechanisms of Nitrosamine Bioactivation and Carcinogenesis, *Advances in Experimental Medicine and Biology* **1996**, *387*, 385.
(13) Mate´, M. J.; Murshudov, G.; Bravo, J.; Melik-Adamy, W.; Loewen, P. C.; Fita, I. *Handbook of Metalloproteins*; Messerschmidt, A., Huber, R., Poulos, T., Weighard, K., Eds.; John Wiley & Sons: New York; Vol. 1, p 486
(14) Kissinger, P. T.; Heineman, W. R. *Laboratory Techniques in Electroanalytical Chemistry*; 2nd ed.; Marcel Dekker: New York, 1996.
(15) Shaw, M. J.; Henson, R. L.; Houk, S. E.; Westhoff, J. W.; Jones, M. W.; Richter-Addo, G. B. Fiber-Optic Infrared Reflectance Spectroelectrochemistry: Isomerization of a Manganese Pyranyl Complex, *Journal of Electroanalytical Chemistry* **2002**, *534*, 47.
(16) Shaw, M. J.; Cranford, D. L.; Rodgers, K. W.; Eilers, J. E.; Noble, B.; Warhausen, A. J.; Richter-Addo, G. B. Facile Determination of the Spectra of Unstable Electrode Products Using Simultaneous Fiber-Optic Chronoabsorptometry and Chronoamperometry, *Inorganic Chemistry* **2010**, *49*, 9590.
(17) Cheng, L.; Powell, D. R.; Khan, M. A.; Richter-Addo, G. B. Synthesis, Characterization, Solid-State Molecular Structures, and Deprotonation Reactions of Cationic Alcohol Complexes of Osmium Nitrosyl Porphyrins, *Inorganic Chemistry* **2001**, *40*, 125.
(18) Bohle, D. S.; Goodson, P. A.; Smith, B. D. Synthesis, Structure and Ligand Exchange Reactions of Ru(TTP)(NO)(OMe), *Polyhedron* **1996**, *15*, 3147.
(19) Fomitchev, D. V.; Coppens, P.; Li, T.; Bagley, K. A.; Chen, L.; Richter-Addo, G. B. Photo-Induced Metastable Linkage Isomers of Ruthenium Nitrosyl Porphyrins, *Chemical Communications* **1999**, 2013.
(20) Chen, L.; Khan, M. A.; Richter-Addo, G. B. Nitrosylation of Octaethylporphyrin Osmium Complexes with Alkyl Nitrites and Thionitrites: Molecular Structures of Three Osmium Porphyrin Derivatives, *Inorganic Chemistry* **1998**, *37*, 533.
(21) Murthy, M. R. N.; Reid, T. J.; Sicignano, A.; Tanaka, N.; Rossmann, M. G. Structure of Beef-Liver Catalase, *Journal of Molecular Biology* **1981**, *152*, 465.
(22) Reid, T. J.; Murthy, M. R. N.; Sicignano, A.; Tanaka, N.; Musick, W. D. L.; Rossmann, M. G. Structure and Heme Environment of Beef-Liver Catalase at

2.5 Å Resolution, *Proceedings of the Natlional Academy of Science-Biology* **1981**, *78*, 4767.
(23) Ko, T. P.; Day, J.; Malkin, A. J.; McPherson, A. Structure of Orthorhombic Crystals of Beef Liver Catalase, *Acta Crystallographica Section D* **1999**, *55*, 1383.
(24) Tanford, C.; Lovrien, R. Dissociation of Catalase into Subunits, *Journal of the American Chemical Society* **1962**, *84*, 1892.
(25) Brown, G. C. Reversible Binding and Inhibition of Catalase by Nitric-Oxide, *European Journal of Biochemistry* **1995**, *232*, 188.
(26) Purwar, N.; McGarry, J. M.; Kostera, J.; Pacheco, A. A.; Schmidt, M. Interaction of Nitric Oxide with Catalase: Structural and Kinetic Analysis, *Biochemistry* **2011**, *50*, 4491.
(27) Cheng, L.; Khan, M. A.; Taylor, R. W.; Richter-Addo, G. B.; Powell, D. R. Structural Consequences of Hydroxamate and Tropolonate Binding to Iron Porphyrins, *Chemical Communications* **1999**, 1941.
(28) Marmion, C. J.; Murphy, T.; Nolan, K. B.; Docherty, J. R. Hydroxamic Acids are Nitric Oxide Donors. Facile Formation of Ruthenium(II)-Nitrosyls and NO-Mediated Activation of Guanylate Cyclase by Hydroxamic Acids, *Chemical Communications* **2000**, 1153.
(29) Griffith, D.; Krot, K.; Comiskey, J.; Nolan, K. B.; Marmion, C. J. Monohydroxamic Acids and Bridging Dihydroxamic Acids as Chelators to Ruthenium(III) and as Nitric Oxide Donors: Syntheses, Speciation Studies and Nitric Oxide Releasing Investigation, *Dalton Transactions* **2008**, 137.
(30) Marmion, C. J.; Griffith, D.; Nolan, K. B. Hydroxamic acids - An Intriguing Family of Enzyme Inhibitors and Biomedical Ligands, *European Journal of Inorganic Chemistry* **2004**, 3003.
(31) Bogatyrenko, T. N.; Kuropteva, Z. V.; Baider, L. M.; Bogatyrenko, V. R.; Fedorov, B. S.; Konovalova, N. P. On the Possibility of the Nitric Oxide Formation Upon Biotransformation of Hydroxamic Acids, *Russian Chemical Bulletin* **2011**, *60*, 1162.
(32) Mizukami, S.; Nagata, K. Metal Complexes of Hydroxamic Acid Analogs, *Coordination Chemistry Reviews* **1968**, *3*, 267.
(33) Miller, M. J. Syntheses and Therapeutic Potential of Hydroxamic Acid Based Siderophores and Analogs, *Chemical Reviews* **1989**, *89*, 1563.
(34) Crumbliss, A. L. Iron Bioavailability and the Coordination Chemistry of Hydroxamic Acids, *Coordination Chemistry Reviews* **1990**, *105*, 155.
(35) Kurzak, B.; Kozlowski, H.; Farkas, E. Hydroxamic and Aminohydroxamic Acids and Their Complexes with Metal Ions, *Coordination Chemistry Reviews* **1992**, *114*, 169.
(36) Neilands, J. B. Siderophores - Structure and Function of Microbial Iron Transport Compounds, *Journal of Biological Chemistry* **1995**, *270*, 26723.
(37) Codd, R. Traversing the Coordination Chemistry and Chemical Biology of Hydroxamic Acids, *Coordination Chemistry Reviews* **2008**, *252*, 1387.
(38) Chaston, T. B.; Richardson, D. R. Iron Chelators for the Treatment of Iron Overload Disease: Relationship Between Structure, Redox Activity, and Toxicity, *American Journal of Hematology* **2003**, *73*, 200.

(39) Natchus, M. G.; Bookland, R. G.; De, B.; Almstead, N. G.; Pikul, S.; Janusz, M. J.; Heitmeyer, S. A.; Hookfin, E. B.; Hsieh, L. C.; Dowty, M. E.; Dietsch, C. R.; Patel, V. S.; Garver, S. M.; Gu, F.; Pokross, M. E.; Mieling, G. E.; Baker, T. R.; Foltz, D. J.; Peng, S. X.; Bornes, D. M.; Strojnowski, M. J.; Taiwo, Y. O. Development of New Hydroxamate Matrix Metalloproteinase Inhibitors Derived From Functionalized 4-Aminoprolines, *Journal of Medical Chemistry* **2000**, *43*, 4948.

(40) Puerta, D. T.; Cohen, S. M. Elucidating Drug-Metalloprotein Interactions with Tris(pyrazolyl)borate Model Complexes, *Inorganic Chemistry* **2002**, *41*, 5075.

(41) Puerta, D. T.; Griffin, M. O.; Lewis, J. A.; Romero-Perez, D.; Garcia, R.; Villarreal, F. J.; Cohen, S. M. Heterocyclic Zinc-Binding Groups for use in Next-Generation Matrix Metalloproteinase Inhibitors: Potency, Toxicity, and Reactivity, *Journal of Biological Inorganic Chemistry* **2006**, *11*, 131.

Chapter 2: Electrochemistry, Infrared and UV-vis Spectroelectrochemistry of (porphyrin)Ru(CO)(L) (L = pyridine and 1-methylimidazole) Complexes

2.1 Introduction

It is well known that heme systems play a crucial role in many important biological redox functions. More specifically, the iron center of heme systems binds many small molecules and ions, the products of which show a array of absorption spectra.[1] Therefore, understanding the redox and spectral properties of these systems will give us greater insight in to their functions that are dependent on their redox behavior. Iron porphyrin complexes can have mixed valencies and spin-states, causing some of the complexes to be difficult to isolate and characterize. Indeed, over the years, ruthenium(II) has become an attractive candidate as a substitute for low-spin iron(II) due to its ability to form stable complexes.[2] I believe that Artemis Antipas et al. said it best in their quote "…it would be nearly impossible to understand iron complexes alone: and only through the relationship to other metals can a sound understanding be reached."[3] There have been electrochemical studies done on ruthenium porphyrin complexes, specifically those involving ruthenium porphyrin carbonyl complexes due to their relative ease of synthesis and characterization.[2-10] Both the porphyrin and ruthenium units are redox active. It has been reported that the first oxidations of (por)Ru(CO)(py) (where por = OEP, TPP) complexes take place on the porphyrin moiety; in contrast, the (por)Ru$(py)_2$ complexes have first oxidations that are metal centered.[4] The roles of other factors such as solvents (in the case of "5-coordinate" (por)Ru(CO)(solvent) complexes)[11], metals[12], and ligands[13] in altering redox behavior

have also been studied. For example, Kadish was able to show, through a study involving several coordinating ligands, that only small changes are observed in the $E_{1/2}$ values for the oxidations of (por)Ru(CO)(L), where L is a σ-donor ligand.[13]

We have probed the redox behavior of the (por)Ru(CO)(L) compounds (por = OEP and TPP; L = pyridine and 1-methylimidazole) shown in Figure 2.1 by cyclic voltammetry and infrared spectroelectrochemistry.

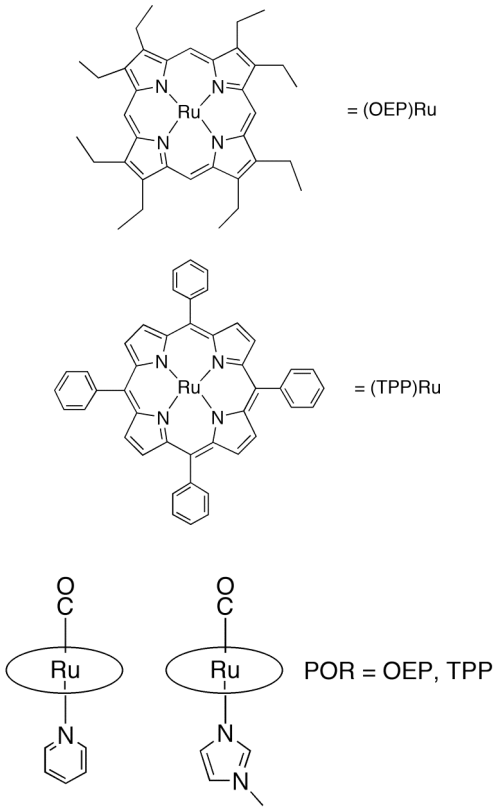

Figure 2.1. Synthetic ruthenium-containing metalloporphyrins.

In addition, we have utilized our recently developed methodology employing simultaneous chronoabsorptometry and chronoamperometry to characterized the redox products in the UV-visible spectral range.[14]

2.2 Experimental Section

Methylene chloride and diethylether used in the experiments were dried using an Innovative Technology Inc. Pure Solv 400-5-MD Solvent Purification System. The supporting electrolyte NBu_4PF_6 (tetrabutylammonium hexafluorophosphate) was obtained from Aldrich. The $NBu_4BAr^F{}_4$ (tetrabutylammonium tetrakis(3,5-bis(trifluoromethylphenyl) borate (BARF)) supporting electrolyte was synthesized according to a literature method.[15] Ferrocene (Fc) and acetylferrocene were purchased from Aldrich and were sublimed before use. (TPP)Ru(CO)(1-MeIm),[5,6] (TPP)Ru(CO)(py),[2,4,7] (OEP)Ru(CO)(1-MeIm),[8] and (OEP)Ru(CO)(py)[3,9,10] were prepared according to previously reported literature methods and their purity was checked by comparison of their IR and ^{1}H NMR spectra with their respective reported values. For example, (OEP)Ru(CO)(py) has a reported ν_{CO} of 1933 cm^{-1} in its IR spectrum compared our experimental value of 1930 cm^{-1} (resolution of the instrument used is 4 cm^{-1}). This was the only band in this region. The reported ^{1}H NMR data in C_6D_6 gives 10.18 (4H, s, por), 4.56 (1H, t, py), 4.05 (2H, t, py), 3.97 (16H, q, por), 1.92 (24H, t, por), 1.26 (2H, d, py) which are very similar to the experimental data collected in $CDCl_3$ which gave 9.78 (4H, s, por), 5.782 (1H, t, py, J = 8 Hz), 4.862 (2H, t, py, J = 8 Hz), 3.958 (16H, m, por), 1.87 (24H, t, por, J = 8 Hz), and 0.84 (2H, d, py, J = 5 Hz).

2.2.1 Cyclic Voltammetry and Infrared Spectroelectrochemistry

Electrochemical measurements were made using a BAS CV50W instrument (Bioanalytical Systems, West Lafayette, IN, USA). Our electrochemical cell has been described previously.[16] For all electrochemical experiments, a 3.0 mm diameter Pt disk

was utilized as the working electrode, a silver wire acted as the pseudo-reference electrode, and a Pt wire served as the auxiliary electrode. The solutions for electrochemical experiments were deaerated by bubbling prepurified nitrogen gas through the solutions for approximately 10 min before each set of measurements. The electrochemistry was performed at room temperature under an atmosphere of nitrogen in a 0.1 M NBu_4PF_6 or a 0.01 M $NBu_4BAr^F{}_4$ (lower concentration of this supporting electrolyte was used due to its limited availability; a slight increase in resistance is observed, but not a significant increase) solution of the analyte (1.0 mM) in CH_2Cl_2. All potentials are referenced to the internal $Cp_2Fe^{0/+}$ couple set to 0.00 V. The infrared spectra for the spectroelectrochemical experiments were collected using a Bruker Vector 22 FTIR spectrometer, which was outfitted with a mid-IR fiber-optic dip-probe, and liquid nitrogen cooled MCT detector (Remspec Corporation, Sturbridge, MA, USA).[16]

2.2.2 Simultaneous Chronoabsorptometry and Chronoamperometry (SCC)

UV-vis data was collected using an Ocean-Optics USB 4000 detector (360-1000 nm), an Ocean Optics LS-1 tungsten lamp, and a T-300-dip-probe as described recently.[14] The cell used is described in Figure 2.2 below.

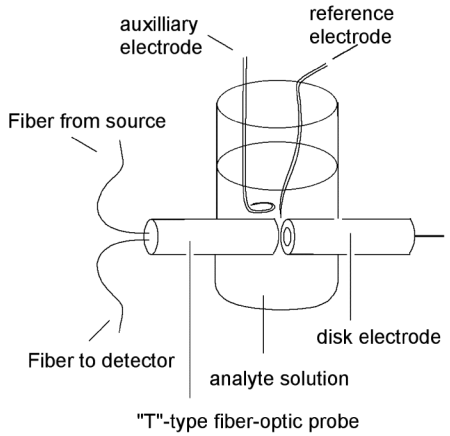

Figure 2.2. Spectroelectrochemical cell used in UV-vis spectroelectrochemical studies.

Solutions were 2×10^{-4} M analyte, 0.1 M NBu_4PF_6 or a 0.01 M (see above) $NBu_4BAr^F{}_4$, in 15 mL of CH_2Cl_2. Potentials and current were supplied using a BAS CV27 instrument. Before data collection, the solutions were deaerated by bubbling prepurified nitrogen gas through the solutions for approximately 10 min, and kept under an atmosphere of nitrogen during data collection. Care was taken to ensure that no potential was applied to the analyte while background spectra were being collected. Solutions were stirred a minimum of 30 seconds to help ensure a uniform diffusion layer before any measurements were performed. Beer's Law plots were collected using a standard 1.0 cm cuvette and an HP 8453 diode array instrument.

2.3 Results and Discussion

2.3.1 Cyclic voltammetry

The cyclic voltammograms of all four (por)Ru(CO)(L) compounds in CH_2Cl_2 using NBu_4PF_6 as a supporting electrolyte are shown in Figure 2.3. The (OEP)Ru(CO)(py) compound displays two well-behaved oxidations ($E_1^{o\prime}$ = 0.18 V; $E_2^{o\prime}$

= 0.78 V) within the solvent-system range available to us. The ΔE_p values for the first and second oxidations of this same compound were found to be 0.14 V along with i_{pc}/i_{pa} values that are equal to 1 suggests that they are electrochemically and chemically reversible processes. A plot of i_{pa} vs. (scan rate)$^{1/2}$ gave a linear relationship, indicating that the processes are diffusion-controlled. These systems studied involve what is referred to as an *EE* mechanism. This is typically described for an electrochemical system involving two consecutive oxidations, which are not complicated by a follow-up chemical step.

The electrochemical behavior for the remaining three compounds are very similar to that of the (OEP)Ru(CO)(py) complex in CH_2Cl_2 solution containing NBu_4PF_6 as supporting electrolyte. In this system they all contain two well-behaved electrochemically reversible oxidations. Their cathodic-to-anodic peak ratios (i_{pc}/i_{pa}) were all ~1.0 for each compound suggesting that they too are chemically reversible. There were no electrochemical reductions observed for these complexes within the solvent limit under the conditions used in our experiments. The electrochemical data for the compounds are summarized in Tables 2.1 and 2.2.

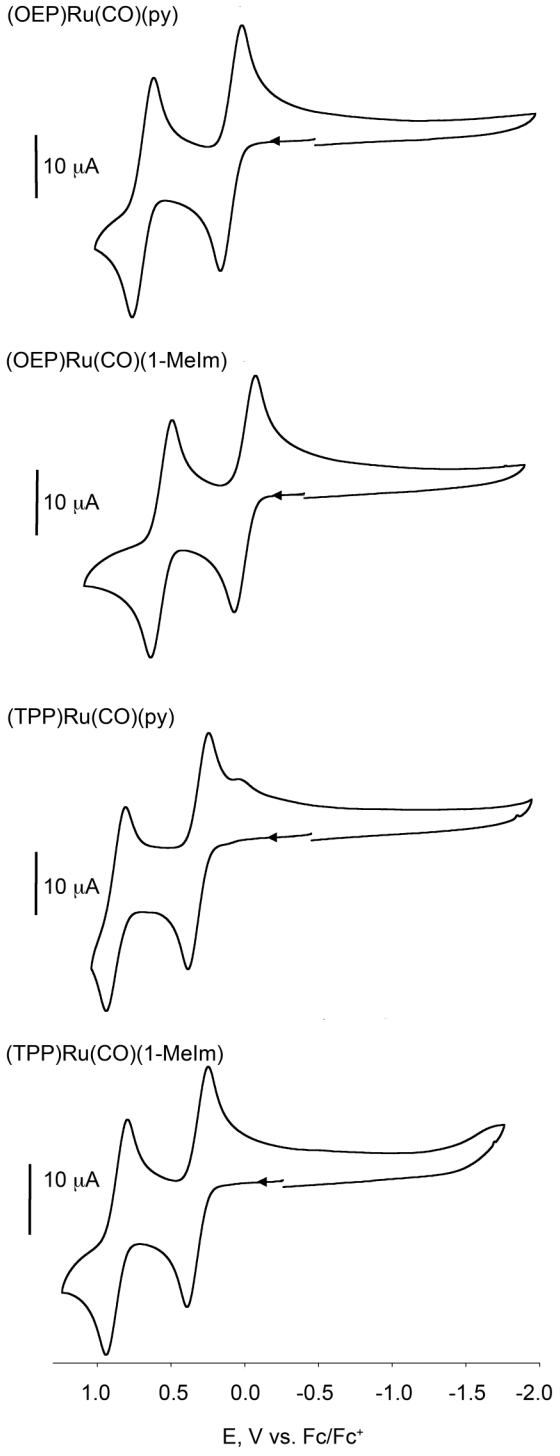

Figure 2.3. Cyclic voltammograms of (por)Ru(CO)(L) (por = TPP, OEP; L = pyridine and 1-MeIm) in CH_2Cl_2 @ 200 mV/s, 1 mM analyte, 0.1 M NBu_4PF_6 at room temperature and referenced against the Fc/Fc^+ couple set to 0.0 V.

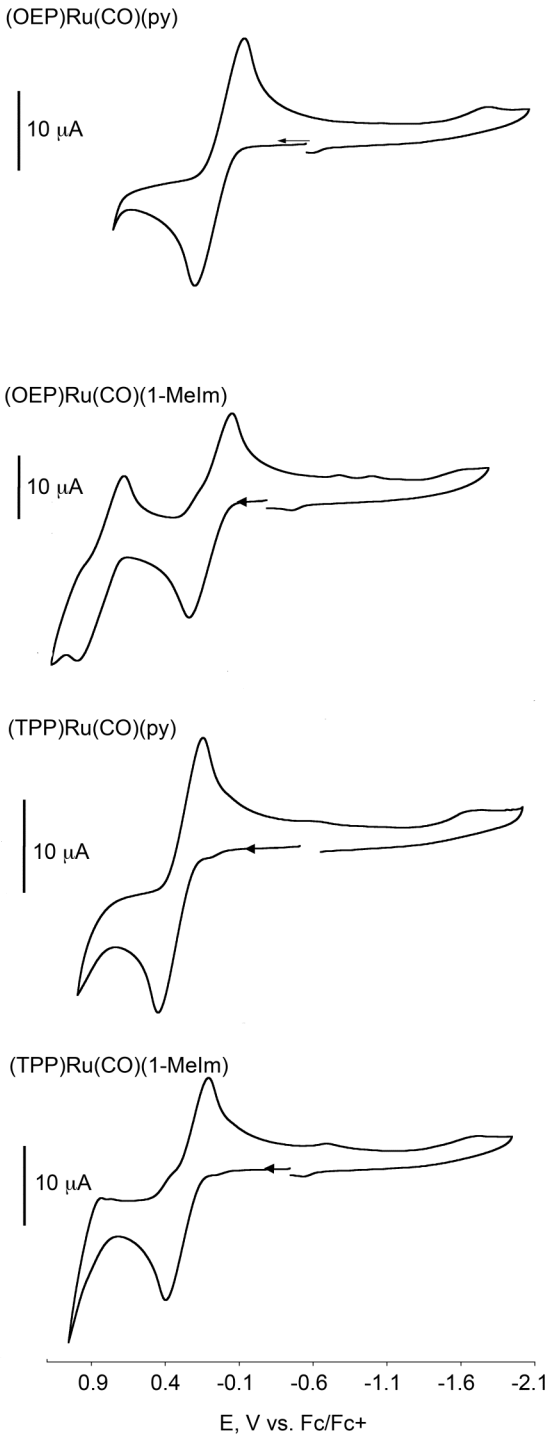

Figure 2.4. Cyclic voltammograms of (por)Ru(CO)(L) (por = TPP, OEP; L = pyridine and 1-MeIm) in CH_2Cl_2 @ 200 mV/s, 1 mM analyte, 0.01 M $NBu_4BAr^F{}_4$ at room temperature and referenced against the Fc/Fc^+ couple set to 0.0 V.

To determine if anion effects complicate the observed redox behavior of the (por)Ru(CO)(L) compounds in CH_2Cl_2, we used $NBu_4BAr^F{}_4$ (containing a weakly coordinating anion) as a supporting electrolyte. Each compound undergoes two oxidations in CH_2Cl_2 containing NBu_4PF_6. However, only (OEP)Ru(CO)(1-MeIm) undergoes a second oxidation while employing $NBu_4BAr^F{}_4$ as the supporting electrolyte as shown in Figure 2.4. This is not unexpected due to the $BAr^F{}_4^-$ anion having a weaker ion-pair interaction than that of PF_6^-.[17] The PF_6^- anion can be thought of as stabilizing a new electrochemically oxidized species ([(por)Ru(CO)(L)]PF_6) that can then be further oxidized. The $BAr^F{}_4^-$ anion has a weak interaction with the species generated after the first oxidation. Hill et al. have shown that $NBu_4BAr^F{}_4$ is a useful non-interacting electrolyte to study systems that generate electrophilic species.[18] This is most likely the reason that we see a second oxidation in the NBu_4PF_6 solution, and not in the $NBu_4BAr^F{}_4$ solution.

In the CH_2Cl_2 solution containing $NBu_4BAr^F{}_4$ as the supporting electrolyte, the (OEP)Ru(CO)(py) compound displays one well-behaved oxidation ($E_1{}^{o\prime}$ = 0.01 V). The ΔE_p for the first oxidation of this compound was found to be 0.39 V along with an i_{pc}/i_{pa} equal to 1 suggests that it is an electrochemically and chemically reversible process. A plot of i_{pa} vs. (scan rate)$^{1/2}$ gave a linear relationship, indicating that the process is diffusion-controlled. By examining Figure 2.4, it is apparent that only the (OEP)Ru(CO)(1-MeIm) compound undergoes two well-behaved oxidations ($E_1{}^{o\prime}$ = -0.034 V and $E_2{}^{o\prime}$ = 0.76 V) within the solvent range available to us during these experiments. Similar to the (OEP)Ru(CO)(py) complex, the other two TPP compounds show only one oxidation with $NBu_4BAr^F{}_4$ as the supporting electrolyte; at 0.37 V (ΔE_p

= 0.13 V) and 0.32 V (ΔE_p = 0.14 V) for (TPP)Ru(CO)(py) and (TPP)Ru(CO)(1-MeIm), respectively. The ΔE_p values obtained for the oxidations of these compounds and their cathodic-to-anodic peak ratios (i_{pc}/i_{pa}), which were all ~1.0 in the $NBu_4BAr^F{}_4$ solutions, suggesting that they too undergo chemically and electrochemically reversible processes. There were no electrochemical reductions observed for these complexes in the $NBu_4BAr^F{}_4$ solutions within the solvent limit under the conditions used in our experiments.

Table 2.1. The oxidation potentials (V) of (por)Ru(CO)(L) (por = TPP, OEP; L = pyridine or 1-MeIm) compounds in CH_2Cl_2.

	$E^{o\prime}$			
	1^{st} Ox.		2^{nd} Ox.	
	NBu_4PF_6	$NBu_4BAr^F{}_4$	NBu_4PF_6	$NBu_4BAr^F{}_4$
(OEP)Ru(CO)(py)	0.18	0.01*	0.78	
(OEP)Ru(CO)(1-MeIm)	0.11	-0.034*	0.69	0.76*
(TPP)Ru(CO)(py)	0.37	0.35	0.93	
(TPP)Ru(CO)(1-MeIm)	0.32	0.29	0.87	

Potentials are in volts, and are referenced to the ferrocene-ferrocenium couple set at 0.00V. Analytes are 1 mM, 200 mV/s, 0.1 M NBu_4PF_6, 0.01 M $NBu_4BAr^F{}_4$ in CH_2Cl_2.
*Potentials were referenced with acetylferrocene and adjusted for ferrocene (0.27 V vs. Ferrocene).

The potential separations obtained are not equal to that of the theoretical 0.059 V. It is commonly accepted that the ferrocene-ferrocenium couple is a reversible system; its ΔE_p in these experiments gave similar values to those of the analytes. Therefore it can be inferred that these oxidations are electrochemically reversible.[12]

Table 2.2. The peak separations ($\Delta E_p = |E_{pa} - E_{pc}|$) for all (por)Ru(CO)(L) (por = TPP, OEP; L = pyridine or 1-MeIm) complexes in CH_2Cl_2.

	1st Ox.		2nd Ox.	
	NBu_4PF_6	$NBu_4BAr^F{}_4$	NBu_4PF_6	$NBu_4BAr^F{}_4$
(OEP)Ru(CO)(py)	0.14 (0.14)	0.39 (0.38)*	0.14 (0.14)	
(OEP)Ru(CO)(1-MeIm)	0.17 (0.12)	0.35 (0.38)*	0.15 (0.12)	0.28 (0.38)*
(TPP)Ru(CO)(py)	0.14 (0.13)	0.31 (0.35)	0.12 (0.13)	
(TPP)Ru(CO)(1-MeIm)	0.15 (0.14)	0.31 (0.36)	0.15 (0.14)	

ΔE_p values ($|E_{pa} - E_{pc}|$) are in volts. Values in ( ) are the ΔE_p for the ferrocene-ferrocenium couple.
*ΔE_p for acetylferrocene-acetylferrocenium couple due to overlap with ferrocene in the CV.

The redox behavior for these (por)Ru(CO)(L) complexes are consistent with those reported earlier.[4,13,19-22]

2.3.2 Infrared Spectroelectrochemistry

In order to investigate the site(s) of oxidation of the (por)Ru(CO)(L) (por = TPP, OEP; L = py, 1-MeIm) compounds, fiber-optic infrared spectroelectrochemistry measurements were performed at room temperature while holding the potential slightly past the E_{pa} of the oxidations (see Table 2.3). An infrared beam was passed through the solution (approximately a 2 – 4 mm path length) and reflected off of the surface of the working electrode and sent to the detector through the fiber-optic cable (the surface of the working electrode thus acts as a mirror). This allows for the collection of an infrared spectrum of the redox-generated product that is formed on the spectroelectrochemical time-scale. The difference spectra obtained show changes that take place in the region of 1500 to 2100 cm^{-1}. The complexes being investigated in this study show strong ν_{CO} absorptions near 1900 cm^{-1} which can be clearly monitored for changes during the experiment.

The difference IR spectra for the first oxidation of (OEP)Ru(CO)(py) in CH_2Cl_2 using NBu_4PF_6 as the supporting electrolyte is shown in Figure 2.5. For this experiment, the applied potential was set at 0.31 V (E_{pa1} = 0.26 V). The difference IR reveal the disappearance of (OEP)Ru(CO)(py) (ν_{CO} = 1926 cm^{-1}) and the appearance of a new ν_{CO} band at 1969 cm^{-1} attributed to the cation $[(OEP)Ru(CO)(py)]^+$. Such a relatively small shift in ν_{CO} upon oxidation ($\Delta\nu_{CO}$ = 43 cm^{-1}) is indicative of the oxidation occurring at a location not too close to the Ru–CO center (where a higher $\Delta\nu_{CO}$ would have been expected, because the reduced Ru → CO backbonding shifts ν_{CO}). Based on this observation, we initially conclude that the first oxidation for (OEP)Ru(CO)(py) is porphyrin-centered (Equation 2.1) as has also been reported previously.[4]

Table 2.3. Difference IR values for the (por)Ru(CO)(L) (por = TPP, OEP; L = py, 1-MeIm) compounds containing 0.1 M NBu_4PF_6 and 0.01 M $NBu_4BAr^F{}_4$ in CH_2Cl_2.

		1st Ox.		2nd Ox.	
	Start*	NBu_4PF_6	$NBu_4BAr^F{}_4$	NBu_4PF_6	$NBu_4BAr^F{}_4$
(OEP)Ru(CO)(py)	1927	1969 (0.31)	1969 (0.25)	1970, 2007 (0.90)	
(OEP)Ru(CO)(1-MeIm)	1920	1961 (0.33)	1961 (0.13)	1959, 2002 (0.89)	1962 (0.83)
(TPP)Ru(CO)(py)	1942	1981 (0.47)	1983 (0.49)	1987, 2010 (1.02)	
(TPP)Ru(CO)(1-MeIm)	1935	1973 (0.49)	1975 (0.43)	1974, 2004 (1.01)	

The values above are for the ν_{CO} (cm^{-1})

* The starting ν_{CO} (cm^{-1}) stretches were within the resolution limits of the instrument for each supporting electrolyte solution

Values in ( ) are the held potentials in Volts vs. Fc/Fc^+ for the IR spectroelectrochemical investigation

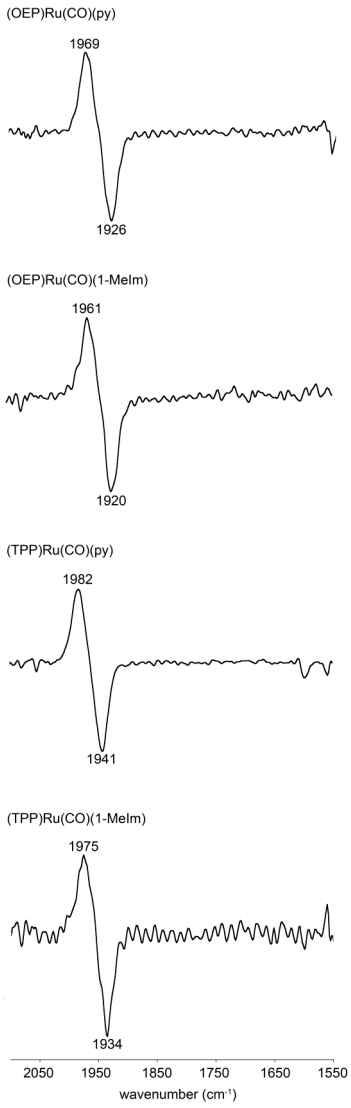

Figure 2.5. Difference IR spectra showing the products from the first oxidations of (por)Ru(CO)(L) (por = TPP, OEP; L = py, 1-MeIm) compounds containing 0.1 M NBu_4PF_6 with potentials held slightly past the first oxidations.

Figure 2.5 shows that during the first oxidation, there is only a small shift in the ν_{CO} band (~ 40 cm^{-1}) in all of the complexes. This is consistent with what has been previously reported for these complexes.[4,20]

The results that were obtained during spectroelectrochemical investigations of the first oxidation of these complexes in CH_2Cl_2 using the $NBu_4BAr^F{}_4$ supporting electrolyte were very similar to the results obtained while using NBu_4PF_6 (see Table

2.3). The results obtained for the (OEP)Ru(CO)(py) compound show the disappearance of ν_{CO} = to 1927 cm^{-1} and the appearance of a new band at 1969 cm^{-1} ($\Delta\nu_{CO}$ = 43 cm^{-1}) again supporting the idea that the first oxidation is taking place at a location other than the Ru–CO center (equation 2.1). As with the compounds in NBu_4PF_6, a $\Delta\nu_{CO}$ = ~40 cm^{-1} was observed in the difference IR spectra for the compounds during spectroelectrochemical studies of their first oxidations while using the $NBu_4BAr^F{}_4$ supporting electrolyte.

$$(por)Ru(CO)(L) \rightleftharpoons [(\dot{p}or)Ru(CO)(L)]^+ + e^- \qquad 2.1$$

The bands that we would expect to see for the porphyrin π-cation radical moiety are not clear in our system. There are features in the IR region (1520 – 1570 cm^{-1})[23] that we would normally assign to the (OEP) π-cation radical, but noise in that area does not allow us to confidently make this particular assignment. As stated above, the spectral window only allows for spectra to be analyzed in the range of 1500 – 2100 cm^{-1}, therefore, the (TPP) π -cation radical bands (1250 – 1295 cm^{-1})[23] are not observable in this study.

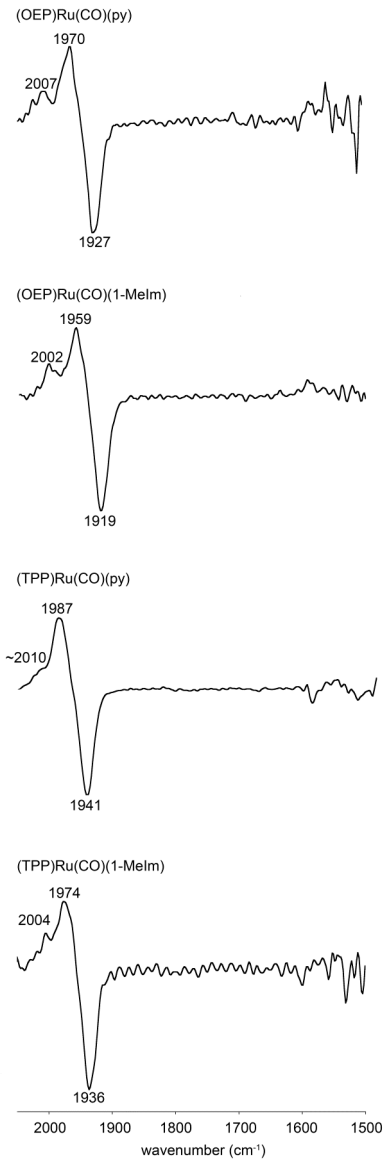

Figure 2.6. Difference IR spectra showing the products from the second oxidations of the (por)Ru(CO)(L) (por = TPP, OEP; L = py, 1-MeIm) compounds containing 0.1 M NBu_4PF_6 with potentials held slightly past the second oxidations.

The difference IR spectrum after the second oxidation of (OEP)Ru(CO)(py) shows two new ν_{CO} bands appearing in the difference IR spectrum at 1970 cm^{-1} and 2007 cm^{-1} while sitting at a potential of 0.90 V (E_{pa2} = 0.85 V). The analysis of the other compounds show similar results with a larger peak appearing in the ranges of 1959 – 1987 cm^{-1} and a much less intense peak in the 2001 – 2010 cm^{-1} area appearing

after the second oxidation (see Figure 2.6). It can be seen that the second (higher energy) new peak is very small and the more intense peak in the spectra is consistent with what was observed after the first oxidation (within the 4 cm^{-1} resolution limits of the instrument). It could be possible that the product from the second electrochemical oxidation is reactive towards the neutral species in solution, as described by equations 2.2 and 2.3.

$$[(\dot{p}or)Ru(CO)(L)]^{+} \rightleftharpoons [(\dot{p}or)Ru(CO)(L)]^{2+} + e^{-} \qquad 2.2$$

$$[(\dot{p}or)Ru(CO)(L)]^{2+} + (por)Ru(CO)(L) \rightleftharpoons 2[(\dot{p}or)Ru(CO)(L)]^{+} \qquad 2.3$$

The reason that the first oxidation product is still visible while sitting at the second oxidation potential is that the first oxidation product may still be the major species near the electrode surface during this time. It is safe to assume that the carbonyl ligand has not been lost from the complex during the first or second oxidation because of (i) the reversibility seen in the CVs, and (ii) both oxidations give rise to new ν_{CO} bands. Equations 2.2 and 2.3 depict the porphyrin radical during the second oxidation. As stated above, the second oxidation gives rise to a new peak that is ~70-80 cm^{-1} shifted from the original neutral species. This could suggest that the second oxidation is taking place somewhere along the axis of the ligands perpendicular to the porphyrin and not on the porphyrin itself. It is not a new claim that the second oxidation species is unstable for (por)Ru(CO)(L) systems. Other reports have also suggested that the second oxidation product of (TPP)Ru(CO)(py) may react with other species in solution.[4,22] To the best of our knowledge, there has not been an infrared spectrum reported that corresponds to the second oxidation products of the (por)Ru(CO)(L) complexes.

2.3.3 Simultaneous Chronoabsorptometry and Chronoamperometry (SCC)

In order to further characterize the redox products of these complexes, we performed simultaneous chronoabsorptometry and chronoamperometry (SCC) to obtain the UV-vis spectra of the products of the first oxidations (to confirm whether or not the first oxidations occur at the porphyrin rings). Details of the methodology have been described previously.[14] This SCC technique is useful and has several advantages over the commonly used optically transparent thin layer electrochemical (OTTLE) cells. OTTLE cells are limited by (i) inaccuracies in cell path length due to a metal electrode grid and non-reproducible spacer lengths (if the cells are disassembled and reassembled often), (ii) an influence of thin-layer resistance on the accuracy of the potential being applied, and (iii) other non-reproducible events that may occur from problems such as leakages. This new SCC technique allows the user to gather quantitative spectral information on the build-up of redox products at or near the electrode surface. This is done without the use of arbitrary spectral subtractions, which are commonly used in the manual generation of difference spectra. Mathematics is used in this technique to determine the plots of absorptivity (ε, extinction coefficient) versus wavelength of the electrode product(s). Another great advantage over OTTLE is that the absorptivities measured with the SCC technique are independent of path length and of the concentration of the starting material. The plots of ε vs. λ that we obtained for the product after the first oxidation of (OEP)Ru(CO)(py) and (OEP)Ru(CO)(1-MeIm) are shown in Figure 2.7. To collect this data, the electrode was set at a potential just positive of the E_{pa} of the first oxidation for the (por)Ru(CO)(L) complexes, similar to

how the IR spectroelectrochemical data was obtained. By using chronoamperometry data, the diffusion coefficients (cm^2/sec) were obtained; (OEP)Ru(CO)(py) = 4.6×10^{-6} (NBu_4PF_6) and 9.3×10^{-6} ($NBu_4BAr^F{}_4$), (OEP)Ru(CO)(1-MeIm) = 3.9×10^{-6} (NBu_4PF_6) and 7.9×10^{-6} ($NBu_4BAr^F{}_4$), (TPP)Ru(CO)(py) = 1.8×10^{-5} (NBu_4PF_6) and 1.2×10^{-5} ($NBu_4BAr^F{}_4$), and (TPP)Ru(CO)(1-MeIm) = 1.0×10^{-5} (NBu_4PF_6) and 9.6×10^{-6} ($NBu_4BAr^F{}_4$).

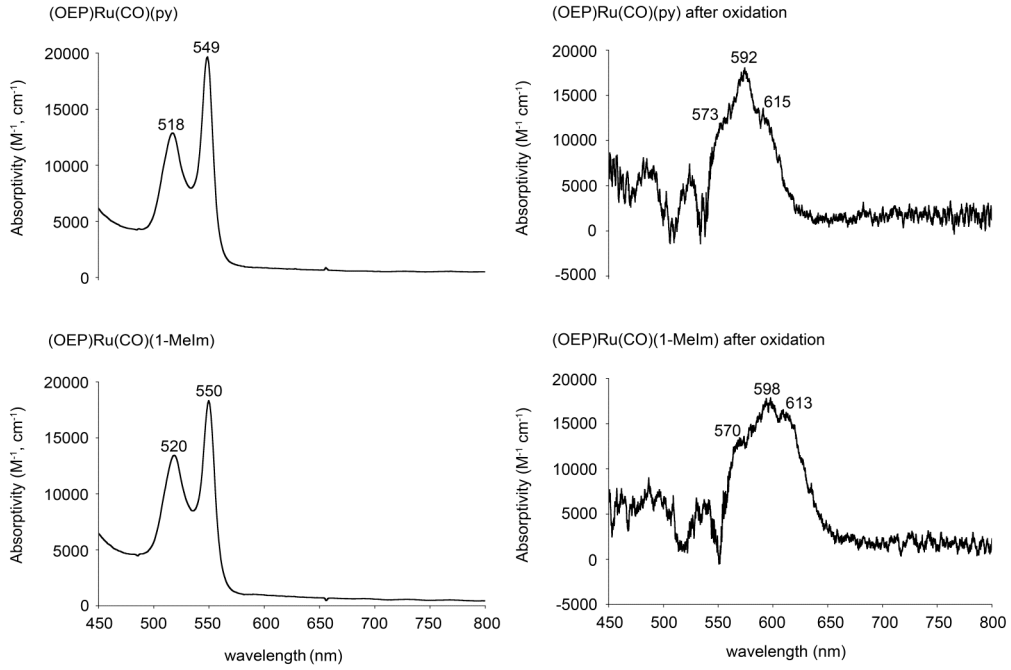

Figure 2.7. UV-vis spectra for the neutral (left) and products (right) of the oxidations of (OEP)Ru(CO)(L) (L = py and 1-MeIm) generated at an electrode surface over a 10 s period. Analytes are 2×10^{-4} M in 0.1 M NBu_4PF_6/CH_2Cl_2 at 298 K.

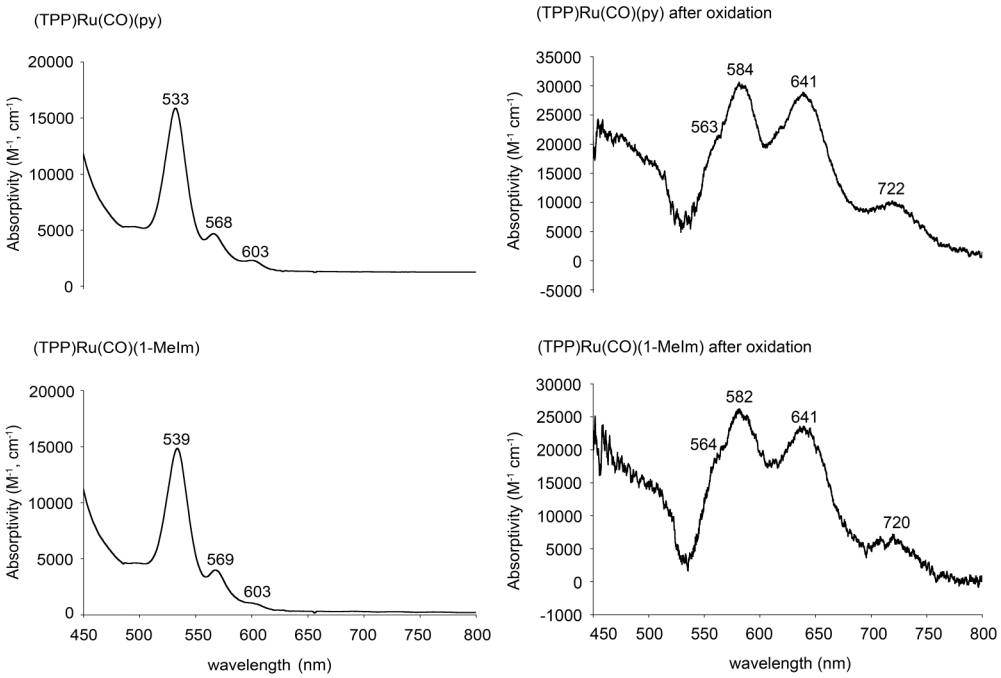

Figure 2.8. UV-vis spectra for the neutral (left) and products (right) of the oxidations of (TTP)Ru(CO)(L) (L = py and 1-MeIm) generated at an electrode surface over a 10 s period. Analytes are 2×10^{-4} M in 0.1 M NBu_4PF_6/CH_2Cl_2 at 298 K.

The plots of the complexes in $NBu_4BAr^F{}_4$ are very similar to those shown above for NBu_4PF_6. The similarities of the spectra of the first oxidation products in both PF_6^- and $BAr^F{}_4^-$ (Table 2.4) suggests that the ion pairing effect is minimal in the first oxidation process, but is much more pronounced in the second oxidation. We are continuing to study this hypothesis; indeed a larger ion-pairing effect might be expected for higher charged species such as the dication.

Table 2.4. UV-vis spectral data of neutral and electrooxidation products of the (por)Ru(CO)(L) (por = TPP, OEP; L = py, 1-MeIm) compounds.

	Neutral complex, λ	*E*	After 1st Ox., λ	
			NBu_4PF_6	$NBu_4BAr^F{}_4$
(OEP)Ru(CO)(py)	518, 549	0.21	573, 592, 615	
(OEP)Ru(CO)(1-MeIm)	520, 550	0.24	570, 598, 613	
(TPP)Ru(CO)(py)	533, 568, 603	0.49	563, 584, 641, 722	561, 583, 641, 720
(TPP)Ru(CO)(1-MeIm)	535, 569, 603	0.44	564, 582, 641, 720	563, 586, 640, 719

Potentials (*E*) are in volts, and are referenced to the Fc/Fc^+ couple set at 0.00 V
Analytes are 1 mM, 0.1 M NBu_4PF_6, 0.01 M $NBu_4BAr^F{}_4$ in CH_2Cl_2

The new features in the ε vs. λ plots suggest that the π-cation radical is being formed during the first oxidation for these complexes. This is supported by previous studies that identify the π-cation radicals for the (por)Ru(CO)(L) complexes which have broad and relatively undefined features in the visible region between 500 and 700 nm.[24-26] The results that we obtained also show red shifted features in the 500 to 700 nm range compared to the neutral species, however we see more detail in the overall shape of spectra instead of broad peaks dominating the visible region of the spectra.

2.4 Conclusion

In this study we have examined a series of (por)Ru(CO)(L) complexes (where por = OEP, TPP and L = pyridine, 1-MeIm) using cyclic voltammetry, infrared and UV-vis spectroelectrochemical techniques. These techniques were utilized in order to gain more information regarding the products that are formed during the oxidations of these complexes. The stability and their relative ease of synthesis of the compounds used have made them ideal for this study. We have also investigated the ion-pairing effects that the supporting electrolytes NBu_4PF_6 and $NBu_4BAr^F{}_4$ have during electrochemical oxidation. All of these compounds show two, well-behaved oxidations in a CH_2Cl_2

solution containing NBu_4PF_6 as a supporting electrolyte but only one oxidation in a CH_2Cl_2 solution containing $NBu_4BAr^F{}_4$ as the supporting electrolyte (with the exception of (OEP)Ru(CO)(1-MeIm), which has two). The weak interaction of the $BAr^F{}_4^-$ electrolyte with the product of the first oxidation leads to the lack of a second oxidation (in our available solvent-system range) as compared to the PF_6^- electrolyte, which does show a second oxidation. The first oxidations of the (por)Ru(CO)(L) complexes show the formation of the π-cation radicals as evidenced by small shifts of the ν_{CO} (~ 40 cm^{-1}) bands in the IR spectra along with features in the 500 – 700 nm range of the UV-vis spectra. Not only have we been able to provide the first difference IR spectra that resulted from the second oxidations, but also we were also able to show in greater detail the UV-vis spectra of the first oxidation products without the use of any manual manipulation of the data. Attempts were made to elucidate the visible product spectra resulting from the second oxidations in these systems. However, the method that was utilized currently lacks the ability to provide reproducible spectra for the second oxidation products. This is most likely due to the fact that there are three species present at the electrode's surface (neutral, monocation, and dication) during the second oxidation and obtaining spectral information specific to the dicationic species is difficult. This is a task that is currently ongoing. Also, another area of interest that needs to be explored involves computational work to make assignments of the spectral intensities, which correspond to the products generated during the first oxidations.

2.5 References

(1) Chien, J. C. W. Correlation of Electronic Spectra of Metalloporphyrins and Metalloproteins, *Journal of the American Chemical Society* **1978**, *100*, 1310.

(2) Seok, W. K.; Kim, M. Y. Spectrosopic Study of a Series of Para-substituted Tetraphenylporphine Carbonyl Complexes of Ruthenium(II) Containing Nitrogenous Bases, *Bulletin of the Korean Chemical Society* **1995**, *16*, 1239.
(3) Antipas, A.; Buchler, J. W.; Gouterman, M.; Smith, P. D. Porphyrins. 36. Synthesis and Optical and Electronic Properties of Some Ruthenium and Osmium Octaethylporphyrins, *Journal of the American Chemical Society* **1978**, *100*, 3015.
(4) Brown, G. M.; Hopf, F. R.; Ferguson, J. A.; Whitten, D. G.; Meyer, T. J. Metalloporphyrin Redox Chemistry - Effect of Extraplanar Ligands on Site of Oxidation in Ruthenium Porphyrins, *Journal of the American Chemical Society* **1973**, *95*, 5939.
(5) Slebodnick, C.; Seok, W. K.; Kim, K. M.; Ibers, J. A. Syntheses and Characterization of the Ruthenium Carbonyl Porphyrin Complexes Ru(TPP)(CO)(1-MeIm) and Ru(α-PocPivP)(CO)(1-MeIm), *Inorganica Chimica Acta* **1996**, *243*, 57.
(6) Salzmann, R.; Ziegler, C. J.; Godbout, N.; McMahon, M. T.; Suslick, K. S.; Oldfield, E. Carbonyl Complexes of Iron(II), Ruthenium(II), and Osmium(II) 5,10,15,20-tetraphenylporphyrinates: A Comparative Investigation by X-ray Crystallography, Solid-State NMR Spectroscopy, and Density Functional Theory, *Journal of the American Chemical Society* **1998**, *120*, 11323.
(7) Bonnet, J. J.; Eaton, S. S.; Eaton, G. R.; Holm, R. H.; Ibers, J. A. Spectroscopic and Structural Characterization of Ruthenium(II) Carbonyl-Porphine Complexes, *Journal of the American Chemical Society* **1973**, *95*, 2141.
(8) Salzmann, R.; McMahon, M. T.; Godbout, N.; Sanders, L. K.; Wojdelski, M.; Oldfield, E. Solid-State NMR, Crystallographic and Density Functional Theory Investigation of Fe-CO and Fe-CO Analogue Metalloporphyrins and Metalloproteins, *Journal of the American Chemical Society* **1999**, *121*, 3818.
(9) Barley, M.; Dolphin, D.; James, B. R.; Kirmaier, C.; Holten, D. Picosecond Flash-Photolysis of Carbonyl-Complexes of Ruthenium(II) Porphyrin Pi-Cation Radicals, *Journal of the American Chemical Society* **1984**, *106*, 3937.
(10) Hopf, F. R.; Obrien, T. P.; Scheidt, W. R.; Whitten, D. G. Structure and Reactivity of Ruthenium(II) Porphyrin Complexes - Photochemical Ligand Ejection and Formation of Ruthenium Porphyrin Dimers, *Journal of the American Chemical Society* **1975**, *97*, 277.
(11) Kadish, K. M.; Chang, D. Solvent-Binding and Solvation Effects on the Electrode-Reactions of Tetraphenylporphyrin Carbonyl-Complexes of Ruthenium(II), *Inorganic Chemistry* **1982**, *21*, 3614.
(12) Brown, G. M.; Hopf, F. R.; Meyer, T. J.; Whitten, D. G. Effect of Extraplanar Ligands on Redox Properties and Site of Oxidation in Iron, Ruthenium, and Osmium Porphyrin Complexes, *Journal of the American Chemical Society* **1975**, *97*, 5385.
(13) Kadish, K. M.; Leggett, D. J.; Chang, D. Investigation of the Electrochemical Reactivity and Axial Ligand-Binding Reactions of Tetraphenylporphyrin Carbonyl-Complexes of Ruthenium(II), *Inorganic Chemistry* **1982**, *21*, 3618.
(14) Shaw, M. J.; Cranford, D. L.; Rodgers, K. W.; Eilers, J. E.; Noble, B.; Warhausen, A. J.; Richter-Addo, G. B. Facile Determination of the Spectra of

Unstable Electrode Products Using Simultaneous Fiber-Optic Chronoabsorptometry and Chronoamperometry, *Inorganic Chemistry* **2010**, *49*, 9590.

(15) Nishida, H.; Takada, N.; Yoshimura, M.; Sonoda, T.; Kobayashi, H. Tetrakis[3,5-Bis(Trifluoromethyl)Phenyl]Borate - Highly Lipophilic Stable Anionic Agent for Solvent-Extraction of Cations, *Bulletin of the Chemical Society of Japan* **1984**, *57*, 2600.

(16) Shaw, M. J.; Henson, R. L.; Houk, S. E.; Westhoff, J. W.; Jones, M. W.; Richter-Addo, G. B. Fiber-Optic Infrared Reflectance Spectroelectrochemistry: Isomerization of a Manganese Pyranyl Complex, *Journal of Electroanalytical Chemistry* **2002**, *534*, 47.

(17) Barriere, F.; Geiger, W. E. Use of Weakly Coordinating Anions to Develop an Integrated Approach to the Tuning of Δ E-1/2 Values by Medium Effects, *Journal of the American Chemical Society* **2006**, *128*, 3980.

(18) Hill, M. G.; Lamanna, W. M.; Mann, K. R. Tetrabutylammonium Tetrakis[3,5-Bis(Trifluoromethyl)Phenyl]Borate as a Noncoordinating Electrolyte - Reversible $1e^-$ Oxidations of Ruthenocene, Osmocene, and $Rh_2(TM4)_4^{2+}$ (TM4 = 2,5-Diisocyano-2,5-Dimethylhexane), *Inorganic Chemistry* **1991**, *30*, 4687.

(19) Kadish, K. M.; Hu, Y.; Tagliatesta, P.; Boschi, T. Synthesis and Electrochemical Characterization of Ruthenium Porphyrins Containing a Bound PF_3 Axial Ligand, *Journal of the Chemical Society, Dalton Transactions* **1993**, 1167.

(20) Kadish, K. M.; Tagliatesta, P.; Hu, Y.; Deng, Y. J.; Mu, X. H.; Bao, L. Y. Evaluation of Electron-Transfer Sites in Ruthenium(II) Octaethylporphyrin Complexes of the Type (OEP)Ru(CO)(L), *Inorganic Chemistry* **1991**, *30*, 3737.

(21) Barley, M.; Becker, J. Y.; Domazetis, G.; Dolphin, D.; James, B. R. Synthesis and Redox Chemistry of Octaethylporphyrin Complexes of Ruthenium(II) and Ruthenium(III), *Canadian Journal of Chemistry* **1983**, *61*, 2389.

(22) Mu, X. H.; Kadish, K. M. Applications of Thin-Layer FTIR, UV-Vis, and ESR Spectroelectrochemistry for Evaluating (TPP)Ru(CO) Redox Reactions in Nonaqueous Media, *Langmuir* **1990**, *6*, 51.

(23) Shimomura, E. T.; Phillippi, M. A.; Goff, H. M.; Scholz, W. F.; Reed, C. A. Infrared-Spectroscopy of Oxidized Metalloporphyrins - Detection of a Band Diagnostic of Porphyrin-Centered Oxidation, *Journal of the American Chemical Society* **1981**, *103*, 6778.

(24) Gross, Z.; Barzilay, C. Spectroscopic Characterization of 2 Types of Tetraarylporphyrin Cation Radicals, *Angewandte Chemie International Edition* **1992**, *31*, 1615.

(25) Felton, R. H.; Owen, G. S.; Dolphin, D.; Fajer, J. Iron(IV) Porphyrins, *Journal of the American Chemical Society* **1971**, *93*, 6332.

(26) Fajer, J.; Borg, D. C.; Forman, A.; Dolphin, D.; Felton, R. H. Pi-Cation Radicals and Dications of Metalloporphyrins, *Journal of the American Chemical Society* **1970**, *92*, 3451.

Chapter 3. Synthesis, Characterization, Electrochemistry, and Spectroelectrochemistry of (por)Ru(NO)(OR) (por = TPP and OEP, R = -C_6H_3-2,6-NHC(=O)CF_3, -C_6H_4-2-NHC(=O)CF_3 and –Ph) Complexes

3.1 Introduction

The chemistry of metal nitrosyl complexes is well established for the most part.[1] The biological chemistry of NO within metalloenzyme active sites is an ever growing field of study.[2] It is known that NO is involved in several bioregulatory processes such as vasodilation, cytotoxicity, neurotransmission, and as a signaling molecule through nitrosylation of iron-containing heme metalloenzymes.[3-10] One area of NO chemistry that is of interest to our research group involves its interactions with heme-containing proteins. In 1995, Guy Brown reported that NO was a competitive inhibitor of heme catalase from bovine liver.[11] Heme-containing catalase enzymes are found in many bacteria and almost all plants and animals and catalyzes the disproportionation of toxic hydrogen peroxide into oxygen and water (Figure 3.1).[12] This is a very important enzyme to organisms that undergo anaerobic respiration because it helps eliminate the reactive oxygen species (ROS) H_2O_2, which can cause oxidative damage to DNA. The structure of bovine liver catalase was initially determined by Murthy et al. in 1981 with

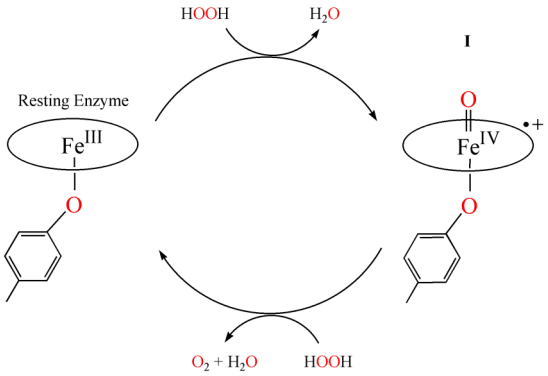

Figure 3.1. Disproportionation of H_2O_2 to H_2O by catalase.[13]

refinement reports becoming available later in 1981 and 1999.[14-16] This structure of catalase was that of a tetramer.[17] Each of the monomers is approximately 60 kDa and contains 507 amino acid residues with a ferric active site.[18-20] Structures of catalase with ligands bound to the active site such as cyanide have been reported.[21] However, until just recently, the structure of the NO bound enzyme was not known until Purwar et al. published the first NO bound structure of catalase in 2011.[22] Their report suggests that the NO is bent with respect to the heme with angles ranging from 5º to 20º with an average of 12º. They also went on to say that the true geometry of the Fe–NO moiety was difficult to determine unambiguously.

Interestingly, a newly recognized class of heme proteins also contains heme-aryloxide moieties. These heme proteins have a tyrosinate ligand coordinated to the iron center of the heme.[23] As stated before, our interests are in the interactions of NO with the metal centers of heme-containing biomolecules and with synthetic models of these types of systems. By preparing synthetic models of the active sites of heme-containing metalloenzymes, it is possible to gain additional insight into the scope of the chemistry available to the active site. Because catalase has a tyrosinate coordinated to the metal center of its active site, along with two hydrogen bonds from the coordinated O–atom to a neighboring arginine,[24] we sought to synthesize a (por)M(NO)(aryloxide) complex with similar H–bonding characteristics. Instead of iron, which can have mixed spin-states making it difficult to isolate and characterize, we sought to use ruthenium as our central metal for these complexes because it is generally accepted as a stable suitable substitute for unstable (low-spin) iron complexes when studying metalloporphyrin complexes.[25]

In this work, we have successfully synthesized and characterized a new series of (porphyrin)Ru(NO)(aryloxide) model complexes that contain an increasing number of internal hydrogen bonds from zero to two as shown in Figure 3.2. Their structures and redox properties are provided to show the effect that the hydrogen bonds have on the properties of these compounds.

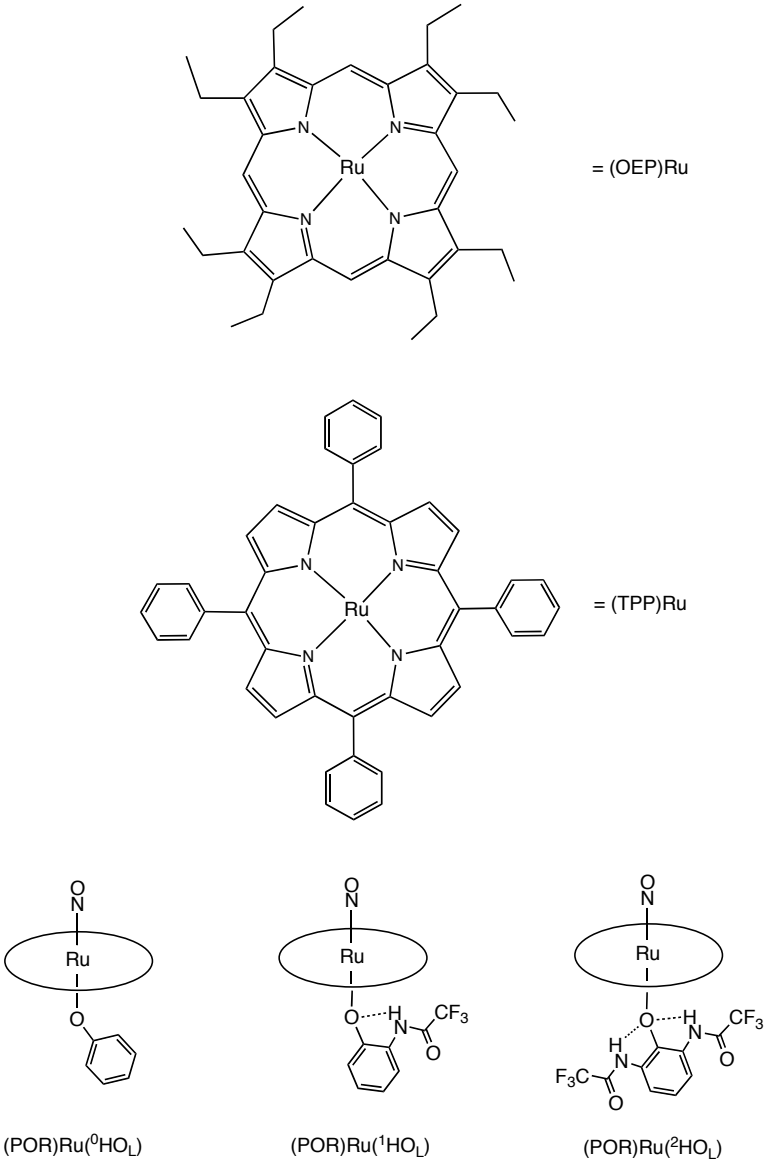

Figure 3.2. Synthetic ruthenium-containing metalloporphyrins.

3.2 Experimental

3.2.1 Materials, Instrumentation, and Methods

All reactions were carried out under an inert atmosphere of nitrogen using standard Schlenk glassware and/or in an Innovative Technology Labmaster 100 Dry Box unless indicated differently. The solvents methylene chloride, hexane, diethyl ether, cyclohexane, and toluene were dried using an Innovative Technology Inc. Pure Solv 400-5-MD Solvent Purification System.

Infrared spectra were collected using a Bio-Rad FT-155 FTIR spectrometer. Proton NMR spectra were acquired on a Varian 300 MHz spectrometer and the signals were referenced to the signal from residual solvent ($CHCl_3$ at 7.24 ppm). Positive and negative ESI mass spectra were obtained on a Micromass Q-TOF mass spectrometer by Dr. Steven Foster of this department. Electrochemical, infrared spectroelectrochemical and UV-vis spectroelectrochemical measurements were made in the same manner that was outlined in Chapter 2 of this dissertation.

3.2.2 Chemicals

$(OEP)H_2$ was purchased from Mid-Century Chemicals. $Ru_3(CO)_{12}$, phenol, and (por)Ru(NO)(OR) (R = Et, C_5H_{11}) were purchased from Sigma-Aldrich. All chemicals were used as delivered. $(TPP)H_2$ was synthesized from known literature methods.[26] (OEP)Ru(CO) was synthesized in the manner given for the preparation of (TPP)Ru(CO) provided in the literature.[27] The only modification to the literature method was that an appreciable amount of product was collected from the decalin fraction after it was chromatographed through a neutral silica gel column (70-230 mesh) with CH_2Cl_2. The

pink-red solution was then dried under vacuum to give a purple-red solid with a yield of approximately 95%. IR (KBr, cm^{-1}): 1925. The HO-*o*-(NHC(=O)CF_3)-C_6H_4 (^1HO_L) and HO-2,6-(NHC(=O)CF_3)$_2$-C_6H_3 (^2HO_L) were synthesized in a manner previously outlined.[28,29]

The supporting electrolyte NBu_4PF_6, for electrochemical experiments was obtained from Aldrich and used as received. The purity of the electrolyte was checked by ^{1}H NMR against a previously re-crystallized (from hot ethanol) sample of NBu_4PF_6 and found to be spectroscopically identical.

3.2.3 Synthesis

3.2.3.1 Synthesis of (OEP)Ru(NO)(O-2,6-(NHC(=O)CF_3)$_2$-C_6H_3)

(OEP)Ru(NO)(^2HO_L)

To a stirred solution of (OEP)Ru(NO)(O-*i*-C_5H_{11}) (0.0323 g, 0.0430 mmol) in toluene (5 mL) was added HO-2,6-(NHC(=O)CF_3)$_2$-C_6H_3 (0.0208 g, 0.0658 mmol) and the mixture was left to stir. The reaction was monitored by IR spectroscopy to observe changes in the ν_{NO} and ν_{CO} regions. A new ν_{NO} stretch at 1842 cm^{-1} and a new ν_{CO} stretch at 1727 cm^{-1} were clearly evident after 30 minutes with no evidence of a ν_{NO} corresponding to the starting (OEP)Ru(NO)(O-*i*-C_5H_{11}) (ν_{NO} = 1795 cm^{-1}). The solvent was removed in vacuo and the residue re-dissolved in CH_2Cl_2 and passed through a silica gel column (70-230 mesh) using CH_2Cl_2 as the eluent. A small amount of pink solution came off of the column first and was discarded. The major red band was collected and then the solvent was removed under vacuum. IR (KBr, cm^{-1}): ν_{NO} =

1845, ν_{CO} = 1722. ^{1}H NMR ($CDCl_3$, ppm): 10.30 (s, 4H, *meso*-H of OEP), 4.13 (m, 16H, CH_3CH_2 of OEP), 1.92 (t, 24H, CH_3CH_2 of OEP, J = 8 Hz), 8.46 (s (broad), 2H from N*H*) 6.46 (d, 2H in *meta*-position on ligand, J = 8 Hz), 5.71 (t, 1H in *para*-position on ligand, J = 8 Hz). ESI^+-MS (m/z): 664.3 $[(OEP)Ru(NO)]^+$ (100%), 634.3 $[(OEP)Ru]^+$ (42%). ESI^--MS (m/z): 315 $[(O\text{-}C_6H_3\text{-}2,6\text{-}(NHC(=O)CF_3)_2)]^-$ (100%).

3.2.3.2 Synthesis of (OEP)Ru(NO)(O-*o*-(NHC(=O)CF_3)-C_6H_4) **(OEP)Ru(NO)(^1HO_L)**

To a stirred solution of (OEP)Ru(NO)(O-*i*-C_5H_{11}) (0.0326 g, 0.0434 mmol) in toluene (5 mL) was added of HO-*o*-(NHC(=O)CF_3)-C_6H_4 (0.0144 g, 0.0701 mmol) and the mixture was left to stir. The reaction was monitored by IR spectroscopy to observe changes in the ν_{NO} and ν_{CO} regions. A new ν_{NO} stretch at 1830 cm^{-1} and a new ν_{CO} stretch at 1731 cm^{-1} were clearly evident after 30 minutes with no evidence of a ν_{NO} corresponding to the starting (OEP)Ru(NO)(O-*i*-C_5H_{11}) (ν_{NO} = 1795 cm^{-1}). The solvent was removed in vacuo and the residue re-dissolved in CH_2Cl_2 and passed through a silica gel column (70-230 mesh) using CH_2Cl_2 as eluent. A small amount of pink solution came off of the column first and was discarded. The major red band was collected, and then the solvent was removed under vacuum. IR (KBr, cm^{-1}): ν_{NO} = 1835, ν_{CO} = 1718. ^{1}H NMR ($CDCl_3$, ppm): 10.31 (s, 4H, *meso*-H of OEP), 4.13 (q, 16H, CH_3CH_2 of OEP, J = 8 Hz), 1.94 (t, 24H, CH_3CH_2 of OEP, J = 8 Hz), 6.43 (m, 1H which is in the 3 position of phenyl moiety of the ligand), 5.17 and 5.48 (3H in the 4,5,6 position of the phenyl moiety of the ligand). ESI^+-MS (m/z): 664.3 $[(OEP)Ru(NO)]^+$ (100%), 634.3 $[(OEP)Ru]^+$ (45%). ESI^--MS (m/z): 204 $[(O\text{-}C_6H_4\text{-}2\text{-}NHCOCF_3)]^-$ (100%).

3.2.3.3 Synthesis of (OEP)Ru(NO)(OPh)

To a stirred solution of (OEP)Ru(NO)(O-*i*-C_5H_{11}) (0.0247 g, 0.0329 mmol) in toluene (5 mL) was added of HO-Ph (0.0085 g, 0.0903 mmol) and the mixture was left to stir. The reaction was monitored by IR spectroscopy to observe a change in the ν_{NO} band. A new ν_{NO} stretch at 1821 cm^{-1} is clearly evident after 45 minutes with no evidence of a ν_{NO} corresponding to the (OEP)Ru(NO)(O-*i*-C_5H_{11}) (ν_{NO} = 1795 cm^{-1}). The solvent was removed in vacuo and the residue re-dissolved in CH_2Cl_2 and passed through a neutral silica column (70-230 mesh) with CH_2Cl_2 as the eluent. A small amount of pink solution came off of the column first and was discarded. The major red band was collected with a CH_2Cl_2/Et_2O (50:50) solution and then the solvent was removed under vacuum. ^{1}H NMR ($CDCl_3$, ppm) 10.25 (s, 4H, *meso*-H of OEP), 4.09 (m, CH_3CH_2 of OEP), 1.94 (t, CH_3CH_2 of OEP, J = 8 Hz), 5.45 (t, 1H, *p-H* of phenyl moiety of the ligand, J = 7 Hz), 5.29 (t, 2H, *m-H* of the phenyl moiety of the ligand, J = 7 Hz), the *o*-H's do not appear to be visible in the collected spectrum, possibly due to overlap with porphyrin H's. ESI$^+$-MS (m/*z*): 664.3 $[(OEP)Ru(NO)]^+$ (100%).

3.2.3.4 Synthesis of (OEP)Ru(NO)(O-NHC(=O)-C_6H_4-*o*-OH) **(OEP)Ru(NO)(SalHate)**

To a stirred solution of (OEP)Ru(NO)(OEt) (0.0202 g, 0.0028 mmol) in toluene (4 mL) was added salicylhydroxamic acid (0.0067 g, (0.0437 mmol) and left to stir at ~70ºC for 4 h. The solvent was removed in vacuo and the residue re-dissolved in CH_2Cl_2 and passed through a silica gel column (70-230 mesh) using CH_2Cl_2 as eluent. A small pink band came off of the column first with a 50:50 hexanes/diethyl ether

mixture and was discarded. The major dark red band was collected with 100% diethyl ether. This dark red band was dried under vacuum and characterized. IR (KBr, cm^{-1}): ν_{NO} = 1835, ν_{CO} = 1637 (weak). ^1H NMR ($CDCl_3$, ppm): 10.35 (s, 4H, *meso*-H of OEP), 4.12 (m, 16H, CH_3CH_2 of OEP), 1.96 (m, 24H, CH_3CH_2 of OEP), 11.20 (s, 1H of ligand), 6.93 (m, 1H of ligand), 6.41 (d, 1H of ligand, J = 8 Hz), 6.22 (t, 1H of ligand, J = 8 Hz), 4.63 (d, 1H of ligand, J = 8 Hz), 0.86 (m, 1H of ligand). ESI^+-MS (m/z): 664.3 $[(OEP)Ru(NO)]^+$ (100%), 634.3 $[(OEP)Ru]^+$ (42%). ESI^--MS (m/z): 137.1 $[(OC_6H_4$-*o*-$COOH)]^-$ (100%), 152.1 $[(OC_6H_4$-*o*-$CONHOH)]^-$ (34%).

3.2.3.5 Synthesis of (TPP)Ru(NO)(O-2,6-$(NHC(=O)CF_3)_2$-C_6H_3) **(TPP)Ru(NO)(^2HO_L)**

To a stirred solution of (TPP)Ru(NO)(OEt) (0.0201 g, 0.0254 mmol) in CH_2Cl_2 (8 mL) was added HO-2,6-$(NHC(=O)CF_3)_2$-C_6H_3 (0.0126 g, 0.0399 mmol) and left to stir at 25ºC for 8 h. The solvent was removed in vacuo and the residue re-dissolved in CH_2Cl_2 and passed through a silica gel column (70-230 mesh) with CH_2Cl_2 as eluent. A yellow band came off of the column first and was discarded. The major red band was collected, and then the solvent was removed under vacuum. IR (KBr, cm^{-1}): ν_{NO} = 1848, ν_{CO} = 1718. ^1H NMR ($CDCl_3$, ppm): 9.02 (s, 8H, *pyrrole*-H of TPP), 7.98 and 8.41 (m, 8H of TPP), 7.83 (m, 12H of TPP), 6.78 (d, 2H in *meta*-position on ligand, J = 8 Hz), 5.79 (t, 1H in *para*-position on ligand, J = 8 Hz) . ESI^+-MS (m/z): 744.1 $[(TPP)Ru(NO)]^+$ (100%), 714.2 $[(TPP)Ru]^+$ (42%). ESI^--MS (m/z): 315 $[(O$-C_6H_4-2,6-$NHCOCF_3)]^-$ (100%).

3.2.3.6 Synthesis of (TPP)Ru(NO)(O-*o*-$(NHC(=O)CF_3)$-C_6H_4) **(TPP)Ru(NO)(^1HO_L)**

To a stirred solution of (TPP)Ru(NO)(OEt) (0.0210 g, 0.0266 mmol) in CH_2Cl_2 (8 mL) was added of HO-*o*-(NHC(=O)CF_3)-C_6H_4 (0.0072 g, 0.0351 mmol) and left to stir at ~30 ºC for 5 h. The solvent was removed in vacuo and the residue re-dissolved in CH_2Cl_2 to pass through a silica gel column (70-230 mesh) with CH_2Cl_2 as eluent. A yellow band came off of the column first and was discarded. The major dark red band was collected, and then the solvent was removed under vacuum. IR (KBr, cm^{-1}): ν_{NO} = 1845, ν_{CO} = 1718. ^{1}H NMR ($CDCl_3$, ppm): 8.98 (s, 8H, *pyrrole*-H of TPP), 8.18 (m, 8H of TPP), 7.78 (m, 12H of TPP), 6.71 (m, 1H which is in the 3 position of phenyl moiety of the ligand), 5.48 and 5.66 (3H in the 4,5,6 position of the phenyl moiety of the ligand). ESI^+-MS (m/*z*): 744.1 $[(TPP)Ru(NO)]^+$ (100%), 714.2 $[(TPP)Ru]^+$ (42%). ESI^--MS (m/*z*): 204.1 $[(O\text{-}C_6H_4\text{-}o\text{-}NHCOCF_3)]^-$ (100%).

3.3 Results

The approach for synthesizing the (por)Ru(NO)(OR) complexes followed the procedure of alcohol exchange similar to that which has been reported for iron porphyrin alkoxide complexes.[30] The six-coordinate complexes belong to the $\{RuNO\}^6$ class according to the Enemark-Feltham notation.[31] A general procedure for the (por)Ru(NO)(OR) complexes was carried out with a CH_2Cl_2 solution of (por)Ru(NO)(OEt)[32] or (por)Ru(NO)(O-*i*-C_5H_{11})[33] and then adding to that an excess of the alcohol (ROH) during the exchange. The reaction mixtures were then taken to dryness under vacuum, re-dissolved in CH_2Cl_2 and passed through a neutral silica column (70 - 230 mesh) and the dark red fraction collected. It should be stated that using either (por)Ru(NO)(OEt) or (por)Ru(NO)(O-*i*-C_5H_{11}) gave the same final

(por)Ru(NO)(OR) product. However, the (por)Ru(NO)(O-*i*-C_5H_{11}) complex was favored by us in these reactions due to its ease of synthesis, and stability of the isoamyl nitrite starting material over the ethyl nitrite starting material that is needed to make the alkoxide complexes from (por)Ru(CO).

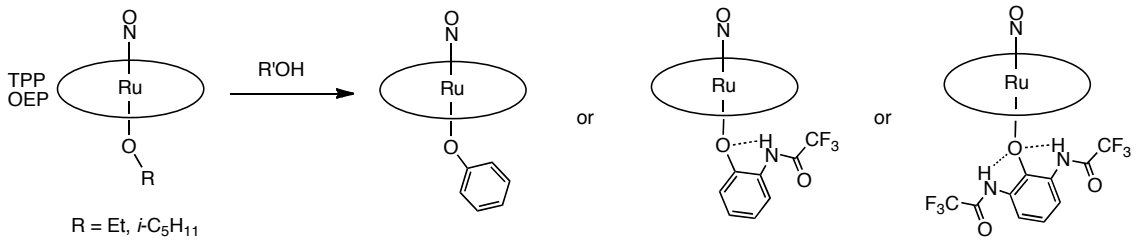

Figure 3.3. General synthetic description for the (por)Ru(NO)(OR) complexes.

3.3.1 Characterization by ^{1}H NMR Spectroscopy

The use of ^{1}H NMR was very useful for two reasons. The first of which was the ability to determine if all of the starting complexes (OEP)Ru(NO)(OEt) or (OEP)Ru(NO)(O-*i*-C_5H_{11}) had been consumed during the reactions. Fortunately, these complexes have very distinguishable features in the negative ppm region of their ^{1}H spectra that correspond to their coordinated alkoxide ligands. Also, the spectra for the products obtained showed identifiable chemical shifts for the coordinated ligands distinct from those of the free ligands (see section 3.2.1 in this chapter).

3.3.2 Mass Spectrometry

The positive and negative ESI mass spectrometry data was collected for all of the (por)Ru(NO)(OR) complexes to aid in their characterization. All complexes showed fragmentation under ESI conditions. None of the analyzed complexes showed

a parent peak for the compound in their respective spectra. For example, the OEP complexes showed *m/z* peaks of 664.3 for the $[(OEP)Ru(NO)]^+$ fragment (base peak, 100%) and 634.3 for the $[(OEP)Ru]^+$ fragment (~40% of the base peak height). The mass spectra of the TPP complexes showed the $[(TPP)Ru(NO)]^+$ fragment of *m/z* 744.1 (base peak, 100%) and the $[(TPP)Ru]^+$ fragment of 714.2 (*m/z*) (~42% of the height of the base peak).

Table 3.1. Mass spectrometry ($ESI^{+/-}$) data for (por)Ru(NO)(OR) complexes.

Compound	ESI^+	ESI^- (ligand)
(TPP)Ru(NO)(^1HO_L)	744.1[a] (100%), 714.2[b] (40%)	204.1 (100%)
(TPP)Ru(NO)(^2HO_L)	744.1 (100%), 714.1 (42%)	315.0 (100%)
(OEP)Ru(NO)(OPh)	664.3[c] (100%)	
(OEP)Ru(NO)(^1HO_L)	664.3 (100%), 634.2[d] (45%)	204.1 (100%)
(OEP)Ru(NO)(^2HO_L)	664.3 (100%), 634.3 (42%)	315.0 (100%)
(OEP)Ru(NO)(SalHate)	664.3 (100%), 634.3 (37%)	137.1 (100%), 152.1 (32%)

[a]744.1 = $[(TPP)Ru(NO)]^+$, [b]714.1 = $[(TPP)Ru]^+$, [c]664.2 = $[(OEP)Ru(NO)]^+$, [d]634.3 = $[(OEP)Ru]^+$

3.3.3 X-ray Crystallography

Crystals of (OEP)Ru(NO)(^1HO_L), (OEP)Ru(NO)(^2HO_L), and (OEP)Ru(NO)(SalHate) were grown from their respective CH_2Cl_2/cyclohexane (4:1) solutions by slow evaporation over a period of several days at room temperature under an N_2(g) atmosphere. Suitable single crystals were then selected for X-ray crystal structure determinations. The molecular structures for these complexes are given in the figures below. The internal hydrogen bonding for all three complexes is shown by dashed lines in the structures.

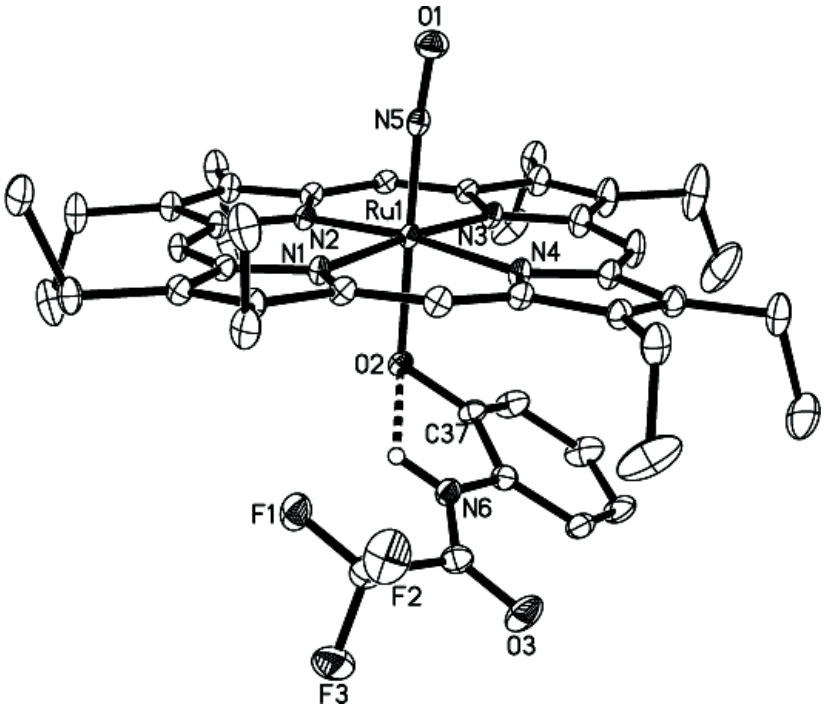

Figure 3.4. Molecular structure of (OEP)Ru(NO)(^1HO_L). Hydrogen atoms have been omitted for clarity (except that which is attached to N6).

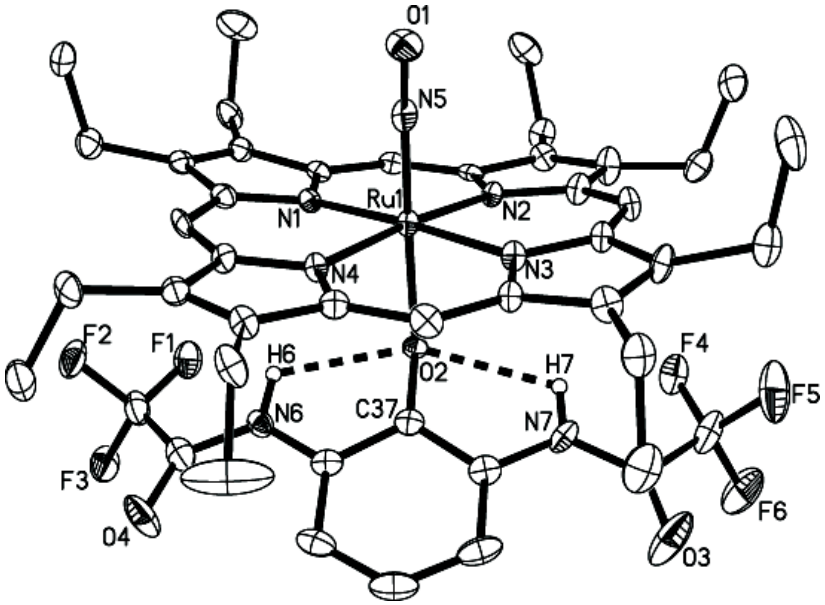

Figure 3.5. Molecular structure of (OEP)Ru(NO)(^2HO_L). Hydrogen atoms have been omitted for clarity (except those attached to N6 and N7).

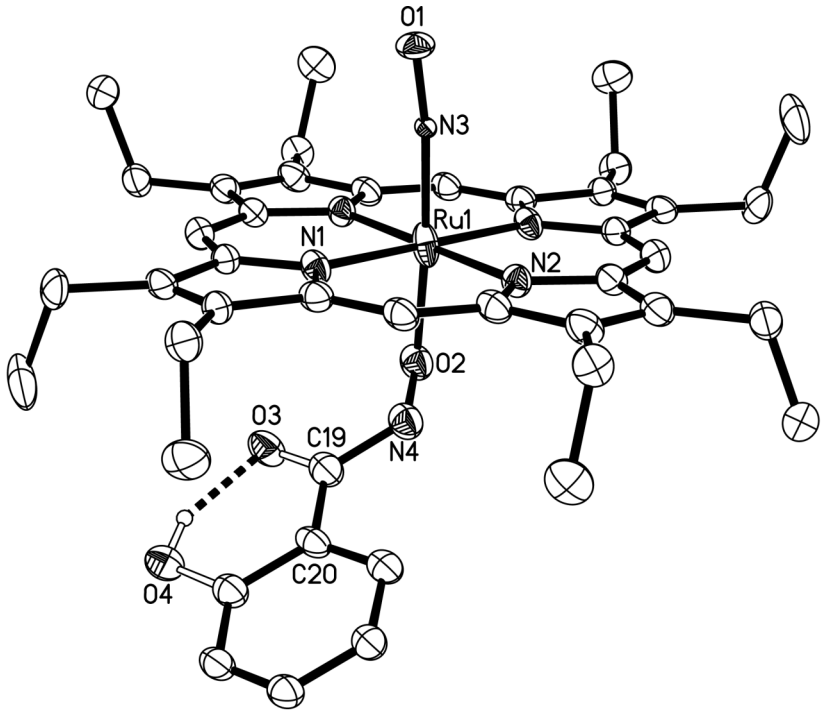

Figure 3.6. Molecular structure of (OEP)Ru(NO)(SalHate). Hydrogen atoms have been omitted for clarity (except that which is attached to O4).

Table 3.2. Selected structural data (in Å and º) for ruthenium-nitrosyl complexes containing aryloxides.

	Ru-N(O) (Å)	∠RuNO (º)	Ru-O(R) (Å)	∠RuOR (º)
(OEP)Ru(NO)(^1HO_L)	1.732(2)	177.80(8)	2.0295(17)	122.26(15)
(OEP)Ru(NO)(^2HO_L)	1.734(5)	177.03(17)	2.045(3)	124.5(3)
(OEP)Ru(NO)(SalHate)[a]	1.806(11)	171.0(9)	1.999(3)	101.3(6)

[a] Two positions of NO and alkoxide ligand observed.

The complexes showed near-linear RuNO bond angles and showed Ru–N(O) bond lengths in the range of 1.732(2) to 1.806(11) Å. Also, the aryloxide ligands on the complexes are fairly bent at the Ru–O–C linkages with the salicylhydroxamate complex having a R–O–C bond angle of 101.3(6)º as the most pronounced bend of these complexes (the ^2HO_L complex has an Ru–O–C of 124.5(3)º).

3.3.4 Cyclic Voltammetry

Cyclic voltammetry was performed on all the OEP complexes but not the TPP complexes, due to the fact that the NMR data for the (difficult to purify) TPP complexes indicated the presence of impurities even after column chromatography.

The CVs for the (OEP)Ru(NO)(OR) complexes with internal H-bonding showed similarities in their appearance. Small redox peaks appear as a shoulder (or a pre-wave) in the CV and have very little separation from the larger reversible feature. Representative examples showing the small irreversible feature before the larger reversible redox feature are given at the top of Figure 3.7 and Figure 3.8. A reduced temperature experiment (205 K) was performed on the (OEP)Ru(NO)(^2HO_L) (bottom of Figure 3.7) complex to determine if the shoulder would move to a position distinct from the larger redox feature. The reduced temperature experiment gave much greater separation as compared to room temperature experiments. It showed two well-defined oxidation features with no shoulders.

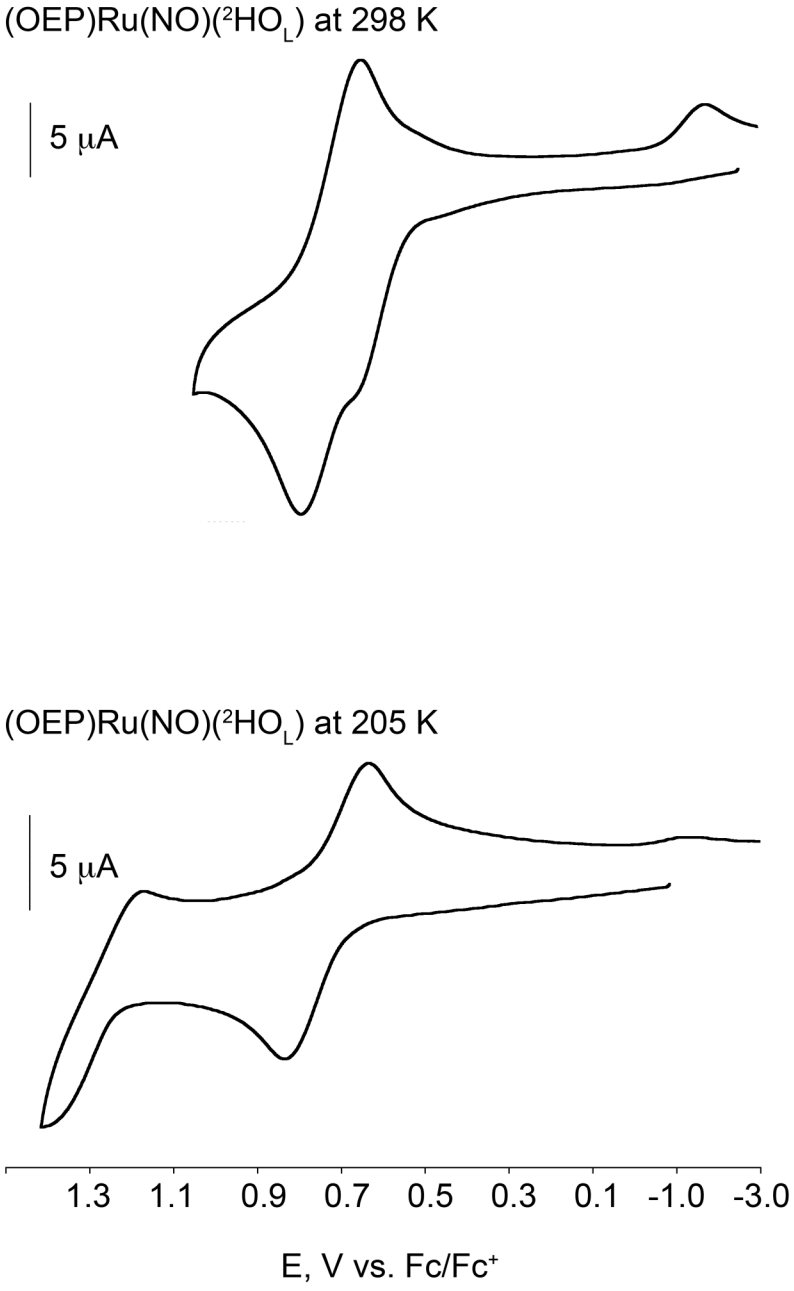

Figure 3.7. Cyclic voltammograms of (por)Ru(NO)(^{2}HO$_L$) in CH_2Cl_2 @ 200 mV/s, 1 mM analyte, 0.1 M NBu_4PF_6 at room temperature (top) and reduced temperature (bottom). Potentials are referenced against the Fc/Fc^+ couple set to 0.0 V.

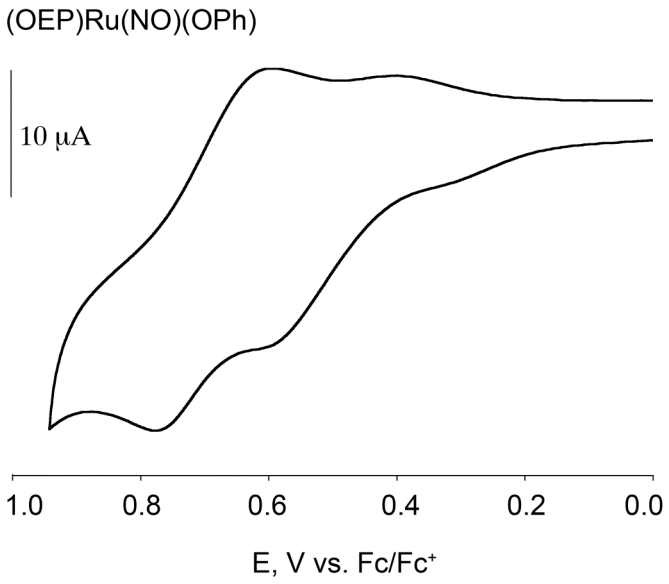

Figure 3.8. Cyclic voltammogram of (OEP)Ru(NO)(OPh) in CH_2Cl_2 @ 200 mV/s, 1 mM analyte, 0.1 M NBu_4PF_6 at room temperature. Potentials are referenced against the Fc/Fc^+ couple set to 0.0 V.

The redox potentials for the (OEP)Ru(NO)(aryloxide) complexes studied are given in

Table 3.3 below.

Table 3.3. Electrochemical data for the (OEP)Ru(NO)(OR) (OR = ^1HO_L, ^2HO_L, and SalHate, phenoxide) complexes.

	1st Oxidation	2nd Oxidation
(OEP)Ru(NO)(OPh)	0.47	0.71
(OEP)Ru(NO)(SalHate)	0.58[a]	0.72
(OEP)Ru(NO)(^1HO_L)	0.62[a]	0.71
(OEP)Ru(NO)(^2HO_L)	0.68[a]	0.72
(OEP)Ru(NO)(^2HO_L)[b]	0.64	1.22

Potentials are in volts, and are referenced to the Fc/Fc^+ couple set at 0.00 V. Analytes are 1 mM, 200 mV/s, 0.1 M NBu_4PF_6 in CH_2Cl_2.
(a) These are E_{pa} values due to irreversibility. (b) CV collected at 205 K.

Table 3.4. The peak separations ($\Delta E_p = |E_{pa} - E_{pc}|$) (V) for all (por)Ru(NO)(OR) (OR = ^1HO_L, ^2HO_L, phenoxide, and SalHate complexes in CH_2Cl_2.

	1st Oxidation	2nd Oxidation
(OEP)Ru(NO)(OPh)	0.14 (0.20)[a]	0.16 (0.20)
(OEP)Ru(NO)(SalHate)		0.17 (0.13)
(OEP)Ru(NO)(^1HO_L)		0.17 (0.16)
(OEP)Ru(NO)(^2HO_L)		0.16 (0.16)
(OEP)Ru(NO)(^2HO_L)[b]	0.25 (0.24)	0.33 (0.24)

[a]Values in ( ) are the ΔE_p for the Fc/Fc^+ couple.
[b]Measurements were taken at 205 K.

3.3.5 Infrared Spectroelectrochemistry

Infrared spectroelectrochemical investigations of the (OEP)Ru(NO)(OR) complexes were performed. While sitting at a potential near the E_{pa} for the first and second oxidation process, difference IR spectra were collected for the redox products generated. Potentials were held "near" the E_{pa} (sometimes slightly before or after) due to minimal separation of the first oxidation response from the second oxidation feature in order to obtain the oxidation product for spectral analysis. This was done in a manner similar to a former group member's analysis of manganese porphyrin complexes in order to obtain an IR spectrum for the first oxidation before any of the second oxidation product could be formed.[34]

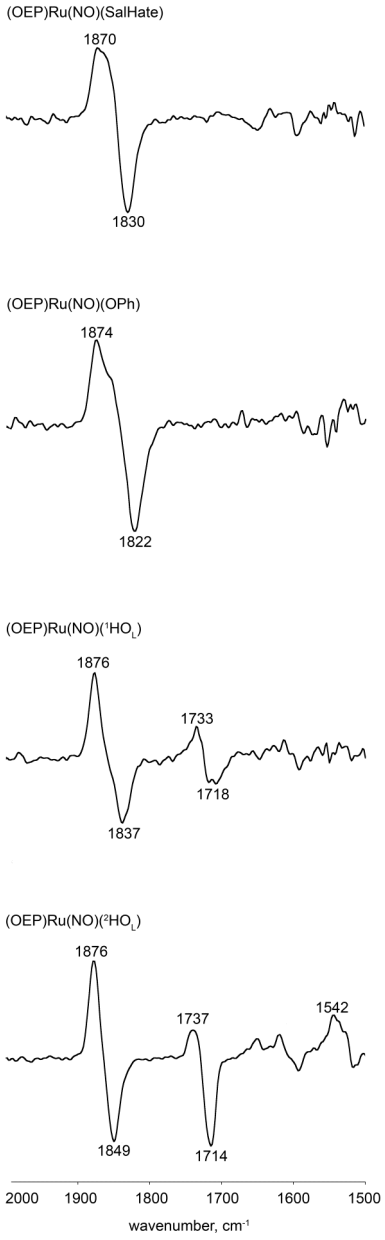

Figure 3.9. Difference IR spectra showing the products from the first oxidations of (OEP)Ru(NO)(OR) (OR = ^1HO_L, ^2HO_L, phenoxide, and SalHate compounds in CH_2Cl_2 solution containing 0.1 M NBu_4PF_6 with potentials held near their first oxidations potential.

New peaks corresponding to the ν_{NO} in the complexes were shifted approximately 40 cm^{-1} to higher values while sitting near the first and second oxidation E_{pa} for 90 seconds.

Table 3.5. The ν_{NO} values of the redox products for (por)Ru(NO)(OR) (OR = ^1HO_L, ^2HO_L, phenoxide, and SalHate) compounds containing 0.1 M NBu_4PF_6 in CH_2Cl_2.

	Neutral	1st Oxidation	2nd Oxidation
(OEP)Ru(NO)(OPh)	1822	1874 (0.59)	1874(0.81)
(OEP)Ru(NO)(SalHate)	1830	1870 (0.59)	1871 (0.83)
(OEP)Ru(NO)(^1HO_L)	1837	1876 (0.60)	1876, 1897 sh (0.81)
(OEP)Ru(NO)(^2HO_L)	1849	1876 (0.60)	1876, 1895 sh (0.95)

(sh) = shoulder

Values in ( ) are the held potentials in Volts vs. Fc/Fc^+ for the IR spectroelectrochemical investigation.

As seen in Figure 3.9, only the (OEP)Ru(NO)(^2HO_L) complex has a distinct signal at 1540 cm^{-1}, which is in the 1520 – 1570 cm^{-1} [35] region that can be assigned to the porphyrin cation radical species. When examining the difference IR spectra corresponding to the second oxidation products in Figure 3.10, we observe that all of the investigated species have a signal in the region of 1520 – 1570 cm^{-1}. This is evidence suggestive of redox process taking place on the porphyrin macrocycle.

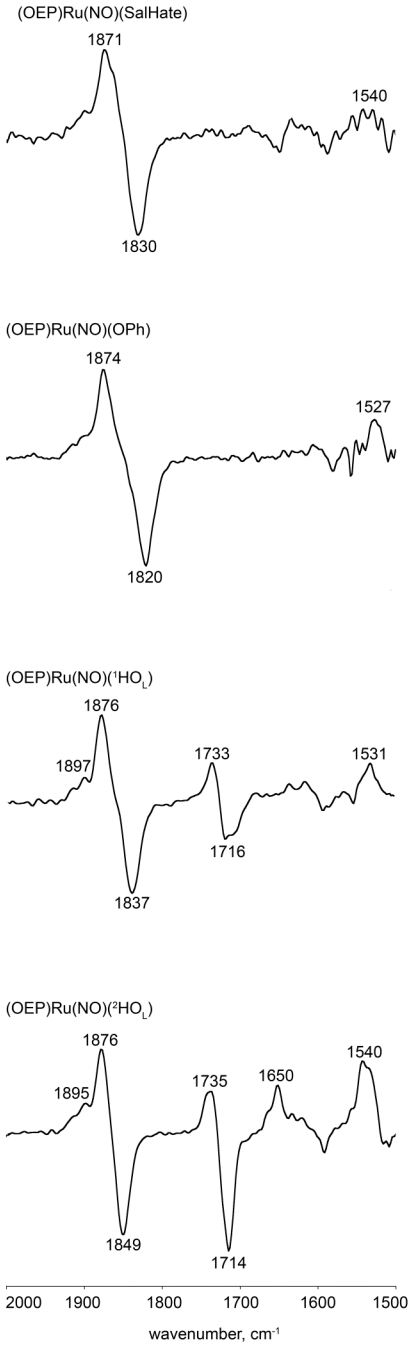

Figure 3.10. Difference IR spectra showing the results of the second oxidations of (OEP)Ru(NO)(OR) (OR = ^1HO_L, ^2HO_L, phenoxide, and SalHate) compounds in CH_2Cl_2 solution containing 0.1 M NBu_4PF_6 with potentials held near their second oxidations potential.

3.3.6 UV-vis Spectroelectrochemistry

The (OEP)Ru(NO)(OR) (OR = phenoxide, $^{1}HO_{L}$ and $^{2}HO_{L}$) complexes were examined by UV-vis spectroelectrochemistry. While sitting at potentials similar to those mentioned for the IR-spectroelectrochemical data collection, electronic absorption difference spectra were collected. The raw data, which is the last spectrum collected minus the initial spectrum collected during the application of the appropriate potential (dependent upon the analyte) over a 10 second period is provided in Figure 3.11. These spectra show a decrease due to a change in the starting complex and an increase in the 495 – 500 nm range due to the formation of the redox product in the three complexes.

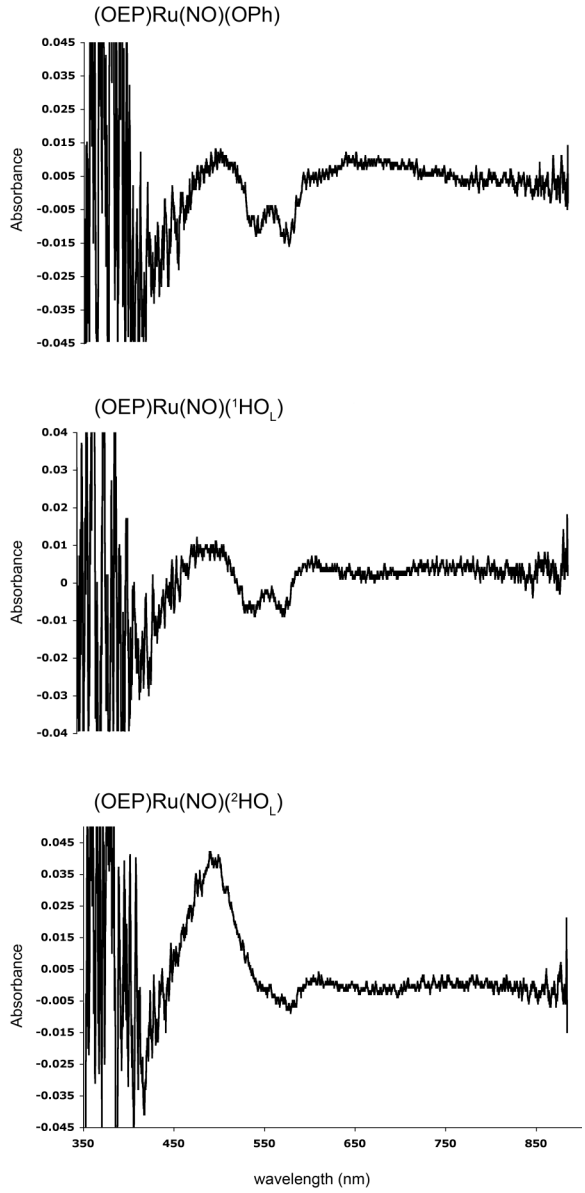

Figure 3.11. Electronic absorption difference spectra for the products formed during the first oxidations of (OEP)Ru(NO)(OR) (OR = phenoxide, $^{1}HO_{L}$, and $^{2}HO_{L}$) at the working electrode's surface over a 10 s period. Analytes are 2×10^{-4} M in 0.1 M NBu_4PF_6/CH_2Cl_2 at 298 K.

3.4 Discussion

The syntheses of other metalloporphyrin nitrosyl with alcohol or alkoxide ligands have been reported.[27,33,36-40] However, these reports do not provide any

examples of metalloporphyrin nitrosyl ***aryl***oxide complexes. In fact, the majority of these synthetic methods utilize the coordination of an alcohol followed by a deprotonation step involving a weak base such as pyridine in order to obtain the desired (por)M(NO)(OR) complexes. The method reported here involves an alcohol exchange similar to what has been reported for (por)Fe(OR) systems.[30] By starting with (por)Ru(NO)(O-*i*-C_5H_{11}) or (por)Ru(NO)(OEt) we have established a more direct route in order to obtain (por)Ru(NO)(OR) complexes by eliminating the step involving deprotonation of a coordinated alcohol. As stated before, the (por)Ru(NO)(O-*i*-C_5H_{11}) complex was preferred over the (por)Ru(NO)(OEt) complex as a precursor due to its ease of synthesis, characterization, and stability of the isoamylnitrite starting material over the ethylnitrite starting material that is needed to make the alkoxide complexes from (por)Ru(CO). However, both gave the same results when used.

The reactions were monitored by solution IR spectroscopy. The reactions were considered complete when the ν_{NO} band for the starting materials was no longer present in the spectrum and a new ν_{NO} band corresponding to the desired product was observed. For example, the ν_{NO} band for the (OEP)Ru(NO)(O-*i*-C_5H_{11}) starting material was 1795 cm^{-1} which reduced in intensity during the reaction and a ν_{NO} of 1842 cm^{-1} was observed upon the formation of the (OEP)Ru(NO)(^2HO_L) product.

Reported IR data for the (por)Ru(NO)(OR) complexes (where OR is an alkoxide ligand and not an aryloxide ligand) show ν_{NO} stretching frequencies ranging from approximately 1790 cm^{-1} to 1810 cm^{-1}.[32,33,41] This range is lower in energy than what we observe for the aryloxide complexes reported here. This is likely due to the alkoxide ligands being better electron donors to the metal center than the aryloxide ligands, (the

conjugation in the phenyl ring found in the aryloxide compounds delocalizes the electron density compared to the alkoxide groups). When the electron-rich metal center back-donates to the nitrosyl ligand, the Ru–N bond is strengthened and the N–O bond is weakened causing a lower stretching vibration for the ν_{NO} to be observed in the alkoxide complexes. This idea of a weaker N-O bond is elaborated in the trend seen within the group of aryloxide complexes and is discussed below.

The trend that we see in the IR spectra relating to the ν_{NO} bands for these complexes is consistent with the increase of internal hydrogen bonds for the complexes studied. To elaborate, if we examine the ν_{NO} values of 1821 cm^{-1}, 1837 cm^{-1}, and 1842 cm^{-1} for the (OEP)Ru(NO)(OPh), (OEP)Ru(NO)(^1HO_L), and (OEP)Ru(NO)(^2HO_L) complexes respectively, we observe that by increasing the number of internal hydrogen bonds from 0 to 1 to 2 we also increase the ν_{NO}.

Table 3.6. Nitrosyl stretching frequencies of (porphyrin)Ru(NO)(OR) complexes in CH_2Cl_2.

Compound	ν_{NO} (cm^{-1})	Reference
(OEP)Ru(NO)(OEt)	1801	[32]
(OEP)Ru(NO)(O-*i*-C_5H_{11})	1800	[33]
(TPP)Ru(NO)(O-*i*-C_5H_{11})	1809	[33]
(T(*p*-OMe)PP)Ru(O-*i*-C_5H_{11})	1808	[42]
(OEP)Ru(NO)(OPh)	1821	This work
(OEP)Ru(NO)(^1HO_L)	1837	This work
(OEP)Ru(NO)(^2HO_L)	1842	This work

The explanation for this phenomenon is that the hydrogen bond(s) is (are) interacting with the oxygen coordinated to the central ruthenium metal, thus capturing some of the oxygen's electron density instead of allowing it to be donated to the central metal. This causes the ruthenium to be less electron rich and thus cannot back-bond as efficiently with the nitrosyl ligand, which allows for a stronger N–O bond causing an increase in the ν_{NO} stretching frequency. The opposite would be expected if an electron rich metal could back-donate to the NO ligand therefore weakening the N–O bond decreasing the ν_{NO} stretching frequency. An example of an electron donating ligand that increases the electron density at the metal center thus decreasing the N–O bond strength and decreasing the ν_{NO} stretching frequency is (T(*p*-OMe)PP)Ru(NO)(Et) which has a ν_{NO} stretch at 1723 cm^{-1} in CH_2Cl_2.[43]

Ruthenium has a great advantage over iron in these studies. This being that even though they are both group 8 transition metals, ruthenium(II) porphyrin complexes are low-spin and diamagnetic making them suitable for NMR characterization as compared to iron being primarily paramagnetic. Therefore, ^{1}H NMR was very beneficial to determine the extent of completion of these reactions. In a manner similar to following the IR spectra, the ^{1}H NMR spectra were examined to see if the signals due to the precursor (por)Ru(NO)(O-*i*-C_5H_{11}) or (por)Ru(NO)(OEt) complexes were present after the reaction was assumed to be complete according to IR spectroscopic monitoring. The negative signals observed at -2.75 ppm (2H of OEt) and -3.07 ppm (3H of OEt) for (OEP)Ru(NO)(OEt) and -0.68 ppm (6H of (CH_3)$_2$), -2.81 ppm (2H, CH_2) and -3.20 ppm (2H of CH_2) for (OEP)Ru(NO)(O-*i*-C_5H_{11}) were not present after the alcohol exchange reaction was complete. Along with the disappearance of the

starting complex, new signals in the NMR spectra were also present which corresponded to the coordinated aryloxide ligands. An example of this can be described with the (OEP)Ru(NO)(^2HO_L) complex. The free ligand has NMR signals of 7.03 ppm (t, 1H, *p*-H on the phenyl ring, J = 8.4 Hz), 7.62 ppm (d, 2H, *m*-H's on the phenyl ring, J = 9 Hz), 8.32 ppm (s, 1H, O*H*), 8.66 ppm (s, 2H, N*H*) are all shifted upfield upon coordination, with the disappearance of the O*H* signal in the product spectrum. The resulting product gives values of 8.46 ppm (s (broad), 2H, N*H*), 6.46 (d, 2H in *meta*-position on ligand, J = 8 Hz) and 5.71 (t, 1H in para-position on ligand, J = 8 Hz) for the complexed ligand. It should be noted that the N*H* protons were only visible when the relaxation time was set to 10 seconds (compared to a delay of one second).

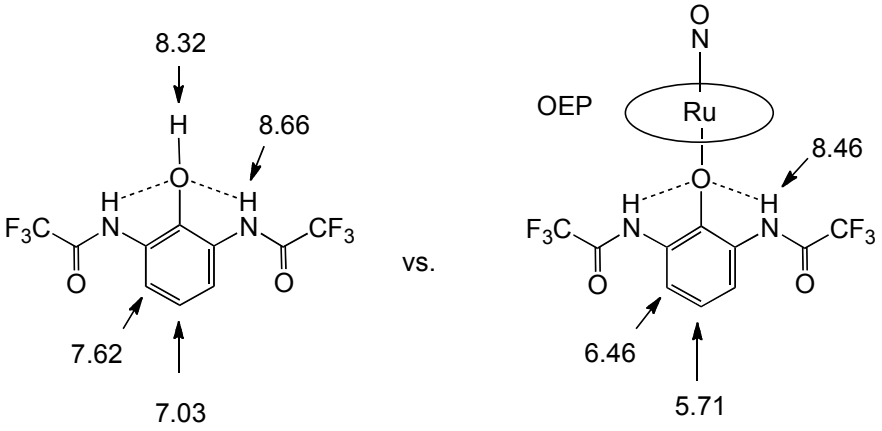

Figure 3.12. ^{1}H NMR chemical shifts (ppm) for (OEP)Ru(NO)(^2HO_L) vs. free ^2HO_L ligand.

When comparing the change in chemical shift for the coordinated ligands in (por)Ru(NO)(aryloxide) complexes, large changes are not observed as seen for those of the organometallic (por)Ru(NO)(R) complexes. For example, the complex (T(*p*-OMe)PP)Ru(NO)(Me) has a signal at -6.72 ppm due to the protons on the axial methyl group.[43] The large upfield shift of the methyl group is caused by a deshielding effect

from the porphyrin macrocycle. A deshielding effect has also been observed for (T(*p*-CF_3)PP)Ru(NO)(Me) -6.71 ppm (CH_3), (T(*p*-OMe)PP)Ru(NO)(Et) at -4.19 ppm (CH_2CH_3) and -6.00 ppm (CH_2CH_3). It has been suggested that under similar environments, the closer the H atoms are to the macrocycle, a more pronounced upfield chemical shift will be observed.[43] In the aryloxide complexes, this large upfield shift is not observed, most likely due to the protons on the phenyl ring being located further away from the porphyrin macrocycle. Also, the Ru–O bond allows for additional distance from the macrocycle compared to the organometallic complexes where the protons are in a much closer proximity to the macrocycle. Therefore, we are only seeing a small change in chemical shift as compared to the organometallic complexes.

Mass spectrometry ($ESI^{+/-}$) was also used for the characterization of these complexes. Unfortunately, peaks corresponding to the parent complexes were not observed in contrast to that the reported (OEP)Ru(NO)(OMe) complex, which gave a peak at *m/z* 695 (61%, $(OEP)Ru(NO)(OMe)^+$) along with the $(OEP)Ru(NO)^+$ fragment at *m/z* 664.[36] Due to the fact that the parent complex was not observed in the ESI^+, it was thought that the use of ESI^- could be used in order to identify the ligand if it was dissociating during ionization. This is what was observed. For example, the (OEP)Ru(NO)(^2HO_L) complex gave a *m*/*z* peak of 315.0 (100%) in the ESI^- spectrum. The ligand (HO-2,6-$(NHC(=O)CF_3)_2$-C_6H_3) has a mass of 316.2, however, the deprotonated ligand has a mass of 315.0, which is what is seen in the ESI^- spectrum. Therefore, the significant data that was collected from the mass spectrometry analysis is that a $(por)Ru(NO)^+$ complex was present in the ESI^+ and a signal corresponding to the appropriate ligand was seen in the ESI^-.

It is understood that the observed mass spectrometry data alone is not sufficient enough to prove that the target complexes were obtained. Such possibilities of having uncoordinated ligand in solution that could show up in the ESI^- spectra and other porphyrin complexes be they unreacted starting materials, dimers, (por)Ru(NO)(Cl), or other ruthenium porphyrin compounds have to be considered. Unreacted porphyrin complexes or signals due to the precursor isoamyl or ethoxide materials were not observed in any of the data collected. The collected data was consistent with other (por)Ru(NO)(L) complexes reported in the literature which showed similar fragmentation.[44] The use of the mass spectrometry, playing a supporting role to the IR and ^1H NMR data, was helpful in order to characterize these (por)Ru(NO)(OR) complexes even without definitive evidence of the parent complexes.

The structural data collected for the (por)Ru(NO)(aryloxide) complexes is given in section 3.3.3. When comparing them to reported crystal structures of known (por)Ru(NO)(alkoxide) complexes, we note that the structural parameters of the new (por)Ru(NO)(aryloxide) complexes are within the reported values. For example, Table 3.7 gives selected bond lengths and angles for known (por)Ru(NO)(alkoxide) complexes. When comparing these values to the those for the (por)Ru(NO)(aryloxide) in Table 3.2, we see that the values are quite similar for all of these $\{Ru(NO)\}^6$ complexes. The Ru-N(O) and Ru-O(R) bond lengths (Å) for the new complexes (1.732(2) – 1.806(11)) fall in the range of 1.708(6) – 1.84(4) for the reported complexes. The ∠RuNO bond angles (171.0(9) – 177.80(8)) are also similar to the values of the complexes found in the literature (170.2(11) – 180.0). The ∠RuNO bond angles are also consistent with other known $\{Ru(NO)\}^6$ complexes that are not alkoxide

complexes.[45] When comparing the RuNO bond angles of these new synthetic porphyrin complexes to that determined from the known protein structure of a NO bound catalase,[22] it is apparent that the synthetic complexes have more linear metal-NO units than the enzyme. The enzyme structure had a slightly bent NO with respect to the heme of ~160º. However, the authors stressed caution when making this assignment because they also observed a bending angle ranging from 175º to 160º depending on the restraints that were used for the structural refinement.[22] Therefore, it is difficult to say if NO binds to the enzyme in a true bent fashion or if it is linear as seen in the synthetic models.

The only difference between the known (por)Ru(NO)(alkoxide) complexes and the (por)Ru(NO)(*aryl*oxide) complexes in the structural data comes from the ∠RuOR bond angles. The (por)Ru(NO)(alkoxide) complexes have reported bond angles ranging from 133.853 – 143.8(5)º shown in Table 3.7. This is different from the 122.26(15) and 124.5(3)º seen in the (OEP)Ru(NO)(^1HO_L) and (OEP)Ru(NO)(^2HO_L) complexes. The only complexes with similarities for the ∠MOR bond angles are found in osmium complexes. (OEP)Os(NO)(O-*n*-Bu)[46] and (OEP)Os(NO)(OEt)[38] give ∠OsOR bond angles of 130.8(9)º and 123.7(15)º respectively. Therefore, the ∠RuOR bond angles for the (OEP)Ru(NO)(^1HO_L) and (OEP)Ru(NO)(^2HO_L) complexes appear to be the smallest known thus far. It is difficult to say exactly what is causing this increased angle. There are two oxygen lone pairs that are nondegenerate on the alkoxide ligand. According to Malcom Chisholm's review article on alkoxides and aryloxides,[47] he described one of these lone pairs as the pπ orbital while the other is an sp lone pair. As the M-O-C angle becomes more linear, the O_{sp}^2 lone pair becomes equivalent, albeit

perpendicular to the other Op_{π} orbital. He states that as a general rule, M–O distances decrease as M–O–C angles increase, which implies increased RO to M donation. Also, it is common to find shorter M–O distances (by a few hundredths of an angstrom) for M–OR groups that have M–O–C angles approaching 180º.[47] This generalization seems to explain the small Ru–O–C bond angles in the $^{1}HO_{L}$ and $^{2}HO_{L}$ complexes because they both possess longer Ru-O bond lengths as compared to the known (POR)Ru(NO)(OR) complexes provided in Table 3.7 below

A structural comparison of the (OEP)Ru(NO)(sal) complex cannot be included with the (OEP)Ru(NO)($^{1}HO_{L}$) and (OEP)Ru(NO)($^{2}HO_{L}$) complexes. The reason for this is that the salicylhydroxamate is not bound in a true "aryloxide" mode. Instead, it is coordinated to the metal through the hydroxyl group in the hydroxamate moiety with a Ru-O-N coordination mode instead of the Ru-O-C coordination that is observed in the rest of the aryloxide complexes (see Figure 3.6).

Table 3.7. Selected structural data (in Å and º) for ruthenium-nitrosyl complexes containing *O*-donors as axial ligands reported from 1999 – 2011.

	Ru-N(O) (Å)	∠RuNO (º)	Ru-O(R) (Å)	∠RuOR (º)	Ref
(TPP)Ru(NO)(OMe)	1.84(4)	180.0	1.80(5)	137.7(31)	40
[(OEP)Ru(NO){O=C(Me)NHCH$_2$C(Me)$_2$SH}]BF$_4$	1.708(6)	177.8(5)	2.049(4)	143.8(5)	48
(OEP)Ru(NO)(O-*i*-C$_5$H$_{11}$)[a]	1.780(10)	170.2(11) 137(3)	1.908(11)	133.853	41,42

[a]Two positions of NO ligand observed

The cyclic voltammetric data collected in this study shows similar results for all of the (OEP)Ru(NO)(aryloxide) complexes studied. As shown above in Figure 3.7, it is seen that at room temperatures, the complexes with internal H-bonding have an

irreversible first oxidation feature (referred to as a shoulder) that is followed by a reversible second oxidation feature at a scan rate of 200 mV/s under the conditions used for these experiments. A graph of (scan rate)$^{1/2}$ vs. i_{pa} for the first oxidation of these complexes gives a straight line, indicating that the processes are diffusion controlled. While scanning from 50 – 200 mV/s, the first shoulders do not show return responses; however, faster scan rates do show an increase in return peaks of the first oxidation response and diminishing second oxidation response (see Figure 3.13).

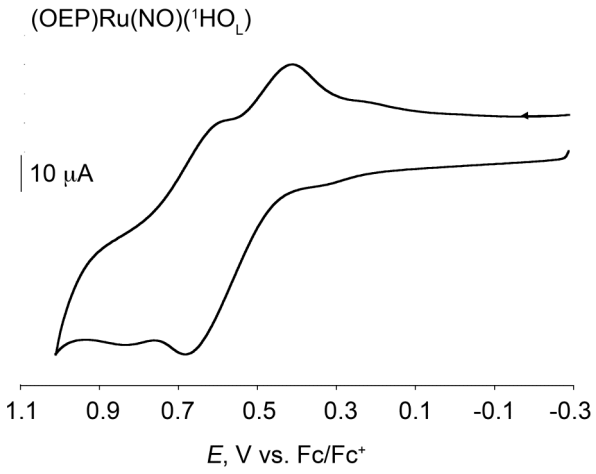

Figure 3.13. Cyclic voltammograms of (OEP)Ru(NO)(^{1}HO$_L$) in CH_2Cl_2 @ 3200 mV/s, 1 mM analyte, 0.1 M NBu_4PF_6 at room temperature. Potentials are referenced against the Fc/Fc$^+$ couple set to 0.0 V.

The first oxidation being observed could lead to a chemical change. This could suggest an oxidation that is followed up by a fast chemical reaction. The fact that there are ionizable protons on all of these complexes complicates the electrochemistry of these systems. Equations 3.1 – 3.3 give a proposed explanation of the electrochemical process of these complexes.

$$E^o(\text{HA}) \qquad \text{HA} \quad \leftrightarrows \quad \text{HA}^+ + \text{e}^- \qquad (3.1)$$

$$HA^{+} \leftrightarrows H^{+} + A \qquad (3.2)$$

$$E^{o}(A) \quad A \leftrightarrows A^{+} + e^{-} \qquad (3.3)$$

By examining the CVs that were obtained for these complexes, it appears that we are dealing with an ECE system, where we have an electrochemical process followed by a chemical change and an additional electrochemical response. During slow scans, the complex is presumed to undergo an oxidation to give a cationic species and loss of electron as shown in equation 3.1, this new cationic species with ionizable protons can be thought of as an acid that can give up a proton (chemical change) after oxidation has occurred, which is reversible if the pKa is large enough to keep the equilibrium of equation 3.2 to the right. The now formed neutral product after the proton loss has a redox process that is reversible during these slow scan experiments giving a redox response explained by equation 3.3. During faster scanning experiments (> 200 mV/s), it is possible that the process in equation 3.1 outraces the proton loss step of equation 3.2 giving a more electrochemically reversible process and loss of the second oxidation response from equation 3.3 that was observed in the CVs.

One more process that should be considered is the idea of the aryloxide ligand dissociating from the metal during oxidation. This is outlined in equations 3.4 and 3.5 below.

$$E^{o}1 \quad e^{-} + (por)Ru(NO)(OR) \rightarrow [(por)Ru(NO)]^{+} + (OR)^{-} \qquad (3.4)$$

$$E^{o}2 \quad [(por)Ru(NO)]^{+} \leftrightarrows [(por)Ru(NO)]^{2+} + e^{-} \qquad (3.5)$$

If this was the result occurring in these complexes, we could expect to see similar oxidation potentials for all of the complexes' second oxidations. It would also give similar ν_{NO} stretching frequencies in the IR spectroelectrochemical experiments. The idea of the ligand decomposition will be considered below with the discussion regarding the IR spectroelectrochemical data.

When (OEP)Ru(NO)(^2HO_L) was cooled to 205 K, we saw two reversible redox couples. The reduced temperature experiment slows down the chemical process. Further decomposition that might be taking place after the first oxidation is minimized at colder temperatures. The cathodic to anodic peak current ratio (i_{pc}/i_{pa}) of the first oxidation is 0.6 at 200 mV/s, and is unity at higher scan rates, compared to ferrocene's (i_{pc}/i_{pa}) of 0.7 at 200 mV/s which also becomes unity at higher scan rates. This suggests that the first oxidation of the (OEP)Ru(NO)(^2HO_L) complex is chemically reversible at reduced temperatures.

The (OEP)Ru(NO)(OPh) complex appears to have a reversible first oxidation at first glance of the CV when scanning at 200 mV/s. However, when comparing its cathodic to anodic peak current ratio (i_{pc}/i_{pa}) of 0.2 to that of ferrocene's (0.9) under the same conditions, it is apparent that the first oxidation is not chemically reversible. All of the complexes show an increase in reversibility of the first oxidation with faster scan rates, which is accompanied by a decrease in reversibility of the second oxidation couple (Figure 3.13).

The fact that the second oxidations are taking place at very similar potentials suggests that the redox products for these complexes are very similar. One possibility is that trace water in the electrochemical cell is coordinating to the ruthenium metal once

the aryloxide leaves forming the $[(OEP)Ru(NO)(H_2O)]^+$ complex. However, attempts were taken to minimize any water that could be present in the electrochemical apparatus such as using supporting electrolyte that was dried in an oven overnight at 100 ºC, using freshly collected methylene chloride that was dried and stored over molecular sieves, and assembling all glassware under a nitrogen gas atmosphere after it was removed from a 110 ºC oven where it was dried overnight. Also, the formation of the water complex was proven to not be the redox product because it was synthesized according to literature methods[44] and characterized by UV-vis, which showed two bands in the visible region at 515 nm and 547 nm. These bands observed for the water complex are different than the bands observed for the oxidation products of the three (OEP)Ru(NO)(aryloxide) complexes being analyzed, which had new bands in the 495 – 500 nm range.

A trend that is apparent from the CV data is that by increasing the number of internal H-bonds, the potential needed for the first oxidation is increased. While comparing the first oxidation potentials from Table 3.3, we see that the phenoxide complex with zero internal H-bonds has a potential of 0.47 V, compared to 0.62 and 0.68 V for the ^1HO_L, and ^2HO_L complexes respectively. This is similar to the trend seen in the ν_{NO} stretching frequency for the IR data. The first oxidation potential of (OEP)Ru(NO)(OEt) is 0.43 V vs. Fc/Fc^+. This alkoxide ligand is a better electron donor than the aryloxide complexes due to the aryloxides being able to delocalize their electron density in the phenyl ring. Therefore, the electron donating ability of the ligand is having an effect on the potential of the first oxidation.

The difference IR spectra which shows the product formation after the first oxidations of the (OEP)Ru(NO)(aryloxide) complexes is presented in Figure 3.9. The electrochemically generated products of the oxidations have ν_{NO} bands ranging from 1870 to 1876 cm^{-1}, which are shifted approximately 30 – 50 cm^{-1} more positive than the starting compounds. The ^1HO_L and ^2HO_L complexes appear to decompose during oxidation. This is supported by the presence of ν_{CO} bands that shift to higher frequencies by 15 cm^{-1} to 1733 cm^{-1} (^1HO_L) and 20 cm^{-1} to 1737 cm^{-1} (^2HO_L) during oxidation are similar to the free ligands' ν_{CO} bands (~1734 cm^{-1}) which are observed after oxidation took place. The (por)Ru(NO)(OPh) and (por)Ru(NO)(Sal) complexes do not have a carbonyl moiety that can be followed during the spectroelectrochemical experiments. The lack of observed IR bands (except for the ^2HO_L complex) in the 1530 – 1550 cm^{-1} range which are normally indicative of a porphyrin π-cation radical for the complexes during IR spectroelectrochemical experiments suggest that the first oxidation is not porphyrin centered. There are several redox sites on these complexes such as the metal center, porphyrin ring, NO ligand, and aryloxide ligand. Because we are not observing a large shift in the ν_{NO}, or a band due to the π-cation radical, it is difficult to say exactly where the site of the first oxidation is taking place. However, since we observe the loss of the aryloxide ligand during oxidation, we can assume that the first oxidation is taking place somewhere along the axis consisting of the (NO)Ru(OR) moiety. It is clear that the π-cation radical is being formed in all of the complexes during the second oxidation. The reason that the π-cation radical is observed during the first oxidation in the ^2HO_L complex is that there is very little peak separation at room temperature between the first and second oxidations in the CV. Therefore, the second

oxidation product could be appearing (generated) at the applied potential of the first oxidation.

In order to have a better understanding of the site of oxidation during these oxidation responses, the simultaneous chronoabsorptivity/chronoamperometry (SCC) technique, which was used in Chapter 2 (this dissertation), was attempted. However, the electrochemical systems that we are studying with the (OEP)Ru(NO)(aryloxide) complexes appear to undergo an ECE mechanism. The capabilities of the SCC technique do not extend to this type of mechanism. Therefore, only the raw difference spectral data can be used from these experiments. The potentials that were applied for the analysis of each of the oxidations are similar to those of the IR spectroelectrochemical study.

The UV-vis data gave difference spectra for the phenoxide, $^{1}HO_{L}$, and $^{2}HO_{L}$ complexes with new features in the 495 – 500 nm range. This is not the accepted range of the π-cation radical, which typically has a broad intensity of 500 – 700 nm in the electronic absorption spectrum.[49-51] There are less intense features in the 600 – 650 range of these complexes during the first oxidations that are reproducible from numerous attempts. The difference spectra used for analysis do not indicate a specific spectral feature that can be assigned to the formation of the π-cation radical during the first oxidation of these complexes. This further supports the idea that the first oxidation is taking place on the axial (NO)Ru(OR) moiety.

Even though the UV-vis data does not specify the site of oxidation for these complexes, the IR spectroelectrochemical data provides very compelling evidence that the first oxidation results in decomposition. This data along with the fact that we see a

very similar second oxidation potential for all of the species at 0.71 – 0.72 V indicates that we are forming an identical redox product, most likely a $[(OEP)Ru(NO)]PF_6$ species. This is not hard to imagine because the aryloxide is not as strong of an electron donor and may not be as tightly bound as a complex such as (T(*p*-OMe)PP)Ru(NO)(Me) which has two chemically and electrochemically reversible oxidations.[43]

An attempt to do a chemical oxidation of the $(OEP)Ru(NO)(^2HO_L)$ complex with $AgPF_6$ provided an IR spectrum with a new ν_{NO} band of 1875 cm^{-1}, which is consistent with the IR spectroelectrochemical investigation. An X-ray quality crystal was obtained from this reaction, and the resulting structure was that of the dimerized ligand, which formed a new C-C bond leaving the hydroxyl oxygens in the *para* position shown in Figure 3.14. It is difficult to say if this was the product formed from the chemical oxidation, or if this was a minor impurity in the starting material not observed in the ^{1}NMR of the ligand, which happened to crystallize from the reaction mixture. The crystals formed appeared to be uniform in appearance, i.e. there was not a mixture of varying colored material. The goal of the current efforts is to obtain an X-ray crystal structure of the product after oxidation of the (por)Ru(NO)(aryloxide) complex.

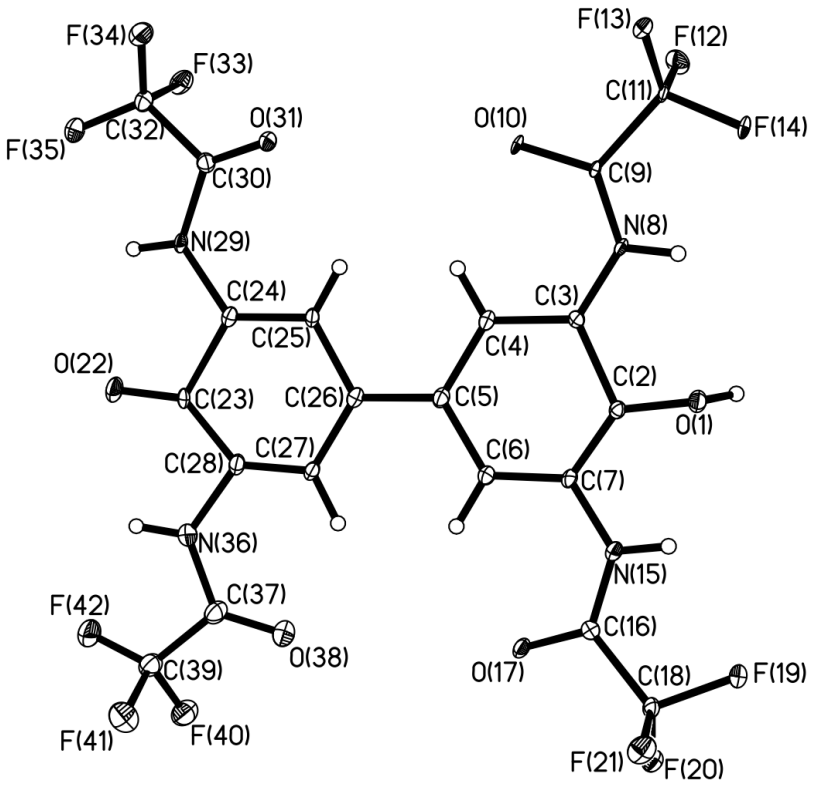

Figure 3.14. Molecular structure of possible product from the chemical oxidation of (OEP)Ru(NO)(^2HO_L) with $AgPF_6$ in CH_2Cl_2.

It should be noted that Dr. Nan Xu, a postdoc from our group, did obtain a similar structure to that seen in Figure 3.14, while working with the same ^2HO_L ligand but instead with iron porphyrins (unpublished results). His structure showed the ligand in Figure 3.14 bridging two iron porphyrins.

3.5 Conclusion

The (por)Ru(NO)(aryloxide) complexes that have been synthesized constitute a new class of compounds that has not been reported. These metalloporphyrin nitrosyl complexes appear to be very good structural models for NO inhibited catalase due to their varying degrees of internal hydrogen bonding. The infrared and solid-state structure characteristics of these new complexes are typical of diamagnetic $\{MNO\}^6$

complexes seen in the literature. To elaborate, the ν_{NO} stretch for these complexes increases with increasing internal hydrogen bonds. This is most likely due to a decrease of electron density at the ruthenium causing a decrease in back-bonding resulting in an increased N–O stretching frequency.

The redox properties observed for these new complexes show that with an increasing number of internal hydrogen bonds, the potential for the first oxidation response also increases. It is unclear where the first oxidation is taking place on the complex by examining the difference IR spectra generated during spectroelectrochemical studies, but it is apparent that a π-cation radical is present during the second oxidation. The use of UV-vis spectroelectrochemistry shows that new features appear in the visible region for the first oxidation products near 495 – 500 nm for all of the complexes investigated, but do not show conclusive evidence of a π-cation radical species which can typically be identified by broad features in the 600 – 700 nm region of the electronic spectra. Attempts at identifying the redox product through chemical oxidations with $AgPF_6$ did not give definitive results. This is an area that needs to be explored further. These ruthenium complexes show a great advantage over unstable iron-nitrosyl models of biological heme prosthetic groups by showing high stability in inert and normal atmospheres. Thus, these derivatives provide an appealing alternative to iron containing models of proteins with metal bound tyrosinate.

3.6 References

(1) Richter-Addo, G. B.; Legzdins, P. *Metal Nitrosyls*; Oxford University Press: New York, 1992.

(2) Richter-Addo, G. B.; Legzdins, P.; Burstyn, J. Introduction: Nitric oxide chemistry, *Chemical Reviews* **2002**, *102*, 857.

(3) Hibbs, J. B.; Vavrin, Z.; Taintor, R. R. L-Arginine Is Required for Expression of the Activated Macrophage Effector Mechanism Causing Selective Metabolic Inhibition in Target-Cells, *Journal of Immunology* **1987**, *138*, 550.
(4) Moncada, S.; Palmer, R. M. J.; Higgs, E. A. Biosynthesis of Nitric-Oxide from L-Arginine - a Pathway for the Regulation of Cell-Function and Communication, *Biochemical Pharmacology* **1989**, *38*, 1709.
(5) Bult, H.; Boeckxstaens, G. E.; Pelckmans, P. A.; Jordaens, F. H.; Vanmaercke, Y. M.; Herman, A. G. Nitric-Oxide as an Inhibitory Nonadrenergic Noncholinergic Neurotransmitter, *Nature* **1990**, *345*, 346.
(6) Shibuki, K.; Okada, D. Endogenous Nitric-Oxide Release Required for Long-Term Synaptic Depression in the Cerebellum, *Nature* **1991**, *349*, 326.
(7) Bredt, D. S.; Hwang, P. M.; Glatt, C. E.; Lowenstein, C.; Reed, R. R.; Snyder, S. H. Cloned and Expressed Nitric-Oxide Synthase Structurally Resembles Cytochrome-P-450 Reductase, *Nature* **1991**, *351*, 714.
(8) Heck, D. E.; Laskin, D. L.; Gardner, C. R.; Laskin, J. D. Epidermal Growth-Factor Suppresses Nitric-Oxide and Hydrogen-Peroxide Production by Keratinocytes - Potential Role for Nitric-Oxide in the Regulation of Wound-Healing, *The Journal of Biological Chemistry* **1992**, *267*, 21277.
(9) Ford, P. C.; Lorkovic, I. M. Mechanistic Aspects of the Reactions of Nitric Oxide with Transition-Metal Complexes, *Chemical Reviews* **2002**, *102*, 993.
(10) Stamler, J. S.; Lamas, S.; Fang, F. C. Nitrosylation: The Prototypic Redox-Based Signaling Mechanism, *Cell* **2001**, *106*, 675.
(11) Brown, G. C. Reversible Binding and Inhibition of Catalase by Nitric-Oxide, *European Journal of Biochemistry* **1995**, *232*, 188.
(12) Mate´, M. J.; Murshudov, G.; Bravo, J.; Melik-Adamy, W.; Loewen, P. C.; Fita, I. *Handbook of Metalloproteins*; Messerschmidt, A., Huber, R., Poulos, T., Weighard, K., Eds.; John Wiley & Sons: New York; Vol. 1, p 486
(13) Andersson, L. A.; Dawson, J. H. EXAFS Spectroscopy of Heme-Containing Oxygenases and Peroxidases, *Structure and Bonding* **1991**, *74*, 1.
(14) Murthy, M. R. N.; Reid, T. J.; Sicignano, A.; Tanaka, N.; Rossmann, M. G. Structure of Beef-Liver Catalase, *Journal of Molecular Biology* **1981**, *152*, 465.
(15) Reid, T. J.; Murthy, M. R. N.; Sicignano, A.; Tanaka, N.; Musick, W. D. L.; Rossmann, M. G. Structure and Heme Environment of Beef-Liver Catalase at 2.5 Å Resolution, *Proceedings of the National Academy of Science-Biology* **1981**, *78*, 4767.
(16) Ko, T. P.; Day, J.; Malkin, A. J.; McPherson, A. Structure of Orthorhombic Crystals of Beef Liver Catalase, *Acta Crystallographica D* **1999**, *55*, 1383.
(17) Tanford, C.; Lovrien, R. Dissociation of Catalase into Subunits, *Journal of the American Chemical Society* **1962**, *84*, 1892.
(18) Torii, K.; Iizuka, T.; Ogura, Y. Magnetic Susceptibility and EPR Measurements of Catalase and its Derivatives. Thermal Equilibrium Between the High- and Low-Spin States in the Catalase-Azide compound, *Journal of Biochemistry* **1970**, *68*, 837.
(19) Stern, K. G. The Constitution of the Prosthetic Group of Catalase, *Journal of Biological Chemistry* **1936**, *112*, 661.

(20) Schroeder, W. A.; Shelton, J. R.; Shelton, J. B.; Robberson, B.; Apell, G.; Fang, R. S.; Bonaventura, J. The Complete Amino-Acid-Sequence of Bovine Liver Catalase and the Partial Sequence of Bovine Erythrocyte Catalase, *Archives of Biochemistry and Biophysics* **1982**, *214*, 397.
(21) Putnam, C. D.; Arvai, A. S.; Bourne, Y.; Tainer, J. A. Active and Inhibited Human Catalase Structures: Ligand and NADPH Binding and Catalytic Mechanism, *Journal of Molecular Biology* **2000**, *296*, 295.
(22) Purwar, N.; McGarry, J. M.; Kostera, J.; Pacheco, A. A.; Schmidt, M. Interaction of Nitric Oxide with Catalase: Structural and Kinetic Analysis, *Biochemistry* **2011**, *50*, 4491.
(23) Gaudin, C. F. M.; Grigg, J. C.; Arrieta, A. L.; Murphy, M. E. P. Unique Heme-Iron Coordination by the Hemoglobin Receptor IsdB of Staphylococcus Aureus, *Biochemistry* **2011**, *50*, 5443.
(24) Fita, I.; Rossmann, M. G. The Active-Center of Catalase, *Journal of Molecular Biology* **1985**, *185*, 21.
(25) Seok, W. K.; Kim, M. Y. Spectrosopic Study of a Series of Para-Substituted Tetraphenylporphine Carbonyl Complexes of Ruthenium(II) Containing Nitrogenous Bases, *Bulletin of the Korean Chemical Society* **1995**, *16*, 1239.
(26) Adler, A. D.; Longo, F. R.; Finarelli, J. D.; Goldmacher, J.; Assour, J.; Korsakoff, L. A Simplified Synthesis for Meso-Tetraphenylporphine, *Journal of Organic Chemistry* **1967**, *32*, 476.
(27) Rillema, D. P.; Nagle, J. K.; Barringer, L. F.; Meyer, T. J. Redox Properties of Metalloporphyrin Excited-States, Lifetimes, and Related Properties of a Series of Para-Substituted Tetraphenylporphine Carbonyl-Complexes of Ruthenium(II), *Journal of the American Chemical Society* **1981**, *103*, 56.
(28) Ueyama, N.; Nishikawa, N.; Yamada, Y.; Okamura, T.-A.; Nakamura, A. Structure and Properties of Tetraphenylporphinate Iron(III) Complexes with an Intramolecular NH...S Benzenethiolate or NH...O Phenolate Hydrogen Bond, *Inorganica Chimica Acta* **1998**, *283*, 91.
(29) Ueyama, N.; Nishikawa, N.; Yamada, Y.; Okamura, T.; Oka, S.; Sakurai, H.; Nakamura, A. Synthesis and Properties of Octaethylporphinato(arenethiolato)iron(III) Complexes with Intramolecular NH…S Hydrogen Bond: Chemical Function of the Hydrogen Bond, *Inorganic Chemistry* **1998**, *37*, 2415.
(30) Shaffer, C. D.; Straub, D. K. The Synthesis and Spectral Properties of Hemins Derived from Tetra(*p*-tolyl)porphyrin, *Inorganica Chimica Acta* **1989**, *158*, 167.
(31) Enemark, J. H.; Feltham, R. D. Principles of Structure, Bonding, and Reactivity for Metal Nitrosyl Complexes, *Coordination Chemistry Reviews* **1974**, *13*, 339.
(32) Carter, S. M.; Lee, J.; Hixson, C. A.; Powell, D. R.; Wheeler, R. A.; Shaw, M. J.; Richter-Addo, G. B. Fiber-Optic Infrared Reflectance Spectroelectrochemical Studies of Osmium and Ruthenium Nitrosyl Porphyrins Containing Alkoxide and Thiolate Ligands, *Dalton Transactions* **2006**, 1338.
(33) Lee, J.; Yi, G.-B.; Khan, M. A.; Richter-Addo, G. B. Synthesis and Characterization of Thiolate-Thiol Complexes of Ruthenium Nitrosyl Porphyrins and Their Symmetrical and Unsymmetrical Dithiolate-Bridged Bimetallic Derivatives, *Inorganic Chemistry* **1999**, *38*, 4578.

(34) Zahran, Z. N.; Shaw, M. J.; Khan, M. A.; Richter-Addo, G. B. Fiber-Optic Infrared Spectroelectrochemical Studies of Six-Coordinate Manganese Nitrosyl Porphyrins in Nonaqueous Media, *Inorganic Chemistry* **2006**, *45*, 2661.
(35) Shimomura, E. T.; Phillippi, M. A.; Goff, H. M.; Scholz, W. F.; Reed, C. A. Infrared-Spectroscopy of Oxidized Metalloporphyrins - Detection of a Band Diagnostic of Porphyrin-Centered Oxidation, *Journal of the American Chemical Society* **1981**, *103*, 6778.
(36) Antipas, A.; Buchler, J. W.; Gouterman, M.; Smith, P. D. Porphyrins. 36. Synthesis and Optical and Electronic Properties of Some Ruthenium and Osmium Octaethylporphyrins, *Journal of the American Chemical Society* **1978**, *100*, 3015.
(37) Yi, G.-B.; Chen, L.; Khan, M. A.; Richter-Addo, G. B. Activation of Thionitrites and Isoamyl Nitrite by Group 8 Metalloporphyrins and the Subsequent Generation of Nitrosyl Thiolates and Alkoxides of Ruthenium and Osmium Porphyrins, *Inorganic Chemistry* **1997**, *36*, 3876.
(38) Cheng, L.; Powell, D. R.; Khan, M. A.; Richter-Addo, G. B. Synthesis, Characterization, Solid-State Molecular Structures, and Deprotonation Reactions of Cationic Alcohol Complexes of Osmium Nitrosyl Porphyrins, *Inorganic Chemistry* **2001**, *40*, 125.
(39) Bohle, D. S.; Hung, C.-H.; Smith, B. D. Synthesis and Axial Ligand Substitution Chemistry of Ru(TTP)(NO)X. Structures of Ru(TTP)(NO)X (X = ONO, OH), *Inorganic Chemistry* **1998**, *37*, 5798.
(40) Bohle, D. S.; Goodson, P. A.; Smith, B. D. Synthesis, structure and ligand exchange reactions of Ru(TTP)(NO)(OMe), *Polyhedron* **1996**, *15*, 3147.
(41) Fomitchev, D. V.; Coppens, P.; Li, T.; Bagley, K. A.; Chen, L.; Richter-Addo, G. B. Photo-Induced Metastable Linkage Isomers of Ruthenium Nitrosyl Porphyrins, *Chemical Communications* **1999**, 2013.
(42) Carter, S. M. Dissertation, University of Oklahoma, 2006.
(43) Xu, N.; Lilly, J.; Powell, D. R.; Richter-Addo, G. B. Synthesis, Characterization, and Infrared Reflectance Spectroelectrochemistry of Organoruthenium Nitrosyl Porphyrins, *Organometallics* **2012**, *31*, 827.
(44) Chen, L.; Yi, G.-B.; Wang, L.-S.; Dharmawardana, U. R.; Dart, A. C.; Khan, M. A.; Richter-Addo, G. B. Synthesis, Characterization, and Molecular Structures of Diethylnitrosamine Metalloporphyrin Complexes of Iron, Ruthenium, and Osmium, *Inorganic Chemistry* **1998**, *37*, 4677.
(45) Richter-Addo, G. B.; Wheeler, R. A.; Hixson, C. A.; Chen, L.; Khan, M. A.; Ellison, M. K.; Schulz, C. E.; Scheidt, W. R. Unexpected Nitrosyl-Group Bending in Six-Coordinate $\{M(NO)\}^6$ σ-Bonded Aryl(iron) and -(ruthenium) Porphyrins, *Jouranal of the American Chemical Society* **2001**, *123*, 6314.
(46) Chen, L.; Khan, M. A.; Richter-Addo, G. B. Nitrosylation of Octaethylporphyrin Osmium Complexes with Alkyl Nitrites and Thionitrites: Molecular Structures of Three Osmium Porphyrin Derivatives, *Inorganic Chemistry* **1998**, *37*, 533.
(47) Chisholm, M. H. Alkoxides, Aryloxides, Trialkylsiloxides, and Related Oxygen Donors as Ancillary Ligands in the Organometallic Chemistry of the Early Transition Metals, *Chemtracts: Inorganic Chemistry.* **1992**, *4*, 273.

(48) Yi, B.-B.; Khan, M. A.; Powell, D. R.; Richter-Addo, G. B. Synthesis, Characterization, and Protonation of an Amide-Containing Thiolate Complex of a Ruthenium Nitrosyl Porphyrin, *Inorganic Chemistry* **1998**, *37*, 208.
(49) Gross, Z.; Barzilay, C. Spectroscopic Characterization of 2 Types of Tetraarylporphyrin Cation Radicals, *Angewandte Chemie International Edition* **1992**, *31*, 1615.
(50) Felton, R. H.; Owen, G. S.; Dolphin, D.; Fajer, J. Iron(IV) Porphyrins, *Journal of the American Chemical Society* **1971**, *93*, 6332.
(51) Fajer, J.; Borg, D. C.; Forman, A.; Dolphin, D.; Felton, R. H. Pi-Cation Radicals and Dications of Metalloporphyrins, *Journal of the American Chemical Society* **1970**, *92*, 3451.

Chapter 4. Synthesis, Characterization, Electrochemistry, Spectroelectrochemistry and Reactivity of (por)Fe(Salicylhydroxamate) and Other Iron Porphyrin Alkoxide Complexes

4.1 Introduction

The chemistry of hydroxamic acids, including their interactions with several different metals, is well established and has been described in several reviews.[1-7] The hydroxamic acid moiety is commonly associated with siderophores; hydroxamates are

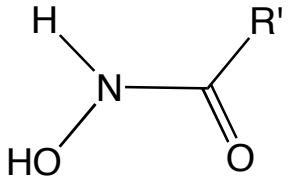

hydroxamic acid

utilized in lower organisms such as fungi and bacteria to sequester ferric iron. Ferric iron has limited bioavailability due to its low solubility in the free state.[8] Hydroxamates are almost exclusively bidentate ligands with respect to iron coordination. However, there is a single report of monodentate coordination to synthetic heme iron complexes.[9]

Some hydroxamic acids have been shown to have pharmaceutical applications such as their use as chelating drugs for iron overload diseases, and, some show anti-tumor activity.[10-13] Some are also proposed as nitric oxide donors.[9,14-17] The simple question "if hydroxamic acids, which are known iron chelators, are administered as drugs to humans, how would they interact with available heme-iron?" along with the possible NO donation character, inspired the work for this dissertation chapter.

The paper by Cheng et al. showed the first structural example of the interaction of a hydroxamate (benzohydroxamate) with a synthetic iron-containing

metalloporphyrin.[9] The observed monodentate coordination was surprising and unexpected; the coordination was through the *O*-atom (M-*O*-NHC(=O)R) of the hydroxamate moiety, with H-bonding to an additional benzohydroxamic acid.[9] In order to follow up on this work to see if this monodentate coordination was a common feature of hydroxamic acids in their interaction with metalloporphyrin centers, we set out to investigate the reactions of additional hydroxamic acids with iron containing metalloporphyrins.

I have successfully synthesized and characterized a new series of (porphyrin)Fe(L) (L = hydroxamate, aryloxide, and carboxylate) complexes for structural and electrochemical studies. The ability of the coordinated hydroxamates to donate NO upon oxidation and their reactivity was investigated. Depictions of the porphyrins and ligand precursors used in these experiments are provided below.

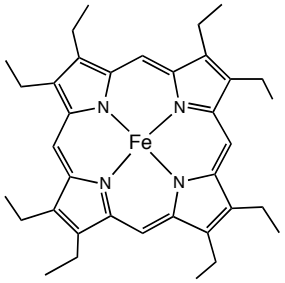

(OEP)Fe

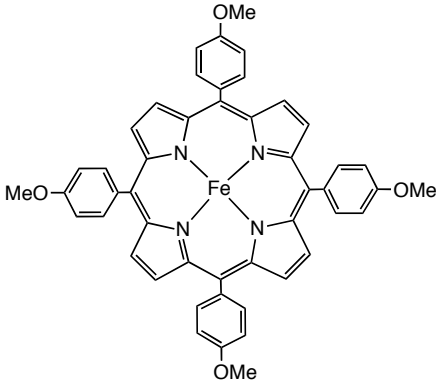

(T(*p*-OMe)PP)Fe

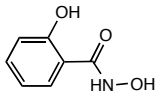

salicylhydroxamic acid

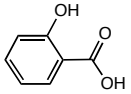

salicylic acid

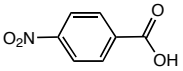

p-nitrobenzoic acid

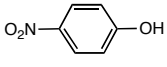

p-nitrophenol

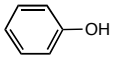

phenol

It should be noted that other hydroxamic acids (aceto-, benzo-, *p*-nitrobenzo-, hexano-, N-phenyl-benzo-, and 2-methoxy-5-methyl-benzohydroxamic acid) were used, however coordination to a metalloporphyrin was not observed with these hydroxamic acids.

4.2 Experimental

4.2.1 Materials, Instrumentation, and Methods

All reactions were carried out under an atmosphere of pre-purified nitrogen using standard Schlenk techniques and/ or in an Innovative Technology Labmaster 100 Dry Box unless mentioned otherwise. Solvents used for these experiments were purified using an Innovative Technology Pure Solv 400-5-MD Solvent Purification System, or distilled using appropriate drying agents under nitrogen just prior to use. Infrared spectra were collected using a Bio-Rad FT-155 FTIR spectrometer. ESI mass spectra were obtained on a Micromass Q-TOF mass spectrometer. UV-vis data was collected using a 1.0 cm cuvette and an HP 8453 diode array instrument.

Electrochemical measurements were made using a BAS CV50W instrument (Bioanalytical Systems, West Lafayette, IN, USA). For all electrochemical experiments, a 3.0 mm diameter Pt disk electrode was utilized as the working electrode, a Ag wire acted as the pseudo-reference electrode, and a Pt wire served as the auxiliary electrode. The solutions for all electrochemical experiments were deaerated by bubbling prepurified nitrogen gas through the solutions for approximately 10 min before each set of measurements, and then the experiments were carried out at room temperature under an atmosphere of nitrogen in a 0.1 M NBu_4PF_6 solution of the

analyte (1.0 mM) in CH_2Cl_2. All potentials are referenced to the $Cp_2Fe^{0/+}$ couple set to 0.00 V. A Bruker Vector 22 FTIR spectrometer, which was outfitted with a mid-IR fiber-optic dip-probe and liquid nitrogen cooled MCT detector (Remspec Corporation, Sturbridge, MA, USA) was utilized for the infrared spectroelectrochemical experiments.[18]

4.2.2 Chemicals

(OEP)H_2 was purchased from Mid-Century Chemicals, (T(*p*-OMe)PP)H_2 was synthesized from pyrrole and the aldehyde precursor as described in the literature.[19] The (por)Fe(Cl) and [(por)Fe]$_2$(μ-O) complexes were synthesized by published procedures and the [(por)Fe]$_2$(μ-O) complexes were identified by their Fe-O stretches which occur in the 880 – 890 cm^{-1} region of their infrared spectra.[20] Salicylhydroxamic acid, salicylic acid, *p*-nitrobenzoic acid, and bis(triphenylphosphoranylidene)ammonium nitrite (PPN-nitrite) were purchased from Sigma-Aldrich and used as received. The compound *p*-nitro-benzohydroxamic acid was received as a gift from Dr. Richard Taylor (OU) and used as received.

4.2.3 Synthesis

The metalloporphyrin hydroxamate complexes were prepared in a manner similar to that previously reported.[9] Two key modifications were (i) application of heat, and (ii) the use of excess hydroxamic acid reagents. The solubility of the ligand precursors in CH_2Cl_2 were poor. This characteristic was found to be very useful for the purification of the product complexes by filtration in the glove box through a disposable pipette containing a small cotton plug to remove excess uncoordinated ligand.

4.2.3.1 Preparation of (T(*p*-OMe)PP)Fe(O-C_6H_4-*o*-C(=O)NHOH)

(T(*p*-OMe)PP)Fe(SalHate)

[(T(*p*-OMe)PP)Fe]$_2$(μ-O) (0.051 g, 0.032 mmol) and salicylhydroxamic acid (0.039 g, 0.25 mmol) were dissolved in toluene (8 mL) in a Schlenk tube. The solution was stirred for 2 hours at 75 °C, during which time a color change from green to brown-red was observed. The solvent was removed in vacuo, and the residue redissolved in CH_2Cl_2 and then filter-cannulated into a clean Schlenk tube. The volume of the solvent was reduced to 1/3 its original volume by the application of vacuum and placed in a freezer at -30 °C for 3 days. The black crystalline precipitate that formed was washed with hexane, dried, and dissolved in CH_2Cl_2/toluene/benzene (5:1:1) mixture. This solution was then allowed to slowly evaporate to give crystalline [(T(*p*-OMe)PP)Fe(O-C_6H_4-*o*-C(=O)NHOH)] (0.058 g, 0.061 mmol, 96% yield (crude)). X-ray quality crystals were generated similarly.

IR (KBr, cm^{-1}): ν_{CO} = 1654 w; also 1607 s, 1560 w, 1511 s, 1492 m, 1464 w, 1441 w, 1411 w, 1338 m, 1290 m, 1248 s, 1204 w, 1175 s, 1107 w, 1073 w, 1033 w, 999 s, 848 w, 806 m, 787 w, 764 w, 729 m, 696 w, 602 m. Mass spectrum *m/z*: (ESI^+) 788.33 [(T(*p*-OMe)PP)Fe]$^+$ (100%); Mass spectrum *m/z* (ESI^-) 136.99 [HO-C_6H_4-C(=O)O]$^-$ (100%), 152.01 [O-C_6H_4-*o*-C(=O)NHOH]$^-$ (45%). UV-vis spectrum (λ, nm (ε, $M^{-1} \bullet cm^{-1}$) 1.0×10^{-5} M in CH_2Cl_2): 421(1.64×10^5), 360 (5.17×10^4).

4.2.3.2 Preparation of (OEP)Fe(O-C_6H_4-*o*-C(=O)NHOH)

(OEP)Fe(SalHate)

[(OEP)Fe]$_2$(μ-O) (0.051 g, 0.043 mmol) and salicylhydroxamic acid (0.052 g, 0.34 mmol) were dissolved in toluene (5 mL) in a Schlenk tube. The solution was stirred for 3 hours at 80 °C during which time the solution changed color from brown-red to red. The solvent was removed under vacuum and the residue redissolved in CH_2Cl_2 and filter-cannulated into a clean Schlenk tube. The solvent of the filtrate was removed by vacuum (to ~2/3 of its original volume) and placed in the freezer at -30 °C for 3 days. The black crystalline precipitate that formed was washed with hexane, dried, and dissolved in CH_2Cl_2/hexane (5:1) mixture. This was then allowed to slowly evaporate to give crystalline [(OEP)Fe(O-C_6H_4-*o*-C(=O)NHOH)] (0.047 g, 0.064 mmol, 74% yield (crude)). X-ray quality crystals were generated similarly.

IR (KBr, cm^{-1}): ν_{CO} = 1647 m; also 1618 w, 1595 w, 1577 w, 1571 w, 1560 m, 1541 w, 1534 w, 1522 w, 1508 w, 1466 s, 1459 m, 1448 m, 1375 w, 1239 m, 1147 m, 1111 w, 1055 m, 1016 m, 982 w, 958 m, 915 w, 843 m, 754 m, 732 w, 700 w, 669 w, 660 w, 604 m. Mass spectrum *m/z*: (ESI$^+$) 588.47 [(OEP)Fe]$^+$ (100%); Mass spectrum *m/z* (ESI$^-$) 152.01 [O-C_6H_4-*o*-C(=O)NHOH]$^-$ (100%). UV-vis spectrum (λ, nm (ε, $M^{-1} \cdot cm^{-1}$) 1.0×10^{-5} M in CH_2Cl_2): 393 (1.39×10^5), 500 (1.53×10^5).

4.2.3.3 Preparation of (T(*p*-OMe)PP)Fe(OC(=O)C_6H_4-*p*-NO_2)

(T(*p*-OMe)PP)Fe(*p*-nitrobenzoate)

[(T(*p*-OMe)PP)Fe]$_2$(μ-O) (0.050 g, 0.032 mmol) and *p*-nitrobenzoic acid (0.041 g, 0.25 mmol) were dissolved in toluene (5 mL) in a Schlenk tube. The solution was

allowed to stir for 2 hours at 75 °C during which time the color changed from green to a brown-red. The solvent was removed under vacuum and the residue redissolved in CH_2Cl_2 and then filter-cannulated into a clean Schlenk tube. The solvent of the filtrate was removed by vacuum and redissolved in CH_2Cl_2/toluene/benzene (5:1:1). This solution was then allowed to slowly evaporate to give crystalline [(T(*p*-OMe)PP)Fe(OC(=O)-C_6H_4-*p*-NO_2] (0.023 g, 0.02 mmol, 36% yield (crude)). X-ray quality crystals were generated similarly.

IR (KBr, cm^{-1}): ν_{CO} = 1662 s, ν_{NO2} 1464 m (sym), ν_{NO2} 1288 s (asym); also 1606 s, 1512 s, 1496 s, 1247 s, 1176 s, 1107 w, 1035 m, 998 s, 848 w, 804 s, 718 s, 601 s, 538 m. Mass spectrum *m/z*: (ESI^-) 165.98 [O-C(=O)-C_6H_4-*p*-NO_2]$^-$ (100%); Mass spectrum *m/z* (ESI^+) 788.33 [(T(*p*-OMe)PP)Fe]$^+$ (100%). UV-vis spectrum (λ, nm in CH_2Cl_2): 419, 519.

It should be noted that the (T(*p*-OMe)PP)Fe(nitrobenzoate) complex was originally obtained by the reaction of [(T(*p*-OMe)PP)Fe]$_2$O with *p*-NO_2-benzohydroxamic acid containing *p*-nitrobenzoic acid as an impurity (~ 20%) (^{1}H NMR spectroscopy).

4.2.3.4 Preparation of (OEP)Fe(OC(=O)C_6H_4-*o*-OH)

(OEP)Fe(sal)

[(OEP)Fe]$_2$(μ-O) (0.032 g, 0.026 mmol) and salicylic acid (0.029 g, 0.21 mmol) were dissolved in toluene (5 mL) in a Schlenk tube. The solution was stirred for 3 hours at 80 °C during which time the solution changed color from brown-red to red. The solvent was removed under vacuum and the residue was redissolved in CH_2Cl_2 and

filter-cannulated into a clean Schlenk tube. The solvent of the filtrate was removed by vacuum and redissolved in CH_2Cl_2/hexane (5:1). This was then allowed to slowly evaporate to give crystalline [(OEP)Fe(OC(=O)C_6H_4-*o*-OH)] (0.021 g, 0.029 mmol, 53% yield). X-ray quality crystals were generated similarly.

IR (KBr, cm^{-1}): ν_{CO} = 1644 m; also 1614 m, 1580 s, 1485 s, 1470 s, 1452 s, 1388 s, 1350 s, 1308 s, 1256 s, 1222 w, 1146 s, 1112 m, 1056 s, 1018 s, 984 m, 962 s, 917 m, 845 m, 788 w, 758 s, 702 s, 660 m. Mass spectrum: (ESI^-) *m/z* 136.96 $[OC(=O)C_6H_4$-*o*-$OH]^-$ (100%); mass spectrum (ESI^+) 588.44 $[(OEP)Fe]^+$ (100%).

4.2.3.5 Preparation of (T(*p*-OMe)PP)Fe(O-C_6H_5)

(T(*p*-OMe)PP)Fe(OPh)

(T(*p*-OMe)PP)FeCl (0.04 g, 0.049 mmol) was added to a Schlenk tube along with $NaOCH_3$ (3.6 mg, 0.066 mmol) and dissolved in of CH_2Cl_2 (7 mL). Then MeOH (2 mL) was added slowly to the solution. This solution was left to stir for 30 minutes. The solution turned green upon the addition of MeOH when stirring. After 30 min., the solvent was removed under vacuum, re-dissolved in CH_2Cl_2 ($NaOCH_3$ is not soluble in CH_2Cl_2), and filter-cannulated into a clean Schlenk tube and dried under vacuum. Benzene (10 mL) and phenol (0.01 g, 0.11 mmol) were added to the remaining solid, and the mixture was left to stir for 4 hours. The benzene solution turned red-brown and was dried under vacuum. The residue was washed with hexanes, dried, re-dissolved in a CH_2Cl_2/hexane solution (3:1) and placed in the glove box to crystallize by slow evaporation to give X-ray quality crystals of the product.

4.2.3.6 Preparation of (T(*p*-OMe)PP)Fe(OC_6H_5-*p*-NO_2)

(T(*p*-OMe)PP)Fe(*p*-nitrophenoxide)

(T(*p*-OMe)PP)FeCl (0.05 g, 0.061 mmol) was added to a Schlenk tube along with $NaOCH_3$ (0.0021 g, 0.039 mmol) and dissolved in CH_2Cl_2 (5 mL). MeOH (2 mL) was then added slowly to the solution. This solution was left to stir for 30 minutes. The solution turned green upon the addition of MeOH while stirring. After 30 minutes, the solvent was removed under vacuum and the residue was redissolved in CH_2Cl_2 ($NaOCH_3$ is not soluble in CH_2Cl_2), and filter-cannulated into a Schlenk tube containing a large excess of 4-nitrophenol (not weighed due to the solubility of 4-nitrophenol) and CH_2Cl_2/toluene (4:1). This solution was left to stir for 1 hour. The solution turned red-brown and the solvent was removed under vacuum. The residue was redissolved in a CH_2Cl_2/hexane solution (3:1), and placed in the glove box to crystallize by slow evaporation, which afforded X-ray quality crystals of the product.

4.3 Results

4.3.1 Synthesis

The complexes reported in this chapter were synthesized in one of two ways. The first was from the acid base reaction of the ligand precursor in excess with the porphyrin μ-oxo dimmer starting materials (Equation 4.1), and the second was from an alcohol exchange reaction (Equation 4.2).

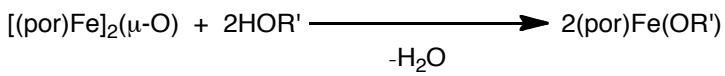

4.1

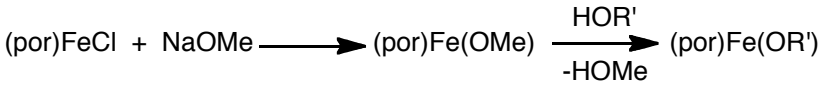

4.2

The products obtained for the salicylhydroxamate complexes showed slight changes in the infrared spectra with respect to the ν_{CO} from the ligand precursor and the coordinated ligand. For example, the ν_{CO} for the free ligand precursor salicylhydroxamic acid is ~1620 cm^{-1} while the coordinated salicylhydroxamate ligand has a ν_{CO} of 1654 cm^{-1}.

4.3.2 Mass Spectrometry

ESI mass spectrometry (positive and negative ion detection) data were collected for the (por)Fe(OR') complexes to aid in characterization. The complexes fragmented under our ESI conditions. None of the spectra of the analyzed complexes showed parent peaks. For example, the OEP complexes showed *m/z* peaks at 588.44 for the $[(OEP)Fe]^+$ fragment. The fragmented ligands were observed in the ESI^- spectra, such as the $[OC(=O)C_6H_4\text{-}p\text{-}NO_2]^-$ ligand which appears at a *m/z* of 165.98. A summary of the mass spectrometry data for the (por)Fe(OR') complexes is provided below in Table 4.1.

Table 4.1. Mass spectrometry ($ESI^{+/-}$) data for (por)Fe(aryloxide/ carboxylate) complexes.

Compound	ESI^+	ESI^- (ligand)
(T(*p*-OMe)PP)Fe(SalHate)	788.33 (100%)	136.99(100%), 152.01(45%)
(OEP)Fe(SalHate)	588.47 (100%)	152.01 (100%)
(T(*p*-OMePP)Fe(*p*-nitrobenzoate)	788.33 (100%)	165.98 (100%)
(OEP)Fe(sal)	588.44 (100%)	136.96 (100%)

Mass spectrometry analyses were done using a Micromass/Waters QTOF-1 (Bedford, MA) equipped with an electrospray ionization source in positive or negative ion mode. Nitrogen gas was used as a nebulizing and drying gas with capillary voltage 3.0 kV, cone voltage ramp 10-85 V, source block temperature 120ºC, desolvation temperature 150ºC, and desolvation flow rate 200 L/hr. Data was collected and analyzed using Mass Lynz (4.0, SP1, 2003).

4.3.3 X-Ray Crystallography

Crystals of (T(*p*-OMe)PP)Fe(SalHate), (OEP)Fe(SalHate), (T(*p*-OMe)PP)Fe(*p*-nitrobenzoate), (OEP)Fe(sal), (T(*p*-OMe)PP)Fe(*p*-nitrophenoxide), and (T(*p*-OMe)PP)Fe(OPh) were grown by slow evaporation of their solutions in an N_2(g) atmosphere. Suitable crystals were then selected for X-ray crystal structure determinations. The molecular structures for these complexes along with the orientations of the Fe-O bonds and their atom displacements of the porphyrin cores from the 24-atom mean porphyrin planes are given in the figures below. The internal hydrogen bonding for the complexes are shown by dashed lines in the figures.

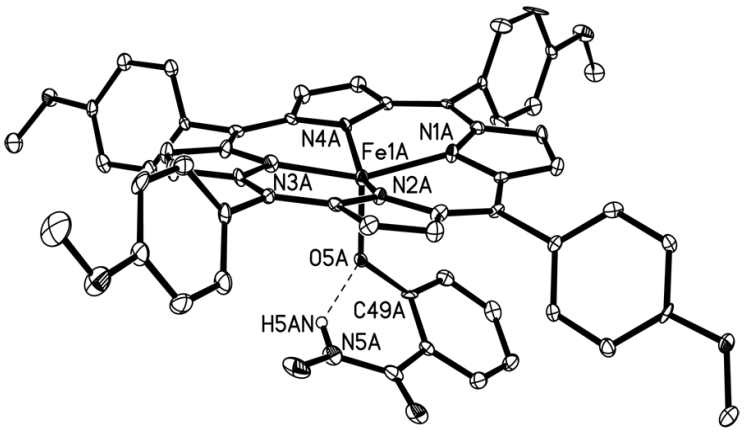

Figure 4.1. Molecular structure of (T(*p*-OMe)PP)Fe(SalHate). Hydrogen atoms (except that attached to N5A) have been omitted for clarity.

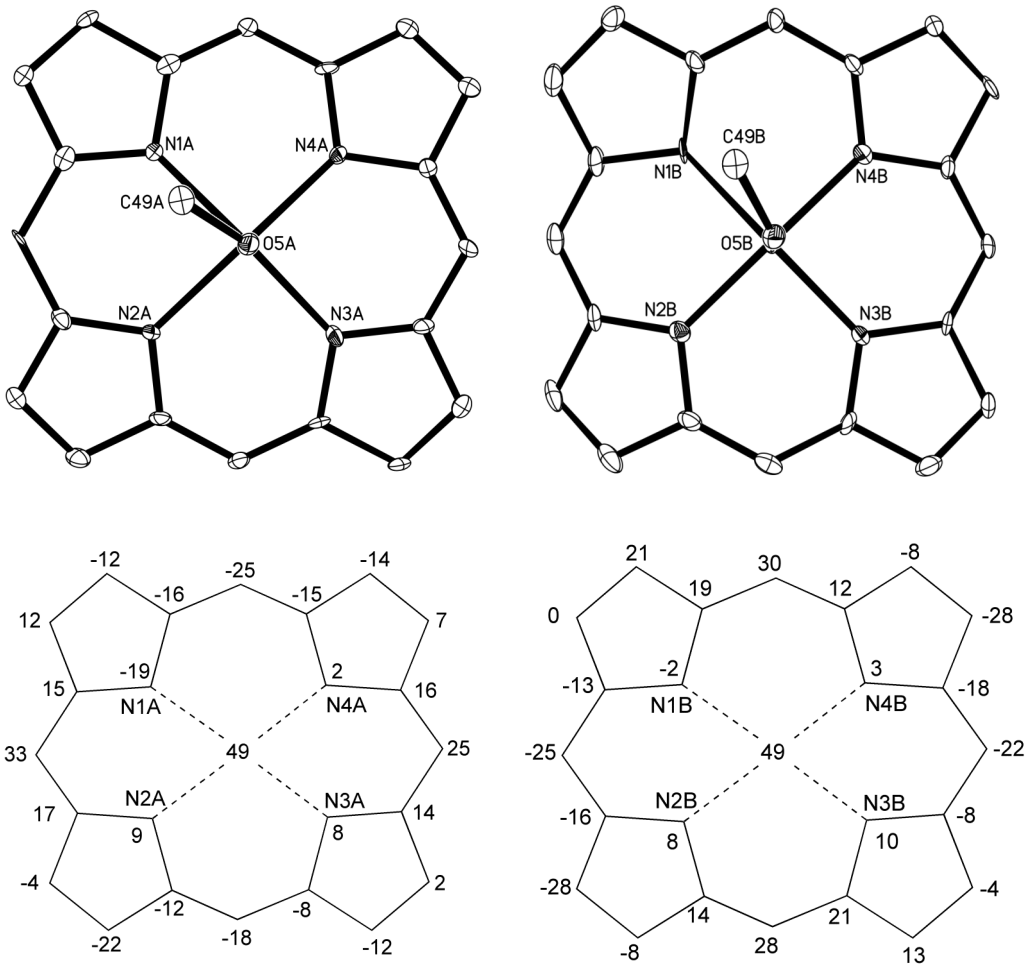

Figure 4.2. (Top) View of (T(*p*-OMe)PP)Fe(SalHate) orientations relative to the porphyrin cores, with the view along the axial OFe bonds. Hydroxamate substituents have been removed for clarity. (Bottom) Perpendicular atom displacements (0.01 Å) of the porphyrin cores from the 24-atom mean porphyrin planes.

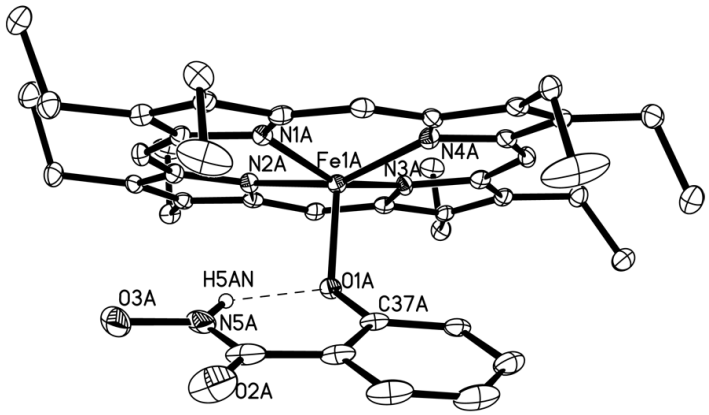

Figure 4.3. Molecular structure of (OEP)Fe(SalHate). Hydrogen atoms (except that attached to N5A) have been omitted for clarity.

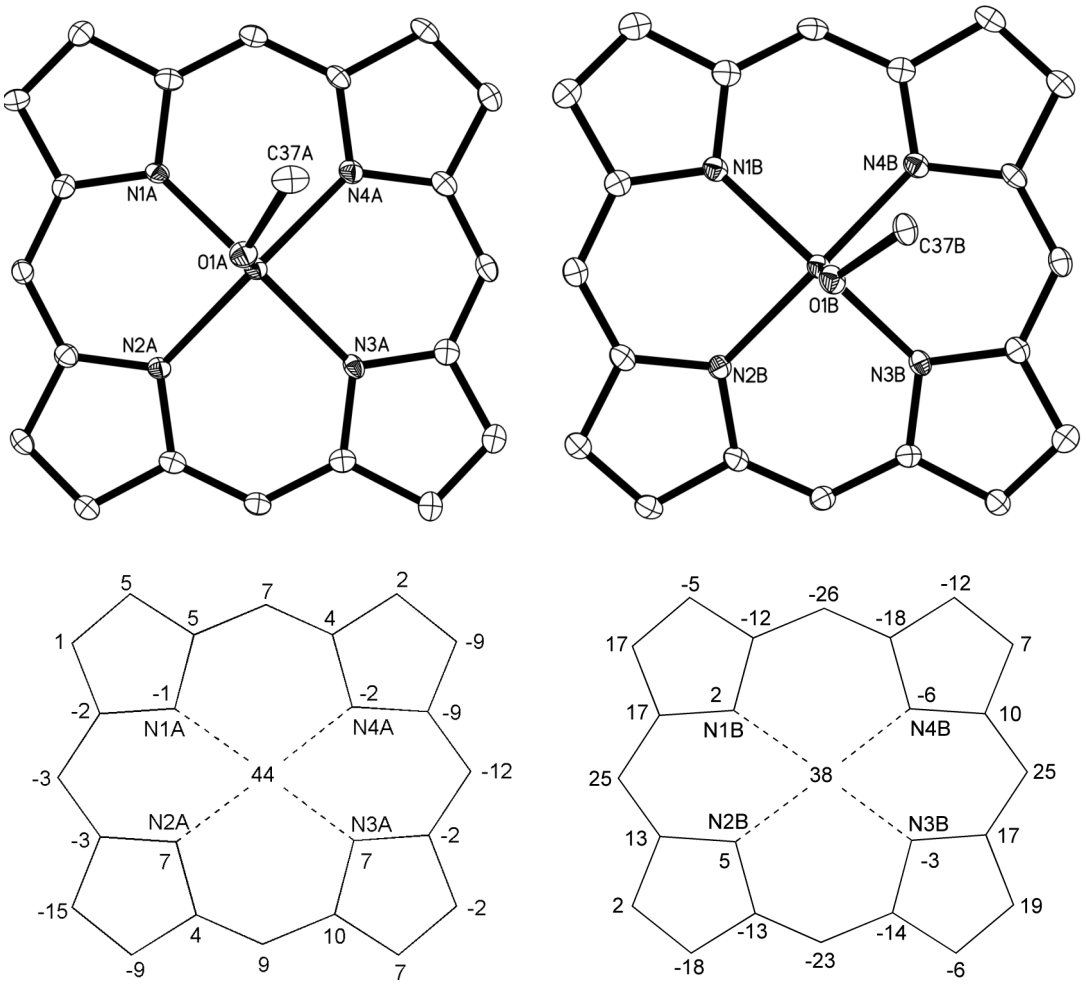

Figure 4.4. (Top) View of (OEP)Fe(SalHate) orientations relative to the porphyrin cores, with the view along the axial OFe bonds. Hydroxamate substituents have been removed for clarity. (Bottom) Perpendicular atom displacements (0.01 Å) of the porphyrin cores from the 24-atom mean porphyrin planes.

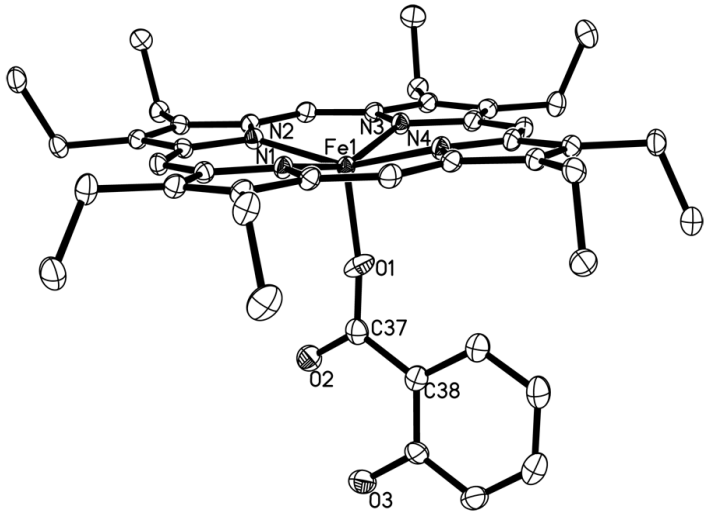

Figure 4.5. Molecular structure of (OEP)Fe(sal). Hydrogen atoms have been omitted for clarity.

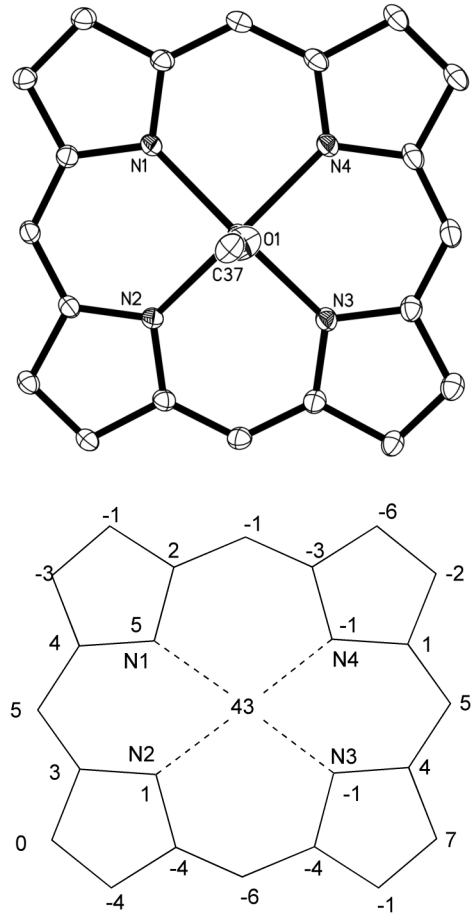

Figure 4.6. (Top) View of (OEP)Fe(sal) orientation relative to the porphyrin core, with the view along the axial O–Fe bond. Salicylate substituents have been removed for clarity. (Bottom) Perpendicular atom displacements (0.01 Å) of the porphyrin core from the 24-atom mean porphyrin plane.

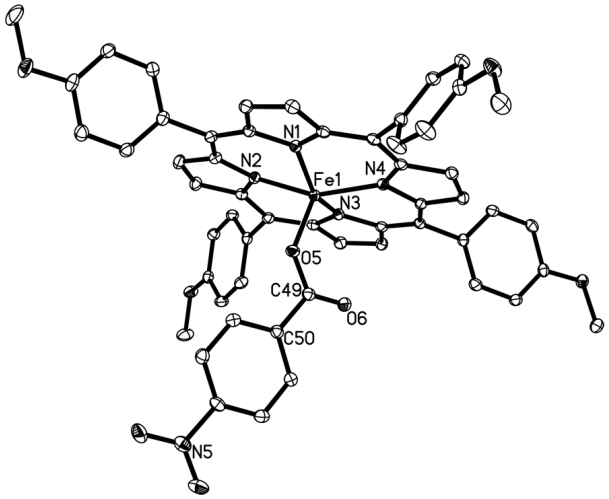

Figure 4.7. Molecular structure of (T(*p*-OMe)PP)Fe(*p*-nitrobenzoate). Hydrogen atoms have been omitted for clarity.

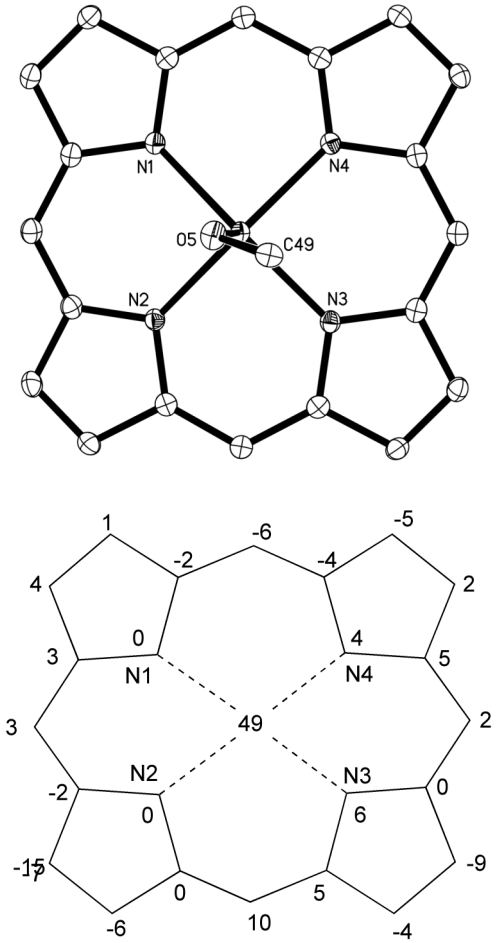

Figure 4.8. (Top) View of (T(*p*-OMe)PP)Fe(*p*-nitrobenzoate) orientation relative to the porphyrin core, with the view along the axial O–Fe bond. The *p*-nitrobenzoate substituents have been removed for clarity. (Bottom) Perpendicular atom displacements (0.01 Å) of the porphyrin core from the 24-atom mean porphyrin plane.

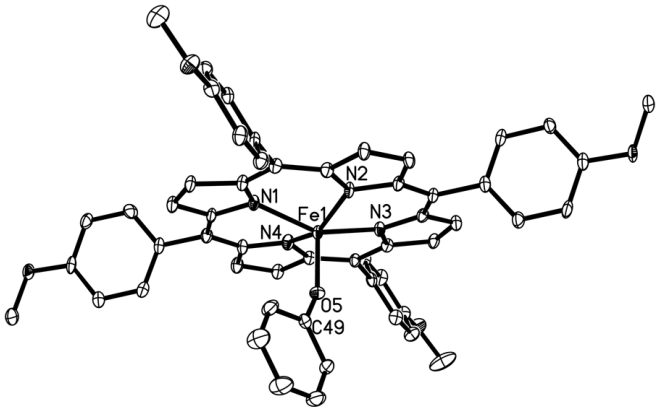

Figure 4.9. Molecular structure of (T(*p*-OMe)PP)Fe(OPh). Hydrogen atoms have been omitted for clarity.

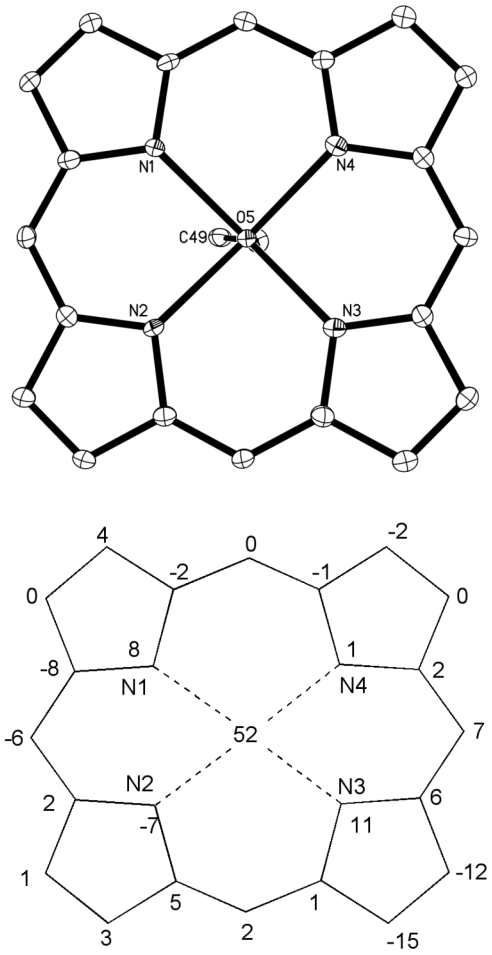

Figure 4.10. (Top) View of (T(*p*-OMe)PP)Fe(OPh) orientation relative to the porphyrin core, with the view along the axial O–Fe bond. Phenoxide has been removed for clarity. (Bottom) Perpendicular atom displacements (0.01 Å) of the porphyrin core from the 24-atom mean porphyrin plane.

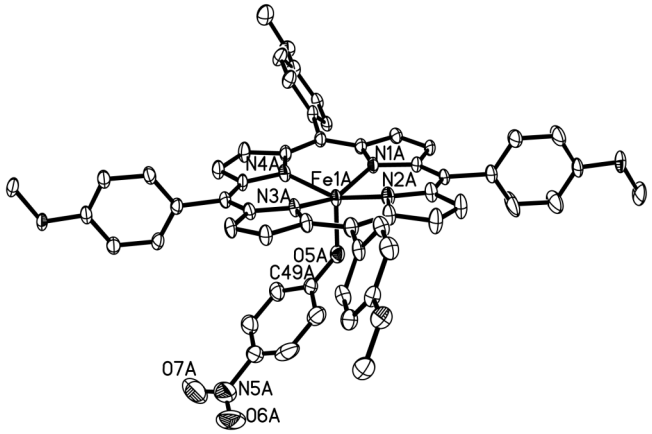

Figure 4.11. Molecular structure of (T(*p*-OMe)PP)Fe(*p*-nitrophenoxide). Hydrogen atoms have been omitted for clarity.

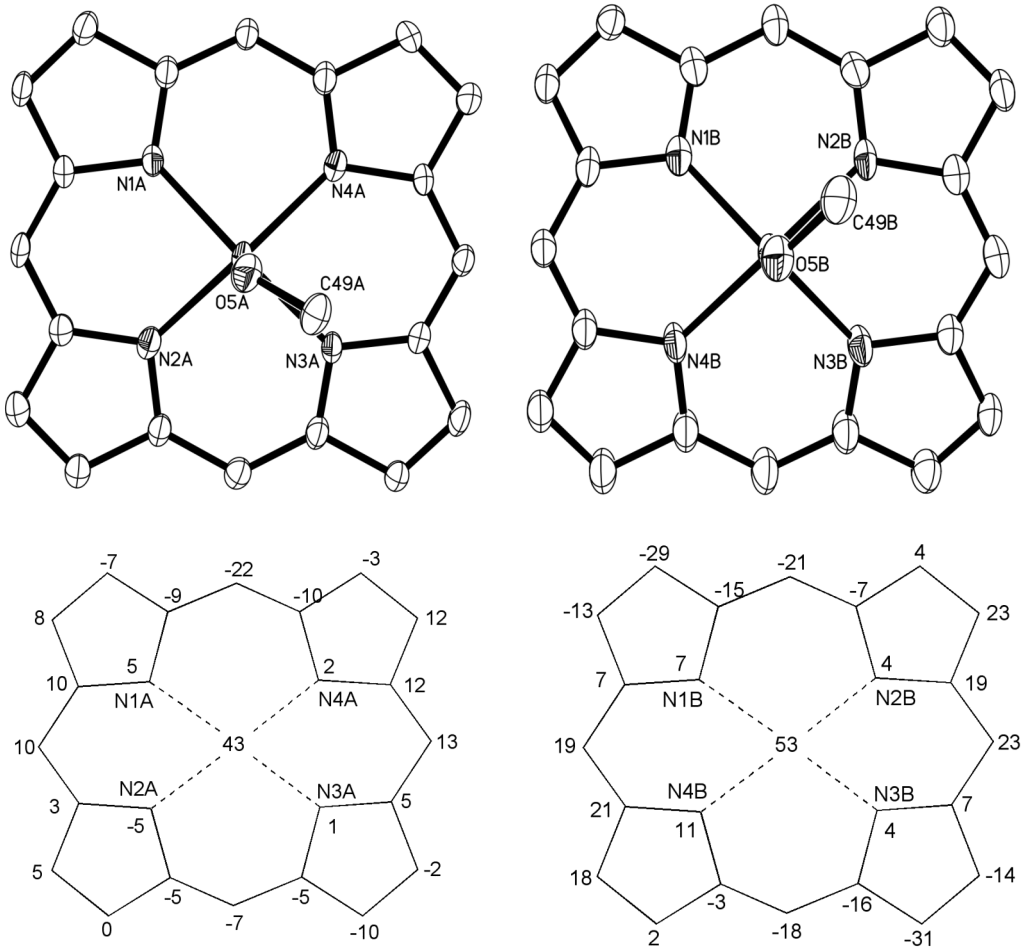

Figure 4.12 (Top) View of (T(*p*-OMe)PP)Fe(*p*-nitrophenoxide) orientation relative to the porphyrin cores, with the view along the axial O–Fe bonds. *p*-nitrophenoxide substituents have been removed for clarity. (Bottom) Perpendicular atom displacements (0.01 Å) of the porphyrin cores from the 24-atom mean porphyrin planes.

Table 4.2. Selected structural data (in Å and º) for iron-porphyrin complexes containing hydroxamate, aryloxides, and carboxylates.

	Fe-N (por)	ΔFe (Å)	Fe-O(C) (Å)	FeO-C (Å)	∠FeOR (º)
(T(*p*-OMe)PP)Fe(SalHate)*	2.050 – 2.062(4)	0.48	1.886(3)	1.352(4)	125.6(2)
	2.042 – 2.066(4)	0.49	1.869(3)	1.370(5)	126.6(2)
(OEP)Fe(SalHate)*	2.043 – 2.061(3)	0.44	1.908(2)	1.355(4)	125.6(2)
	2.032 – 2.056(3)	0.38	1.911(2)	1.348(4)	126.3(2)
(T(*p*-OMe)PP)Fe(*p*-nitrobenzoate)	2.0578 – 2.0757(15)	0.49	1.8997(13)	1.312(2)	129.44(12)
(OEP)Fe(sal)	2.0548 – 2.0673(17)	0.43	1.8888(17)	1.250(3)	170.22(17)
(T(*p*-OMe)PP)Fe(OPh)	2.061 – 2.091(2)	0.52	1.839(2)	1.321(5)	143.9(3)
(T(*p*-OMe)PP)Fe (nitrophenoxide)*	2.060 – 2.062(3)	0.43	1.871(3)	1.327(5)	129.5(3)
	2.061 – 2.066(4)	0.53	1.870(4)	1.332(6)	122.1(3)

*Two unique structures in the unit cell

The complexes show a range of ∠FeOR(º) bond angles from 122º to 145º. The 170º bond angle in the (OEP)Fe(salicylate) appears to be the outlier in this group even though the carboxylic group by which it coordinates is unhindered sterically, similar to the nitrobenzoate ligand used in the (T(*p*-OMe)PP)Fe complex. The structures appear to have very similar Fe-O(R) bond lengths in the 1.88 – 1.91Å range. These characteristics will be discussed below.

4.3.4 Cyclic voltammetry (CV)

The CVs of (T(*p*-OMe)PP)Fe(*p*-nitrophenoxide) and (T(*p*-OMe)PP)Fe(OPh) show two reversible oxidations each. The major difference between the CVs for these

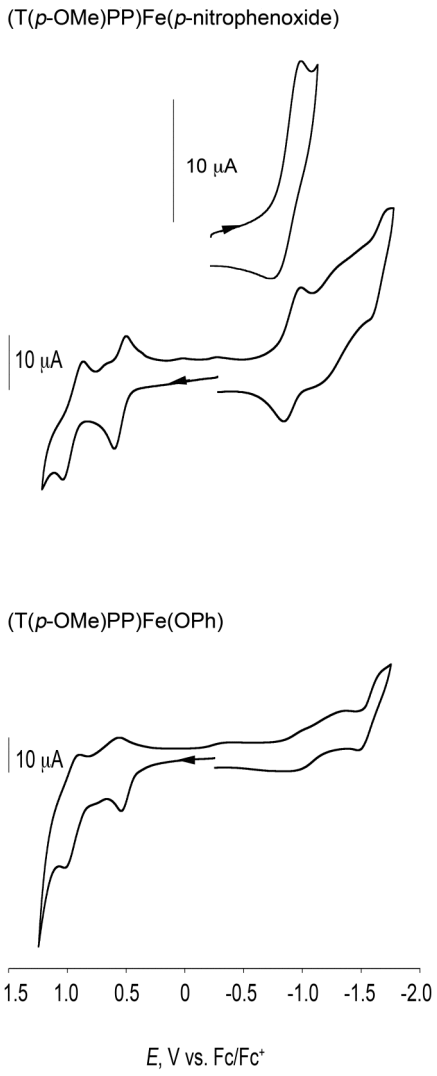

Figure 4.13. Cyclic voltammograms of (T(*p*-OMe)PP)Fe(*p*-nitrophenoxide) and (T(*p*-OMe)PP)Fe(OPh) at 200 mV/s, 1 mM analyte, 0.1 M NBu_4PF_6 at room temperature. Potentials are referenced against the Fc/Fc^+ couple set to 0.0 V.

complexes is that the nitrophenoxide complex yields a reversible reduction at -0.89 V vs. Fc/Fc^+ (i_{pa}/i_{pc} = 0.80, ΔE = 0.25 V) while the phenoxide compound does not provide

a reduction that was reproducible in the solvent window that was utilized in these experiments (Figure 4.13). When studying the first oxidation of (T(*p*-OMe)PP)FeOPh by itself (Figure 4.14 (inset) and Figure 4.15), it does show very good electrochemical and chemical reversibility at $E_1°' = 0.47$ V with a $\Delta E_p = 0.11$ V and an $i_{pc}/i_{pa} = 0.81$ are in good agreement with the Fc/Fc^+ couple's values of $\Delta E_p = 0.19$ V and $i_{pc}/i_{pa} = 0.82$.

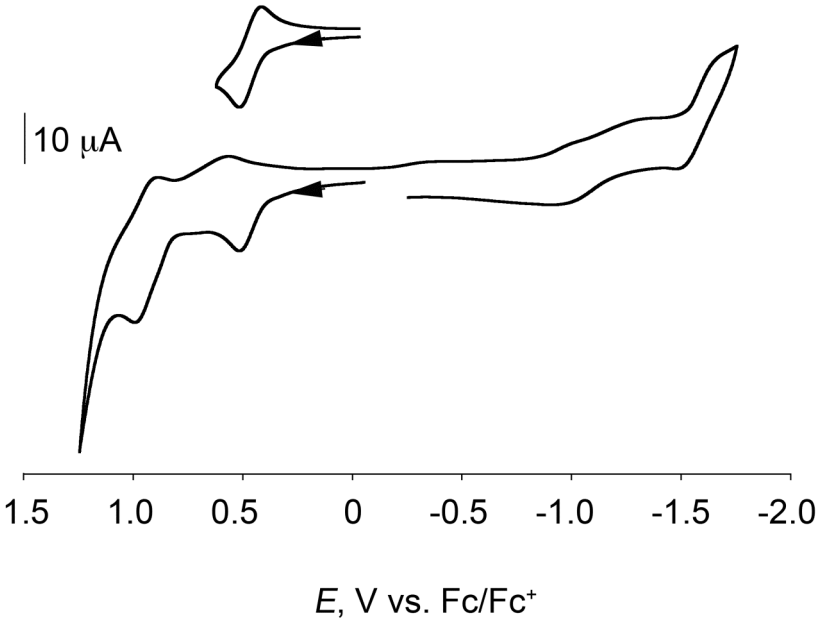

Figure 4.14. Cyclic voltammograms of (T(*p*-OMe)PP)Fe(OPh) at 200 mV/s, 1 mM analyte, 0.1 M NBu_4PF_6 at room temperature. Potentials are referenced against the Fc/Fc^+ couple set to 0.0 V.

Similar to what was observed with the (T(*p*-OMe)PP)FeOPh complex, the first oxidation for (T(*p*-OMe)PP)Fe(*p*-nitrophenoxide) is indeed reversible when studying

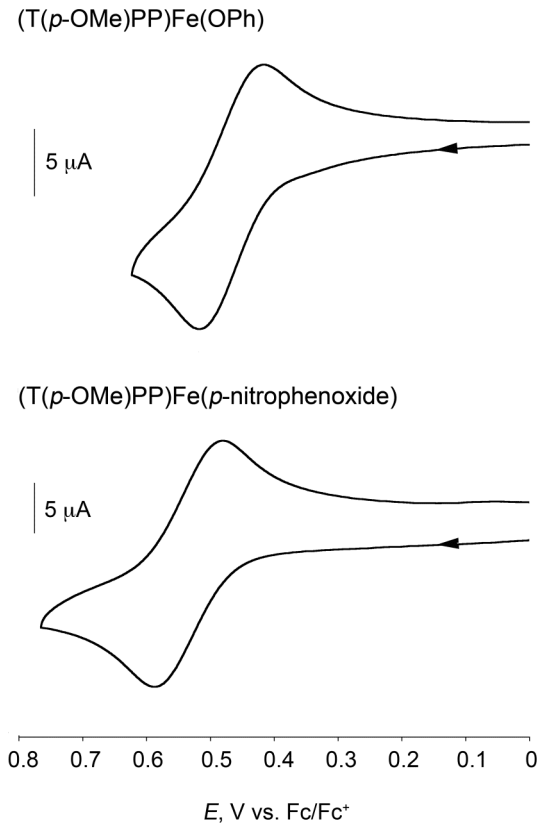

Figure 4.15. Cyclic voltammograms of the first oxidations of (T(*p*-OMe)PP)Fe(*p*-nitrophenoxide) and (T(*p*-OMe)PP)Fe(OPh) at 200 mV/s, 1 mM analyte, 0.1 M NBu_4PF_6 at room temperature. Potentials are referenced against the Fc/Fc^+ couple set to 0.0 V.

the first oxidation by itself which can be observed in Figure 4.15.

The (OEP)Fe(sal) complex had two reversible oxidation features in its CV ($E_1^{o\prime}$ = 0.51 V, $E_2^{o\prime}$ = 1.06 V) with an irreversible reduction at E_{pc1} = -1.2 V within the solvent limits used for these experiments (Figure 4.16). The oxidations were both electrochemically reversible with ΔE_p values of 0.15 V and 0.20 V for the first and second oxidations respectively compared to a ΔE_p value of 0.12 V for ferrocene. The i_{pc}/i_{pa} values of 0.9 (~1) and 0.7 suggest chemical reversibility for the first oxidation.

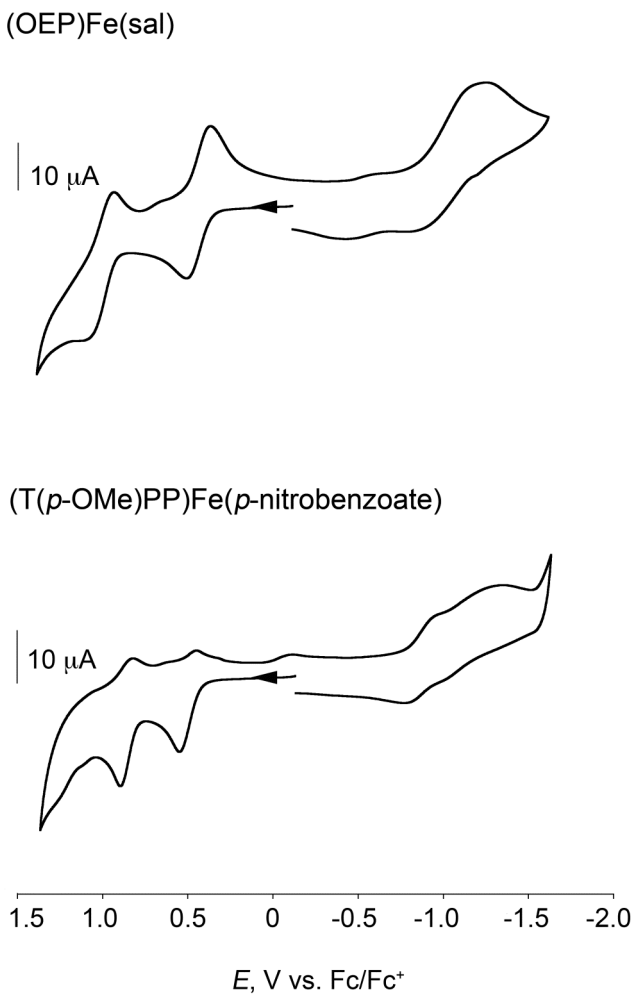

Figure 4.16. Cyclic voltammograms of (from top to bottom) (OEP)Fe(sal) and (T(*p*-OMe)PP)Fe(*p*-nitrobenzoate) at 200 mV/s, 1 mM analyte, 0.1 M NBu_4PF_6 at room temperature. Potentials are referenced against the Fc/Fc^+ couple set to 0.0 V.

The first oxidation of the (T(*p*-OMe)PP)Fe(*p*-nitrobenzoate) complex (bottom of Figure 4.16) was similar to what was observed for the (T(*p*-OMe)PP)Fe(OPh) and (T(*p*-OMe)PP)Fe(*p*-nitrophenoxide) complexes in that while investigating the first oxidation peak by itself showed chemical and electrochemical reversibility as shown in Figure 4.17.

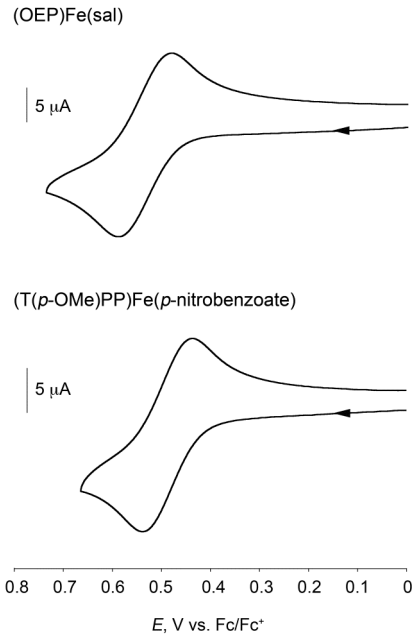

Figure 4.17. Cyclic voltammograms of the first oxidation of (OEP)Fe(Sal) and (T(*p*-OMe)PP)Fe(*p*-nitrobenzoate) at 200 mV/s, 1 mM analyte, 0.1 M NBu_4PF_6 at room temperature. Potentials are referenced against the Fc/Fc^+ couple set to 0.0 V.

The (T(*p*-OMe)PP)Fe(SalHate) complex displays one irreversible oxidation (E_{1pa} = 0.52 V). Additional irreversible oxidations are present at E_{2pa} = 0.73 V and E_{3pa} = 1.01 V. Also observed in the CV when scanning in the negative direction is the presence of two reductions at –0.86 V (ΔE = 0.18 V, i_{pc}/i_{pa} = .81) and –1.58 V (ΔE = 0.16, i_{pc}/i_{pa} = 0.48). These reductions disappear after several scans, most likely due to decomposition or fouling of the electrode from various components in the solution depositing on the electrode's surface. The oxidation peaks were studied first and did not show any fouling during multiple scans. A plot of i_{pa} vs. (scan rate)$^{1/2}$ for the first oxidation feature provided a linear relationship, indicating that the process is diffusion-controlled.

The (OEP)Fe(SalHate) complex behaves in a similar manner as the (T(*p*-OMe)PP)Fe(SalHate) complex. The OEP compound undergoes an irreversible first

oxidation (E_{1pa} = 0.44 V), followed by two more oxidation features at E_{2pa} = 0.72 V and E_{3pa} = 1.15 V, there are three return peaks at 0.41 V, 0.58 V, and 0.94 V that accompany the oxidations. When examining the oxidation features individually, they showed no reversibility (Figure 4.19). Also observed during initial scans of (OEP)Fe(SalHate) were two reductions at E_{1pc} = -0.79 V and -1.1 V (ΔE = 0.48 V, i_{pc}/i_{pa} = 0.85). Again, the reduction feature disappears during the CV experiment after several scans have been performed.

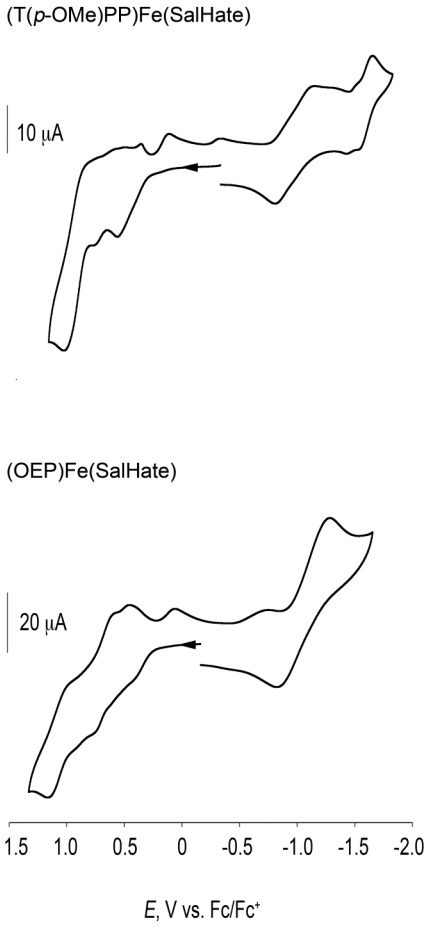

Figure 4.18. Cyclic Voltammograms of (from top to bottom) (T(*p*-OMe)PP)Fe(SalHate) and (OEP)Fe(SalHate) in CH_2Cl_2 at 200 mV/s, 1 mM analyte, 0.1 M NBu_4PF_6 at room temperature. Potentials are referenced against the Fc/Fc^+ couple set to 0.0 V.

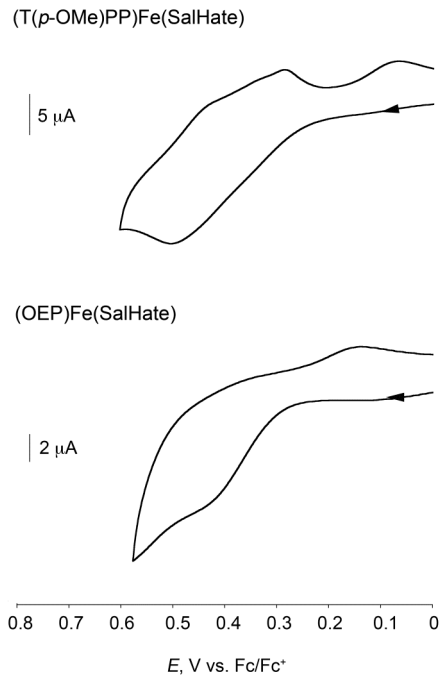

Figure 4.19. Cyclic Voltammograms of the first oxidation of (T(*p*-OMe)PP)Fe(SalHate) and (OEP)Fe(SalHate) in CH_2Cl_2 at 200 mV/s, 1 mM analyte, 0.1 M NBu_4PF_6 at room temperature. Potentials are referenced against the Fc/Fc^+ couple set to 0.0 V.

A summary of the electrochemical information is provided in Tables 4.3 below.

Table 4.3. The redox potentials in (V) of the (por)Fe(OR) compounds in CH_2Cl_2.

	$E^{o\prime}$				
	1st Ox.	2nd Ox	3rd Ox	1st Red.	2nd Red
(T(*p*-OMe)PP)Fe(SalHate)	0.52*	0.73*	1.01*	-0.86	-1.58
(OEP)Fe(SalHate)	0.44*	0.72*	1.15*	-0.79*	-1.1
(T(*p*-OMe)PP)Fe(*p*-nitrophenoxide)	0.53	0.95		-0.89	
(T(*p*-OMe)PP)Fe(OPh)	0.47	0.90			
(OEP)Fe(sal)	0.51	1.06		-1.2	
(T(*p*-OMe)PP)Fe(*p*-nitrobenzoate)	0.49	0.85			

Potentials are in volts, and are referenced to the ferrocene-ferrocenium couple set at 0.00V. Analytes are 1 mM, 200 mV/s, 0.1 M NBu_4PF_6 in CH_2Cl_2.
*These are E_{pa} and E_{pc} values due to irreversibility.

4.3.5 Infrared Spectroelectrochemistry

The spectroelectrochemical measurements for (T(*p*-OMe)PP)Fe(SalHate) were carried out in a CH_2Cl_2 solution containing 1 mM analyte and 0.1 M NBu_4PF_6. While holding the potential at 0.58 V (just past the E_{pa} for the first oxidation) for 90 seconds, a new peak in the difference IR spectrum is observed at 1839 cm^{-1} that corresponds to the oxidation product (Figure 4.20 top).

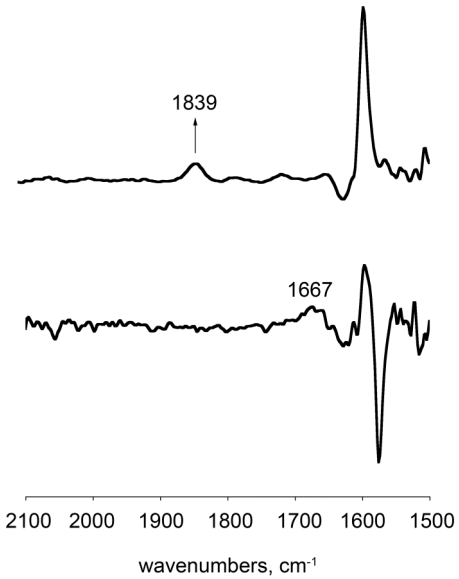

Figure 4.20. Difference IR spectra showing the products from the first oxidation of the (T(*p*-OMe)PP)Fe(SalHate) compound containing 0.1 M NBu_4PF_6 with potentials held near the E_{pa} of the first oxidation (top) and with a proton sponge (bottom).

If the reaction is carried out in the same way, but in the presence of a proton sponge (Figure 4.21), the 1839 cm^{-1} peak is not observable in the difference IR spectrum as

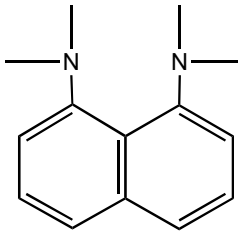

Figure 4.21. Proton sponge (N,N,N',N'-tetramethyl-1,8-naphthalenediamine) used in spectroelectrochemical experiments.

indicated by Figure 4.20.

The same occurrence can be observed for (OEP)Fe(SalHate). Sitting at a potential of 0.65 V (past the E_{pa} of the first oxidation) yields a new peak in the difference IR spectrum at 1855 cm^{-1}. Much like the (T(*p*-OMe)PP)Fe(SalHate), if a proton sponge is added, this new peak is not observed during the spectroelectrochemical experiment (Figure 4.22).

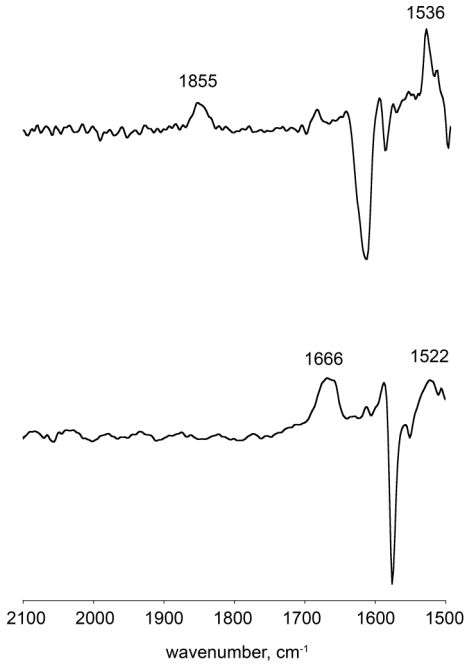

Figure 4.22. Difference IR spectra showing the products from the first oxidation of (OEP)Fe(SalHate) compound containing 0.1 M NBu_4PF_6 with potentials held near their first oxidation potential (top) and with a proton sponge (bottom).

4.3.6 Reactions with Nitric Oxide

I attempted to produce a never before reported neutral 6-coordinate (por)Fe(OR)(NO) complex by exposing the solid (crystalline and powder) (por)Fe(OR) complexes to NO gas for varying amounts of time.[21] On one occasion, a new band near

1890 cm^{-1} in the IR spectrum was obtained after the powder of (T(*p*-OMe)PP)Fe(SalHate) was soaked with NO gas for ~14 hours.

4.3.7 Reactions with bis(triphenylphosphoranylidene)ammonium nitrite (PPN-nitrite)

The reactivity of some of the (por)Fe(OR) complexes with PPN-nitrite was carried out. The reactions were monitored by UV-vis spectroscopy. After a UV-vis spectrum of a 5×10^{-6} M CH_2Cl_2 solution containing (T(*p*-OMe)PP)Fe(OPh) was collected, a >50 mole excess of PPN-nitrite (0.0010 g) added to it in the glove box under anaerobic conditions. Spectra were then collected every 60 seconds for 20 minutes, and then every 5 minutes for a total of 110 minutes. The collection of spectra ceased after 110 minutes due to a lack of change in the spectra for 30 minutes. The sealed cuvette containing the reaction solution was then placed in an area that was free of light for 24 hours so an additional spectrum could be collected. Examples of the spectra are provided below.

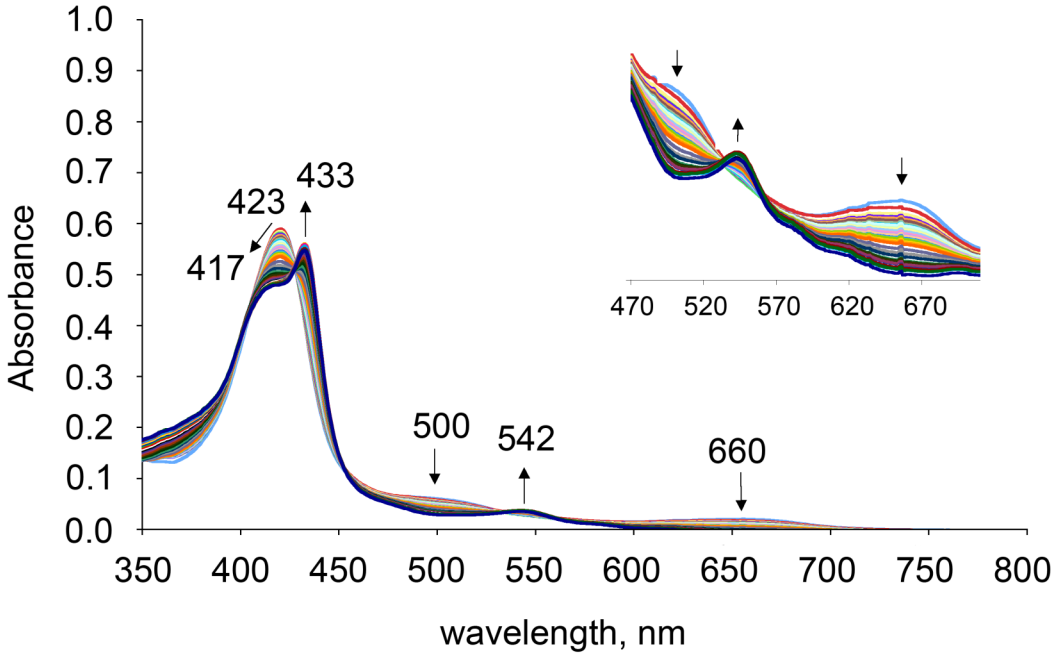

Figure 4.23. UV-vis spectra of the reaction of (T(*p*-OMe)PP)Fe(OPh) (5×10^{-6}) with PPN-nitrite (50 X's excess) in CH_2Cl_2 using anaerobic conditions. Reaction spectra collected for 110 min, the final spectrum was collected 24 hours after the initial spectrum.

The beginning of the reaction spectra displays a shift in the Soret band from 423 nm to 417 nm with a new peak near 433 nm. Also observed were diminishing peaks near 500 nm and 660 nm accompanied by a new band increasing at 542 nm. The following 85 minutes of the reaction spectra indicates a shift from 417 nm to 434 nm with diminishing 500 nm and an increase to the 542 nm band. Similar results were seen for the (T(*p*-OMe)PP)Fe(SalHate) complex using the same conditions. Care was taken to eliminate contact with oxygen from the atmosphere due to previous reports in the literature suggesting stability of nitrite in the absence of oxygen.[22] However, experiments were also done without the precaution to eliminate an interaction with atmosphere and they showed similar results to those done under anaerobic conditions.

Additional anaerobic experiments were carried out. For example, a 3 mM CH_2Cl_2 solution of (T(*p*-OMe)PP)Fe(SalHate) was used along with a 5 times excess of PPN-nitrite (15 mM). The starting complex's Soret band shifts from 422 nm to 419 nm after 50 minutes followed by a shift to 413 nm after 100 minutes had passed (Figure 4.24). The peaks in the visible region show a disappearance of a peak at 510 nm with increasing peaks at 482 nm (shoulder), 542 nm and 620 nm. There were no changes observed after 100 minutes had passed after initial mixing of the reactants.

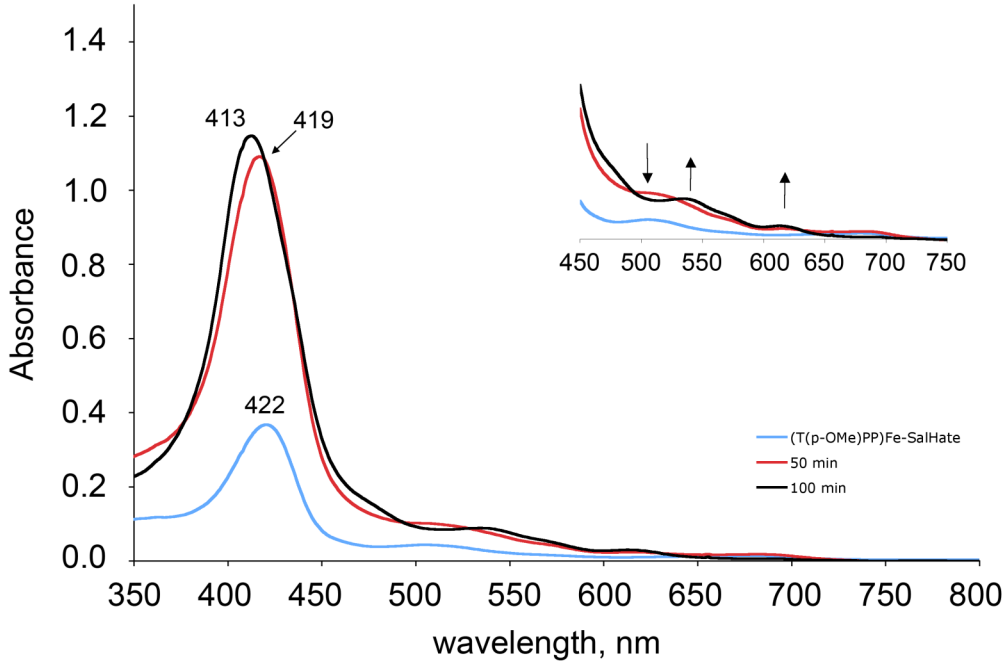

Figure 4.24. UV-vis spectra for the reaction of a CH_2Cl_2 solution containing (T(*p*-OMe)PP)Fe(SalHate) (3 mM) with PPN-nitrite (5 X's excess) under anaerobic conditions. Reaction spectra were collected every 10 minutes for 100 minutes.

An infrared dip-probe experiment was also done in order to aid in the determination of the reaction product of the (por)Fe(OR) complexes with PPN-nitrite.

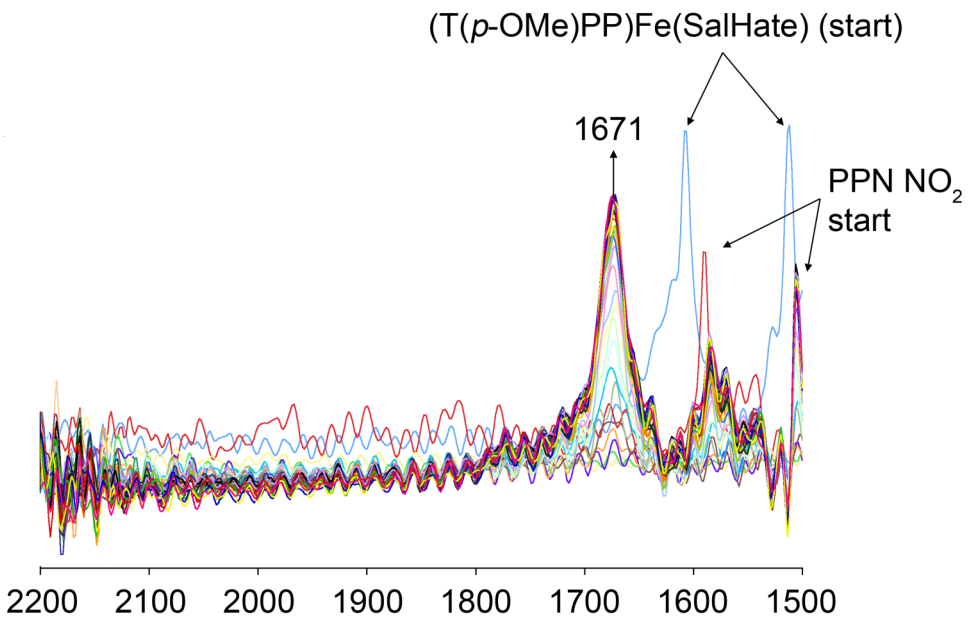

Figure 4.25. Dip-probe IR investigation of the reaction of a solution of (T(*p*-OMe)PP)Fe(SalHate) (3 mM) with PPN-nitrite (15 mM) in CH_2Cl_2 monitored for 180 minutes using anaerobic conditions.

The presence of a new band at 1671 cm^{-1} that appears after PPN-nitrite has been introduced to a CH_2Cl_2 solution of (T(*p*-OMe)PP)Fe(SalHate) at room temperature that was not there when just the starting (T(*p*-OMe)PP)Fe(SalHate) was present (see Figure 4.25). This peak grows in intensity over the 180 minutes of spectral collection.

4.4 Discussion

Mass spectrometry ($ESI^{+/-}$) was used to aid in the characterization of these complexes. The peaks that correspond to the parent complexes were not observed. I figured that since the parent complex was not observed in the ESI^+, the use of ESI^- could possibly be used in order to observe the ligand if it was dissociating during ionization. This was indeed case. For example, the (T(*p*-OMe)PP)Fe(SalHate) complex gave a *m/z* signal of 788.33 (base peak, 100%) in the ESI^+ spectrum. The

ligand (HO-C_6H_4-*o*-C(=O)NHOH) has a mass of 153.1, however, the deprotonated ligand has a mass of 152.01, which is what is seen in the ESI^- spectrum. Therefore, the significant data that was collected from the mass spectrometry analysis is that a (por)Fe^+ complex was present in the ESI^+ spectra and a *m/z* peak corresponding to the appropriate ligand was seen in the ESI^- spectrum.

The data collected from these MS experiments does not give enough information as an analytical tool to definitively characterize the complexes studied. There are other factors such as the possibility of having uncoordinated ligands in the sample that could show up in the ESI^- spectra and other porphyrin complexes that may be present including unreacted starting materials, porphyrin dimers, (por)Fe(Cl), or other iron porphyrin compounds that might give similar fragmentation patterns. These "contaminants" were not observed in any of the spectra that were collected. Therefore, it is a safe assumption that the target complexes were synthesized successfully because the collected data was consistent with other (por)Fe(OR) complexes reported in the literature which showed similar fragmentation.[23] The use of the mass spectrometry, playing a supporting role to the other spectroscopic data, was helpful in order to characterize these (por)Fe(OR) complexes even without definitive evidence of the parent complexes.

The ability to obtain X-ray quality crystals for small molecule X-ray crystallography was very beneficial in determining the nature of coordination for these complexes.

Table 4.4. Selected structural data (in Å and º) for iron-porphyrin complexes containing *O*-donors as axial ligands reported from 1965 – 2011.

	Fe-O(R) (Å)	∠FeOR (º)	Ref.
(PPIX)Fe(Hf) (Hf = halofantrine)	1.843	126.1	[24]
(TTP)Fe(OC(=O)CH_3)	1.898(4)	129.6(4)	[23]
(OEP)Fe(OC(=O)CCl_3)	1.928(2)		[25]
(OEP)Fe(O-2,6-$(CF_3C(=O)NH)_2C_6H_3$)	1.926(3)	122.8(3)	[26]
(OEP)(O-2-$CF_3C(=O)NHC_6H_4$)	1.887(2)	125.5(2)	[26]
(OEP)Fe(OPh)	1.848(4)	142.2(3)	[26]
(OEP)(O-2,6-(i-Pr)$_2C_6H_3$)	1.816(4)	170.6(4)	[26]
(5,15-(o,o′)-(2-methyl-2′-hydroxy-3,3′-diamidobiphenyl)-diphenyl)porphyrin)Fe(OMe)	1.867(3)	122.9(3)	[27]
(TPP)Fe(O-2-$CF_3C(=O)NHC_6H_4$)	1.847(5)	146.0(5)	[28]
(PPDME)Fe(OMe)[a]	1.842(4)	125.9(6)	[29]
(TPP)Fe(OMe)	1.8155(15)	129.10(9)	[30]
(TDFPP)Fe(OMe)[b]	1.788(5)	128.3(5)	[31]
(OEP)Fe(OMe)	1.843(2)	125.5(3)	[32]
(TPP)Fe(OPh)	1.859(7)		[33]
(TPP)Fe(OC(=O)CF_3)	1.921(4)	129.3(6)	[34]
(OEP)Fe(OCH_2CH_3)	1.8232(13)	128.6(3)	[35]
(OEP)(O-4-t-butyl-2-OHC_6H_3)	1.874(2)	125.13(19)	[36]
(OEP)Fe(O-2-OHC_6H_4)-iron(III)	1.9120(14)	119.48(13)	[36]
(OEP)Fe(O-2-$C(=O)HC_6H_3$)	1.912(3)	124.3(4)	[36]
(OEP)Fe(O-2-OH-5-$NO_2C_6H_3$)	1.909(3)	122.2(3)	[36]

[a]PPDME = mesoporphyrinIX dimethyl ester
[b]TDFPP = 5,10,15,20-meso-tetrakis(2,6-difluorophenyl)porphyrinato

The information provided in Table 4.4 above gives the reported structural data of known (por)Fe(OR) complexes, possessing a carboxylate or alkoxide ligand. The Fe(O)R bond lengths (Å) the ∠FeOR bond angles (º) appear to be very similar to the new complexes reported in this work (Table 4.2). The Fe-O bond lengths of the complexes that have been reported in the literature range from 1.79 – 1.93 Å which encompasses the 1.88 – 1.91Å range observed for the new (por)Fe(OR) complexes. The same can be said of the 129º – 170º ∠FeOR bond angles for the new (por)Fe(carboxylate) complexes are similar to the reported (por)Fe(carboxylate)

complexes which have reported ∠FeOR bond angles of 126º – 130º. The obvious outlier is the (OEP)Fe(sal) complex. The new (por)Fe(aryloxide) complexes which have ∠FeOR bond angles of 125º - 144º fall in the range of 120º – 170º that has been previously reported for other (por)Fe(OR) complexes. The majority of the previously reported ∠FeOR bond angles (º) appear to be in the 120º - 145º range with one outlier of 170º belonging to (OEP)Fe(O-2,6-$(CF_3C(=O)NH)_2C_6H_3$).[26] This aryloxide complex's ∠FeOR bond angle (º) is very similar to that of the (OEP)Fe(salicylate) complex. The authors of this paper believed that complexes such as these would need a longer Fe-O bond length (Å) and a reduction in the *s*-character (possibly via H-bonding) of the coordinated oxygen to obtain smaller Fe-O-C bond angles. I do not believe that this explanation is completely adequate. By examining Table 4.4 above, it is apparent that there are several complexes that have shorter or similar Fe-O bong lengths and relatively small (~125º) Fe-O-C bond angles. The reduction of *s*-character does however seem to be somewhat valid as shown in the (por)Fe(SalHate) complexes from this present work, which both possess H-bonding to the coordinated oxygen. They both have Fe-O-C bond angles of ~125º which according to the authors that reported the (OEP)Fe(O-2,6-$(CF_3C(=O)NH)_2C_6H_3$) complex is small. However, this does not explain the other complexes in this current work that possess long Fe-O bond lengths (relative to the (OEP)(O-2,6-$(CF_3C(=O)NH)_2C_6H_3$) complex) with no internal H-bonding while still having small (<< 170º) Fe-O-C bond angles. A much simpler explanation could be weak Fe-O interactions resulting in longer Fe-O bond lengths. This weak Fe-O interaction could also explain the ease at which the complexes fragment in the mass spectrometry experiments.

The structural parameters of Fe-N_{por} bond length and distance by which the central iron atom has been displaced from the plane of the 24-atom porphyrin macrocycle are good indicators of spin-state according to the review by Scheidt and Reed.[37] The Fe-N_{por} bond length range of 2.03 – 2.07 that were observed for these complexes are similar to the accepted range of 2.060 – 2.087 Å for 5-coordinate high-spin iron porphyrin complexes.[37] The out of plane displacements of the central iron from the 24-atom porphyrin plane for these new (por)Fe(OR) complexes ranges from 0.38 – 0.52 Å which is typical (0.39 – 0.62 Å) of high-spin iron porphyrin species.[37] Therefore, it appears that these complexes possess high-spin iron centers.

Another interesting aspect of the salicylhydroxamate complexes is that the hydroxamate ligands used in this chapter coordinated to the central metal via the phenyl hydroxyl oxygen and not the hydroxamate moiety (C(=O)NHOH) as might have been expected based on the literature. However, salicylhydroxamic acid has the potential to coordinate in a number of varying ways as shown below in Figure 4.26. Our group's published (OEP)Fe(benzohydroxamate) complex had coordination of the ligand to the metal in a monodentate fashion via the hydroxamate moiety's O-NHC(=O)R

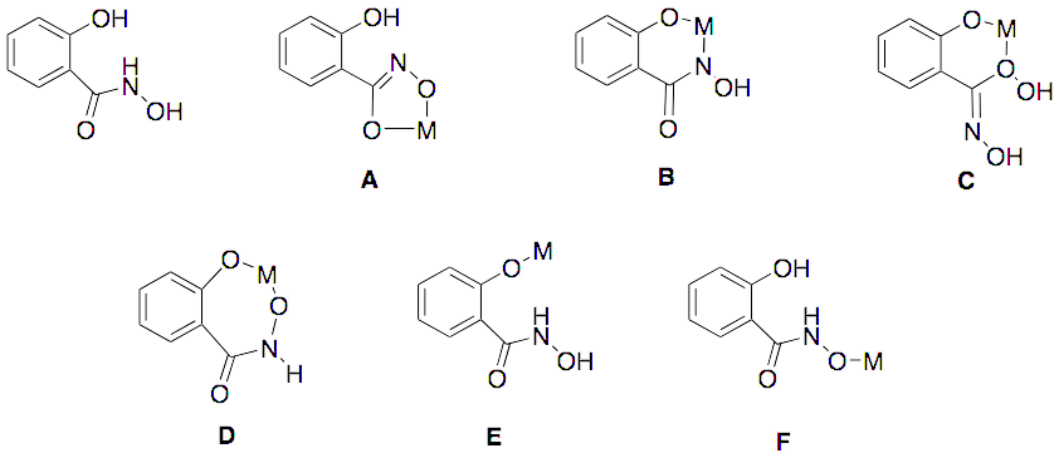

Figure 4.26. Possible binding modes of salicylhydroxamic acid to metals.

($R = C_6H_5$).[9] This was the first structural evidence of a hydroxamate coordinated to a metalloporphyrin complex. The report by Shaffer et al. claimed that the coordination of several hydroxamates (including salicylhydroxamate) to metalloporphyrins were monodentate,[38] they too believed that the coordination was through the NO moiety of the hydroxamate (F in Figure 4.26). Their conclusions were based on the relative increase in the ν_{CO} = 1650 cm^{-1} upon monodentate coordination (TTP)Fe(benzohydroxamate) as opposed to the expected decrease in the ν_{CO} stretching frequency upon bidentate coordination ν_{CO} = 1626 cm^{-1} (K[benzohydroxamate]).

In this work, we investigated the (por)Fe-hydroxamate, -aryloxide, and -carboxylate compounds. The electrochemical data that was collected is consistent within the individual (por)Fe(hydroxamate), (por)Fe(aryloxide), and (por)Fe(carboxylate) classes, but differs across them.

For example, the (T(*p*-OMe)PP)Fe(OPh) (E_{ox} = 0.47 V) and (T(*p*-OMe)PP)Fe(*p*-nitrophenoxide) (E_{ox} = 0.53 V) complexes both show two reversible

oxidations in their respective CVs with only the *p*-nitrophenoxide complex showing a reversible reduction (-0.92 V) in the solvent window used for these experiments.

The (OEP)Fe(sal) (0.51 V, 1.06 V, vs. Fc/Fc^{+}) and (T(*p*-OMe)PP)Fe(*p*-nitrobenzoate) (0.49 V, 0.85 V vs. vs. Fc/Fc^{+}) compounds each show two oxidation features in the solvent window used in these experiments. The observation of oxidations for (por)Fe(carboxylate) complexes is rare in the current literature. The only other (por)Fe(carboxylate) complex in the current literature that provides information on the oxidation features of the complex is (OEP)Fe($OC(=O)CH_3$). This complex in a CH_2Cl_2 solution with NBu_4ClO_4 as a supporting electrolyte and referenced against SCE gave reversible oxidation features at 1.01 V and 1.41 V. It appears that the studies by Richard et al. were focused on the influence of pKa of the axially bound OR ligands on the reduction potentials of Fe(III) to Fe(II), which is why the majority of complexes in Table 4.5 report only a single reduction feature. Dr. Nan Xu, a research assistant professor in our group, has recently synthesized a few new (por)Fe(carboxylate) complexes for electrochemical studies which includes (OEP)Fe($OC(=O)CCl_3$), (TPP)Fe($OC(=O)CH_2Cl$), and (TPP)Fe($OC(=O)CCl_3$).[39] In Dr. Xu's work, he found that his complexes undergo two oxidations and one reduction each. By examining Figure 4.16, the (OEP)Fe(sal) and (T(*p*-OMe)PP)Fe(*p*-nitrobenzoate) compounds display reduction features when scanning in the negative direction. The (OEP)Fe(sal) complex displays the same irreversible feature near -1.2 V when the initial scan is in the negative direction, however, the (T(*p*-OMe)PP)Fe(*p*-nitrobenzoate) complex does appear to show a more reversible feature near -0.9 V. Neither of reductions for these

complexes were investigated in this study due to electrode fouling issues during data collection.

The complexes listed in Table 4.5 depict the reported redox potentials for known (por)Fe(OR) complexes. By examining this table it is apparent that there are few reports of oxidation potentials for (por)Fe(OR) complexes as compared to reduction potentials. The authors did not give a reason as to why the oxidations were not investigated.

Table 4.5. Electrochemical data for reported iron-porphyrin complexes containing *O*-donors (carboxylates) as axial ligands. All complexes were analyzed in CH_2Cl_2 solution containing NBu_4ClO_4 as supporting electrolyte.

Compound	Ref Electrode	Ox 1	Ox 2	Red 1	Ref
(TPP)Fe(OC(=O)CH_3)	$Ag/AgNO_3$			-0.79	[40]
(OEP)Fe(O-C(=O)CH_3)	SCE	1.01	1.41	-0.40	[41]
(T(*p*-Me)Fe($O_2C(3\text{-}ClC_2H_4)$)	SCE			-0.37	[42]
(T(*p*-Me)Fe(O_2C(*o*-C_6H_3Cl))	SCE			-0.35	[42]
(T(*p*-Me)Fe(O_2C-*m*-$C_6H_3NO_2$)	SCE			-0.32	[42]
(T(*p*-Me)Fe(O_2CCCl_3)	SCE			-0.10	[42]
(T(*p*-Me)Fe(O_2CCH_2Cl)	SCE			-0.17	[42]
(T(*p*-Me)Fe(O_2CCH_2Ph)	SCE			-0.40	[42]
(T(*p*-Me)Fe(O_2CCHCl_2)	SCE			-0.11	[42]
(T(*p*-Me)Fe(O_2CCMe_3)	SCE			-0.47	[42]
(T(*p*-Me)Fe(O_2CEt)	SCE			-0.41	[42]
(T(*p*-Me)Fe(O_2CMe)	SCE			-0.36	[42]

(T(*p*-Me)Fe(O_2CPh)	SCE			-0.39	[42]
(T(*p*-Me)Fe(O_2CPr)	SCE			-0.44	[42]
(OEP)Fe(O(C=O)CCl_3)	Fc/Fc^+	0.55	1.04	-0.99*	[39]
(TPP)Fe(O(C=O)CH_2Cl)	Fc/Fc^+	0.69	1.13*	-0.78	[39]
(TPP)Fe(OC(=O)CCl_3)	Fc/Fc^+	0.72	1.14*	-0.76*	[39]

* Irreversible redox process

If we examine the CVs of the (por)Fe-hydroxamate complexes, we observe that the first feature is an irreversible oxidation for both the (T(*p*-OMe)PP)Fe(SalHate) (0.52 V) and (OEP)Fe(SalHate) (0.44 V) complexes (Figure 4.18). The OEP complex has two additional oxidation features in the CV (0.72 V and 1.15 V) whereas the (T(*p*-OMe)PP complex only has one additional oxidation (0.73 V). Both hydroxamate complexes possess two reduction features with the T(*p*-OMe)PP complex having two reductions (-0.86 V and -1.58 V) in the solvent window used in these experiments, and the OEP complex having reduction features at -0.79 V and -1.1 V. To the best of my knowledge, this is the first report of the redox behavior of (por)M(hydroxamate) complexes. However, there are a few reports in the literature that provide information regarding the oxidations and reductions of other metal-hydroxamate complexes. The trihydroxamate iron(III) complexes Fe(ONPhC(=O)Ph)$_3$ and Fe(ONHC(=O)Ph)$_3$ each undergo one oxidation at 1.34 V and 1.36 V vs. Ag/AgCl respectively at room temperature measured at 200 mV/s in acetone using NBu_4PF_6 as the supporting electrolyte.[43] The authors did not report any reductions for these complexes. The iron(III) complexes based on the tris-(2-pyridylmethyl)amine (TPA) ligand provided

only one observable reduction in their CVs. $[Fe(TPA)(CH_3C(O)NHO)](ClO_4)_2$, $[Fe(TPA)(PhC(O)NHO)](ClO_4)_2$, and $[Fe(TPA)(pyrC(O)NHO)](ClO_4)_2$ showed quasi-reversible Fe^{III}/Fe^{II} reduction waves at $E_{1/2}$ at +0.18, +0.21, and +0.32 V vs. SCE, respectively, with no reported oxidations.[44]

The complication of ionizable protons on the (por)Fe(SalHate) complexes makes it a very difficult system to study because the site of oxidation is difficult to predict. It is difficult to deduce from CV alone what the products are, more specifically what is being generated after the first oxidation. It should be noted that the CV of salicylhydroxamic acid itself was collected and it did not reveal any oxidation feature within the solvent limits used in the experiment.

It is apparent that these systems undergo what is referred to as an *EC* mechanism (electrochemical step followed by a chemical reaction).[45] This type of mechanism involves an electrogenerated species, which rearranges or reacts with some other solution component as described in Equation 4.3 and 4.4 below.

$$O + e^- \leftrightarrows R \qquad 4.3$$

$$R + Z \rightarrow \text{Products(s)} \qquad 4.4$$

Table 4.6. Electrochemical data for reported iron-porphyrin complexes containing *O*-donors (alkoxides/aryloxides) as axial ligands. All complexes were analyzed in CH_2Cl_2 solution containing NBu_4ClO_4 as supporting electrolyte.

Compound	Ref electrode	Ox 1	Ox 2	Ox 3	Red 1	Red 2	Ref
(TPP)Fe(OMe)	$Ag/AgNO_3$				-1.19		40
(TPP)Fe(OMe)	SCE	1.11	1.16	1.64			46
(TPP)Fe(OPh)	$Ag/AgNO_3$				-1.04		40
(TPP)Fe(OPh)	SCE	1.08	1.44				47
(TMP)Fe(OMe)	SCE	0.98	1.10	1.25	-0.86	-1.21	48
(T(*p*-Me)Fe(O-*m*,*p*-$C_6H_3Me_2$)	SCE				-0.72		42
(T(*p*-Me)Fe(O-*o*,*p*-$C_6H_3(NO_2)_2$)	SCE				-0.27		42
(T(*p*-Me)Fe(O-*o*,*p*-$C_6H_3Me_2$)	SCE				-0.74		42
(T(*p*-Me)Fe(O-*p*-C_6H_3CN)	SCE				-0.54		42
(T(*p*-Me)Fe(O-*p*-$C_6H_3NO_2$)	SCE				-0.42		42
(T(*p*-Me)Fe(OBu)	SCE				-0.86		42
(T(*p*-Me)Fe(OC_2F_5)	SCE				-0.72		42
(T(*p*-Me)Fe(OC_3HF_6)	SCE				-0.60		42
(T(*p*-Me)Fe($OC_6H_2(NO_2)_3$)	SCE				-0.06		42
(T(*p*-Me)Fe(OCH_2Ph)	SCE				-0.82		42
(T(*p*-Me)Fe(OEt)	SCE				-0.96		42
(T(*p*-Me)Fe(OMe)	SCE				-0.28		42
(T(*p*-Me)Fe(OPh)	SCE				-0.68		42

Infrared spectroelectrochemical investigations were carried out for the (T(*p*-OMe)PP)Fe(SalHate) and (OEP)Fe(SalHate) complexes. During these experiments, new bands appeared in the difference IR spectra while a potential was applied to the complex in solution. The oxidation of the (T(*p*-OMe)PP)Fe-SalHate complex gave rise to a new band in the IR spectrum at 1839 cm^{-1} while (OEP)Fe-SalHate yielded at new band at 1855 cm^{-1} during oxidation. These bands are consistent with the ν_{NO} associated with 5-coordinate cationic $[(por)Fe(NO)]^{+}$ complexes in CH_2Cl_2. For example, $[(TPP)Fe(NO)]ClO_4$ and $[(OEP)Fe(NO)]ClO_4$ have a ν_{NO} of 1848 cm^{-1} 1854 cm^{-1} respectively, while $[(OEP)Fe(NO)]SbF_6$ has a ν_{NO} of 1853 cm^{-1}.[49,50] This would suggest that the hydroxamate ligand is dissociating from the complex during oxidation. This supports the irreversible character for the first oxidation that was observed in the cyclic voltammograms for each of the (por)Fe-Salhate complexes. The observation of NO donation from a hydroxamic acid is not a new claim,[9,14,15,51] however; this is the first observation of NO donation from a metal coordinated hydroxamate. The paper published by the Richter-Addo group in Chemical Communications in 1999 describes the formation of a $[(por)Fe(NO_2)(py)]$ complex from the reaction of a [(por)Fe(Cl)] in the presence of a small amount of pyridine with a 1:1 mixture of excess benzohydroxamic acid and NaH. This was the first report of a hydroxamic acid donating its "NO" group to a metal center. The reports by Nolan et al. describe a possible denitrosylation of hydroxamic acid with a $[Ru(Hedta)Cl]^{-}$ complex to give a $[Ru(edta)(NO)(Cl)]^{2-}$ complex.[14,15] They claim that the mechanism involves a nucleophilic attack of a hydroxo conjugate base ligand on the hydroxamic acid carbonyl group that provides an intermediate from which hydroxylamine (a known NO donor) is

produced. Generation of NO from the hydroxylamine displaces coordinated edta carboxylate by chloride to generate the nitrosyl-coordinated product.

In the experiments done in this current work, a possible 5-coordinate cationic [Fe(por)(NO)] complex is being generated during oxidation from the 6-coordinate (por)Fe(hydroxamate) complex. As suggested from the CV data, the first oxidation is irreversible implying a chemical change to the complex during oxidation. This could be the dissociation of the hydroxamate ligand from the metal. However, the possibility of generating a cationic species (free hydroxamate) during a one-electron loss process seems unlikely. However, it is not completely impossible due to the large excess of counter ions available to stabilize this anion from the supporting electrolyte in solution. A more plausible mechanism could involve the oxidation of the porphyrin moiety, which leads to the dissociation of the salicylhydroxamate ligand and the formation of a "phenoxide" radical, which is provided in Scheme 4.1 below.

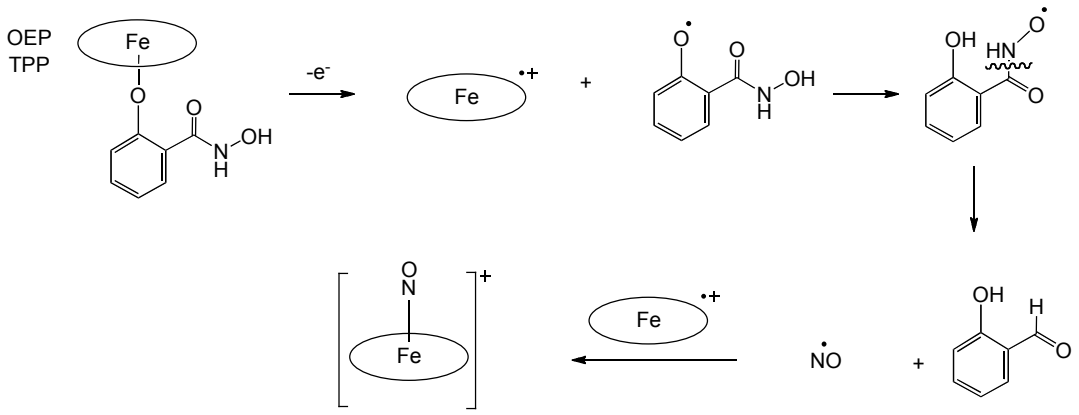

Scheme 4.1. Proposed mechanism for the formation of $[(por)Fe(NO)]^+$ from (por)Fe(SalHate) (por = TPP and OEP) during electrochemical oxidation.

The scheme above shows the formation of an aldehyde and NO radical. The NO radical could possibly react with the porphyrin cation radical forming the final 5-coordinate $[(por)Fe(NO)]^+$. As stated above, the 5-coordinate $[(por)Fe(NO)]^+$ complex does not

form in the presence of a proton sponge. Isolation of the possible aldehyde and/or other products of the oxidation were not attempted, therefore further work will need to be done in order to identify to the components after NO coordination is complete. Such attempts may include the use of an aprotic solvent or the addition of a radical trap such as TEMPO ((2,2,6,6-tetramethylpiperidin-1-yl)oxyl).

Attempts to generate a neutral six-coordinate (por)Fe(NO)(OR) complex via exposure of the 5-coordinate (por)Fe(OR) to NO gas did produce a new stretch at 1890 cm^{-1} for (T(*p*-OMe)PP)Fe(SalHate) in the IR spectrum. This new 1890 cm^{-1} stretch suggested the formation of the desired six-coordinate complex. The first compound to consider is the neutral (T(*p*-OMe)PP)Fe(NO) complex which we would expect to have a ν_{NO} near 1690 - 1670 cm^{-1}.[52,53] The possibility of generating the (T(*p*-OMe)PP)Fe(NO)(NO_2) complex during these reactions should lead to a new ν_{NO} of 1874 cm^{-1} which we do not observe.[54,55] The other conceivable complex that could be generated during this experiment would be the neutral six-coordinate (por)Fe(NO)(OR) species. There are currently no other neutral six-coordinate nitrosyl complexes with an *O*-donor ligand reported. The small number of six coordinate cationic $[(por)Fe(NO)(HOR)]^+$ complexes possess a ν_{NO} of 1897 cm^{-1} – 1937 cm^{-1}.[56-58] With this in mind, it was thought that the 1890 cm^{-1} peak obtained from 14 hours of exposure of NO gas with (T(*p*-OMe)PP)Fe(SalHate) powder generated a never before observed neutral six-coordinate (T(*p*-OMe)PP)Fe(NO)(OR) compound. Unfortunately, this spectrum could not be duplicated after exhaustive attempts.

The PPN-nitrite reactions with (por)Fe(OR) complexes were initially carried out in order to seek evidence for a (por)Fe(OR)(ONO) species. By thinking about

Compound I in Figure 3.1 (this dissertation), it can be perceived that nitric oxide could possibly interact with the Fe^{IV}oxo intermediate to inhibit catalase activity instead of reacting with the resting state enzyme. If this were the case, one could predict the formation of a (por)Fe(OR)(ONO) complex. However, the results that were had from the reaction of PPN-nitrite (50 times excess) with the (por)Fe(OR) (5×10^{-6} M) complexes did not suggest this envisioned compound. Instead, I believe that nitrite from PPN-nitrite is displacing the hydroxamate and aryloxide ligands to form new (por)Fe$(NO_X)_y$ complexes. The evidence for this is that the UV-vis spectra are very similar to what has been reported by Ryan et al. In their work, they reacted (TPP)Fe(Cl) with PPN-nitrite and monitored the reactions by UV-vis.[59] The changes in the spectra for the experiments done for this dissertation suggest the formation of a (por)Fe(NO)$(NO)_2$ complex when PPN-nitrite concentrations are high relative to the (por)Fe(OR) complex (the concentrations were both low (por)Fe(OR) = 5×10^{-6} M and PPN-nitrite = 2.5×10^{-4} M) is in line with the reported UV-vis spectra for (T(*p*-OMe)PP)Fe(NO)$(NO)_2$. The reported values for this complex provides a Soret of 437 nm with bands in the visible region at 549 nm and 586 nm (spectrum collected in C_6H_5Cl).[60] This is very similar to the final spectrum obtained for the (T(*p*-OMe)PP)Fe(OR) with PPN-nitrite reaction done in CH_2Cl_2, which produced a Soret band of 434 with additional bands at 542 nm and a smaller feature in the 583 nm area.

When the reaction was carried out in higher concentrations with PPN-nitrite in 5 times excess (15 mM) as compared to the concentration of (por)Fe(SalHate) (3 mM), the Soret band shifts to 413 nm after 100 minutes along with the appearance of bands at 482 nm (shoulder) 542 nm, and 620 nm. The large difference in the Soret band is

somewhat puzzling for this reaction compared to the previous experiments which had lower overall concentrations but larger differences in the amount of excess of PPN-nitrite. This spectrum is more consistent with the reported spectrum for (T(*p*-OMe)PP)Fe(NO) complex. Yoshimura et al. reported a Soret of 410 nm along with bands of 473 nm (shoulder), 541 nm, and 615 nm for (T(*p*-OMe)PP)Fe(NO).[61]

In order to determine if possible organonitro compounds were being formed in the CH_2Cl_2 solution which could alter the reaction,[62] a UV-vis experiment was carried out in a DMF solution with PPN-nitrite in great excess (50 times excess) compared to the (T(*p*-OMe)PP)Fe(SalHate) (5×10^{-6} M). The spectra for this experiment are provided in Figures 4.27 and 4.28 below.

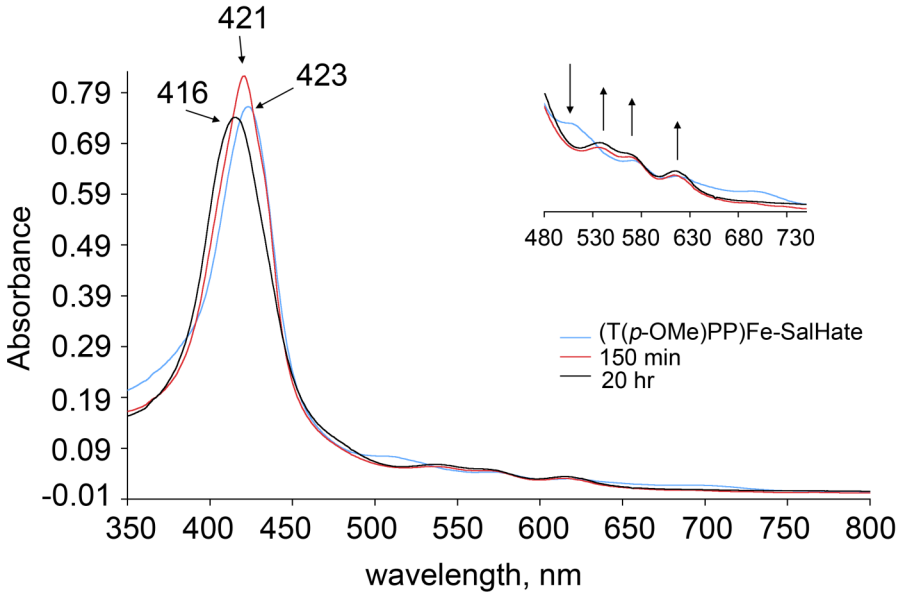

Figure 4.27. UV-vis spectra of the reaction of (T(*p*-OMe)PP)Fe(SalHate) (5×10^{-6} M) with PPN-nitrite (50 times excess) in DMF using anaerobic conditions. Reaction spectra collected at 0 min, 150 min, and 20 hrs.

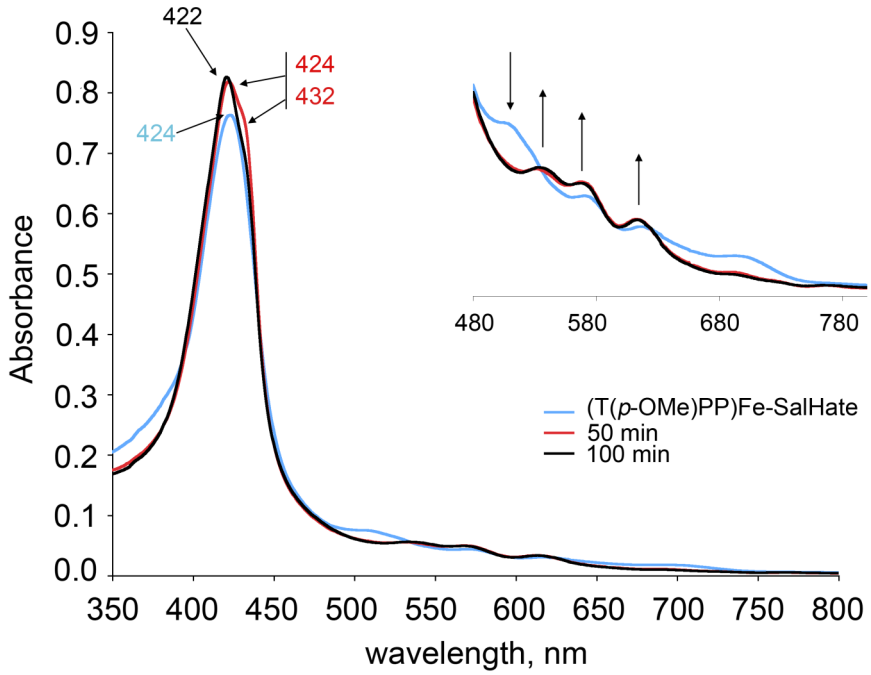

Figure 4.28. UV-vis spectra of the reaction of (T(*p*-OMe)PP)Fe(SalHate) (5×10^{-6} M) with PPN-nitrite (50 times excess) in DMF using anaerobic conditions. Reaction spectra collected at 50 and 100 minutes.

The general appearance of Figure 4.28 displays the change in the spectra that are very similar to those observed in Figure 4.24 above suggesting that the 5-coordinate nitrosyl complex is formed in DMF. The spectra shown in Figure 4.28 provides the first 100 minutes of the reaction mixture. The 50-minute spectrum displays a shoulder at 434 nm that could suggest that there is another species generated in solution that does not persist after 100 minutes have passed.

Infrared dip-probe experiments were also done in order to help identify the products formed from the reaction of PPN-nitrite with the (por)Fe(OR) complexes. The results obtained in CH_2Cl_2 containing 3 mM of (T(*p*-OMe)PP)Fe-SalHate and 15 mM PPN-nitrite support the idea of the formation of the five coordinate nitrosyl complex. As shown in Figure 4.25, a new band at 1671 cm^{-1} appears in the spectra during the first few minutes of the reaction and is lasting for 180 minutes of spectral collection. The

1671 cm^{-1} band is in line with other (por)Fe(NO) complexes available in the literature and falls between reported values of (TPP)Fe(NO) (1678 cm^{-1}) and (OEP)Fe(NO) (1665 cm^{-1}).[50,63] The ν_{NO} for these complexes supports the idea that the OEP macrocyle is a more electron rich and therefore a better electron donor than that of the TPP macrocycle and the (T(*p*-OMe)PP) species falling somewhere in between the two due to the electron rich OMe units on the phenyl groups of the macrocylce.[64] This electron-rich character of the OEP macrocyle provides better backbonding of electron density to the NO ligand relative to the TPP and (T(*p*-OMe)PP counterparts.

Attempts were made to repeat the ratios of excess PPN-nitrite to (por)Fe(OR) (50:1) with the IR dip-probe, but they were unsuccessful due to the PPN-nitrite drowning out any observable signal for the other species in solution. Also, efforts were put forth with IR dip-probe experiments with organic solvents other than CH_2Cl_2, however, solubility issues and spectral overlap impeded such endeavors.

From the PPN-nitrite experiments, it appears that during experiments in CH_2Cl_2 where the concentrations of PPN-nitrite (2.5×10^{-4} M) are low, the predominant species in solution is the (por)Fe(NO)(NO_2) complex, however in DMF using the same concentrations it appears that the 5-coordinate (por)Fe(NO) complex is the prevalent complex produced. When concentrations were increased ((por)Fe(OR) = 3 mM and PPN-nitrite = 15 mM), the UV-vis data and dip-probe IR data suggest the formation of the 5-coordinate (por)Fe(NO) complex. The formation of the five-coordinate (por)Fe(NO) complex from (por)Fe(NO)(NO_2) has been previously reported, so it is acceptable that we are seeing this complex in our final spectrum of these experiments.[55]

4.5 Conclusion

The (por)Fe(SalHate) complexes that have been synthesized in this work are unique in their unexpected phenoxide coordination of a hydroxamic acid to the metal center of porphyrin complexes. Other (por)Fe(hydroxamate) complexes that have been reported either show or propose coordination through the hydroxamate moiety to the metal center. The X-ray crystallographic structures that were collected for the salicylhydroxamte complexes in this current work display coordination through the phenylhydroxyl group instead of the hydroxamate moiety. This is different than that which was observed in the 6-coordinate (por)Ru(NO)(SalHate) complex described in Chapter 3 of this dissertation which showed *O*-atom coordination of the hydroxamate moiety.

The (por)Fe(OR) (R = aryloxide and carboxylate) complexes have provided a set of complexes by which structural and electrochemical comparisons were made. Through electrochemical comparisons with known (por)Fe(OR) complexes it was apparent that the (por)Fe(SalHate) complexes undergo a more complicated redox process. The carboxylate and aryloxide complexes were in agreement with reported complexes regarding reversibility and relative redox potentials. However, the (por)Fe(SalHate) complexes both showed irreversibility which is associated with a decomposition or the occurrence of a chemical change upon oxidation.

The use of infrared spectroelectrochemical analysis was a very useful technique to help identify the products formed during the oxidation of the (por)Fe(SalHate) complexes. The data suggests the formation of a 5-coordinate $[(por)Fe(NO)]^{+}$ cationic species upon oxidation. To my knowledge, this is the first report of a metal-coordinated

hydroxamate complex acting as an NO donor. Other reports have observed NO donation when reacting metal complexes with a hydroxamic acid, but none have been coordinated to the metal before observance of NO donation.

A very exciting result from a solid soak of (T(*p*-OMe)PP)Fe(SalHate) with NO gas without the presence of solvent did yield an IR spectrum which contained a new band at 1890 cm^{-1} which was not present in the starting materials. This hinted at the possibility of forming a new never before reported (por)Fe(NO)(OR) complex. However, this result could not be repeated so it is difficult to say with absolute certainty that the six-coordinate complex was indeed obtained.

Reactivity studies were carried out with PPN-nitrite and were monitored by UV-vis spectroscopy. These reactions showed that the PPN-nitrite reacts with the (por)Fe(OR) complexes to generate (por)Fe$(NO_X)_y$ complexes under anaerobic conditions more specifically (por)Fe(NO) and (por)Fe(NO)(NO_2) which depend on solvent and concentration of reactants.

Additional work remains for the elucidation of a mechanism by which NO is generated during oxidation of the (por)Fe(SalHate) complexes to yield the $[(por)Fe(NO)]^+$ species. It would also be interesting to see if other (por)Fe(Hydroxamate) complexes behave similarly to the (por)Fe(SalHate) complexes with regards to NO donation upon oxidation. Also, I believe that a structure of a cationic $[(por)Fe(NO)(SalHate)]^+$ complex could be had in a manner similar to that which has been previously outlined.[65] A qualitative experiment done with this approach with carbon monoxide gas suggested to me that this may be possible but it was never followed up.

4.6 References

(1) Mizukami, S.; Nagata, K. Metal Complexes of Hydroxamic Acid aAalogs, *Coordination Chemistry Reviews* **1968**, *3*, 267.

(2) Munson, J. W. Chemistry and Biologic Activity of Hydroxamic Acids - An Overview, **1982**.

(3) Miller, M. J. Syntheses and Therapeutic Potential of Hydroxamic Acid Based Siderophores and Analogs, *Chemical Reviews* **1989**, *89*, 1563.

(4) Crumbliss, A. L. Iron Bioavailability and the Coordination Chemistry of Hydroxamic Acids, *Coordination Chemistry Reviews* **1990**, *105*, 155.

(5) Kurzak, B.; Kozlowski, H.; Farkas, E. Hydroxamic and Aminohydroxamic Acids and Their Complexes with Metal Ions, *Coordination Chemistry Reviews* **1992**, *114*, 169.

(6) Neilands, J. B. Siderophores - Structure and Function of Microbial Iron Transport Compounds, *Journal of Biological Chemistry* **1995**, *270*, 26723.

(7) Codd, R. Traversing the Coordination Chemistry and Chemical Biology of Hydroxamic Acids, *Coordination Chemistry Reviews* **2008**, *252*, 1387.

(8) Kaim, W.; Schwederski, B. *Bioinorganic Chemistry: Inorganic Elements in the Chemistry of Life. An Introduction and Guide*; Wiley, 1994.

(9) Cheng, L.; Khan, M. A.; Taylor, R. W.; Richter-Addo, G. B.; Powell, D. R. Structural Consequences of Hydroxamate and Tropolonate Binding to Iron Porphyrins, *Chemical Communications* **1999**, 1941.

(10) Chaston, T. B.; Richardson, D. R. Iron Chelators for the Treatment of Iron Overload Disease: Relationship Between Structure, Redox Activity, and Toxicity, *American Journal of Hematology* **2003**, *73*, 200.

(11) Natchus, M. G.; Bookland, R. G.; De, B.; Almstead, N. G.; Pikul, S.; Janusz, M. J.; Heitmeyer, S. A.; Hookfin, E. B.; Hsieh, L. C.; Dowty, M. E.; Dietsch, C. R.; Patel, V. S.; Garver, S. M.; Gu, F.; Pokross, M. E.; Mieling, G. E.; Baker, T. R.; Foltz, D. J.; Peng, S. X.; Bornes, D. M.; Strojnowski, M. J.; Taiwo, Y. O. Development of New Hydroxamate Matrix Metalloproteinase Inhibitors Derived from Functionalized 4-Aminoprolines, *Journal of Medical Chemistry* **2000**, *43*, 4948.

(12) Puerta, D. T.; Cohen, S. M. Elucidating Drug-Metalloprotein Interactions with Tris(pyrazolyl)borate Model Complexes, *Inorganic Chemistry* **2002**, *41*, 5075.

(13) Puerta, D. T.; Griffin, M. O.; Lewis, J. A.; Romero-Perez, D.; Garcia, R.; Villarreal, F. J.; Cohen, S. M. Heterocyclic Zinc-Binding Groups for Use in Next-Generation Matrix Metalloproteinase Inhibitors: Potency, Toxicity, and Reactivity, *Journal of Biological Inorganic Chememistry* **2006**, *11*, 131.

(14) Marmion, C. J.; Murphy, T.; Nolan, K. B.; Docherty, J. R. Hydroxamic Acids are Nitric Oxide Donors. Facile Formation of Ruthenium(II)-Nitrosyls and NO-Mediated Activation of Guanylate Cyclase by Hydroxamic Acids, *Chemical Communications* **2000**, 1153.

(15) Griffith, D.; Krot, K.; Comiskey, J.; Nolan, K. B.; Marmion, C. J. Monohydroxamic Acids and Bridging Dihydroxamic Acids as Chelators to Ruthenium(III) and as Nitric Oxide Donors: Syntheses, Speciation Studies and Nitric Oxide Releasing Investigation, *Dalton Transactions* **2008**, 137.

(16) Marmion, C. J.; Griffith, D.; Nolan, K. B. Hydroxamic acids - An Intriguing Family of Enzyme Inhibitors and Biomedical Ligands, *European Journal of Inorganic Chemistry* **2004**, 3003.
(17) Bogatyrenko, T. N.; Kuropteva, Z. V.; Baider, L. M.; Bogatyrenko, V. R.; Fedorov, B. S.; Konovalova, N. P. On the Possibility of the Nitric Oxide Formation Upon Biotransformation of Hydroxamic Acids, *Russian Chemical Bulletin* **2011**, *60*, 1162.
(18) Shaw, M. J.; Henson, R. L.; Houk, S. E.; Westhoff, J. W.; Jones, M. W.; Richter-Addo, G. B. Fiber-Optic Infrared Reflectance Spectroelectrochemistry: Isomerization of a Manganese Pyranyl Complex, *Journal of Electroanalytical Chemistry* **2002**, *534*, 47.
(19) Adler, A. D.; Longo, F. R.; Finarelli, J. D.; Goldmacher, J.; Assour, J.; Korsakoff, L. A Simplified Synthesis for Meso-Tetraphenylporphine, *Journal of Organic Chemistry* **1967**, *32*, 476.
(20) Fleischer, E. B.; Srivastava, T. S. Structure and properties of μ-oxobis(tetraphenylporphineiron(III)), *Journal of the American Chemical Society* **1969**, *91*, 2403.
(21) Xu, N.; Powell, D. R.; Cheng, L.; Richter-Addo, G. B. The First Structurally Characterized Nitrosyl Heme Thiolate Model Complex, *Chemical Communications* **2006**, 2030.
(22) Castro, C. E. Ozone from Iron(III) Porphyrin, Nitrite Ion, and Oxygen, *Journal of the American Chemical Society* **1996**, *118*, 3984.
(23) Oumous, H.; Lecomte, C.; Protas, J.; Cocolios, P.; Guilard, R. Pentacoordinate Iron(III) Porphyrin Carboxylates:
Synthesis, Physicochemical Characteristics and X-ray Crystal Structure of Acetato(5,10,15,20-tetra-*p*-tolylporphyrinato)iron(III), *Polyhedron* **1984**, *3*, 651.
(24) de, V. K. A.; Marques, H. M.; Egan, T. J. The Crystal Structure of Halofantrine-Ferriprotoporphyrin IX and the Mechanism of Action of Arylmethanol Antimalarials, *Journal of Inorganic Biochemistry* **2008**, *102*, 1660.
(25) Neal, T. J.; Cheng, B.; Ma, J.-G.; Shelnutt, J. A.; Schulz, C. E.; Scheidt, W. R. Conformational Diversity in (Octaethylporphinato)(trichloroacetato)iron(III) Derivatives, *Inorganica Chimica Acta* **1999**, *291*, 49.
(26) Kanamori, D.; Yamada, Y.; Onoda, A.; Okamura, T.-a.; Adachi, S.; Yamamoto, H.; Ueyama, N. Structures and Properties of Octaethylporphinato(henolate)iron(III) Complexes with NH...O Hydrogen Bonds: Modulation of Fe-O Bond Character by the Hydrogen Bond, *Inorganica Chimica Acta* **2005**, *358*, 331.
(27) Prevot, L.; Jaquinod, L.; Fischer, J.; Weiss, R. Molecular Structure of the Methoxy-Iron(III) Derivative of 5,15-(o,o'(2-methyl-2'-hydroxy-3,3'-diamidobiphenyl)-diphenyl)-porphyrin and CO Binding Properties of Iron(II)-Pyridine Complexes of 2,2'-Substituted Biphenyl Strapped Porphyrins, *Inorganica Chimica Acta* **1998**, *283*, 98.
(28) Ueyama, N.; Nishikawa, N.; Yamada, Y.; Okamura, T.-A.; Nakamura, A. Structure and Properties of Tetraphenylporphinate Iron(III) Complexes with an Intramolecular NH...S Benzenethiolate or NH...O Phenolate Hydrogen Bond, *Inorganica Chimica Acta* **1998**, *283*, 91.

(29) Hoard, J. L.; Hamor, M. J.; Hamor, T. A.; Caughey, W. S. The Crystal Structure and Molecular Stereochemistry of Methoxyiron (III) Mesoporphyrin-IX Dimethyl Ester, *Journal of the American Chemical Society* **1965**, *87*, 2312.
(30) Lecomte, C.; Chadwick, D. L.; Coppens, P.; Stevens, E. D. Electronic Structure of Metalloporphyrins. 2. Experimental Electron Density Distribution of (*meso*-tetraphenylporphinato)iron(III) methoxide, *Inorganic Chemistry* **1983**, *22*, 2982.
(31) Kim, Y.; Nam, W.; Lim, M. H.; Jin, S. W.; Lough, A. J.; Kim, S. J. Methoxy[meso-5,10,15,20-tetrakis(2,6-difluorophenyl)porphyrinato]iron(III), [Fe(TDFPP)(OCH_3)], *Acta Crystallographica, Section C: Crystal Structure Communications* **2001**, *C57*, 556.
(32) Hatano, K.; Uno, T. Preparation and Molecular Structure of (methoxo)(octaethylporphinato)iron (III), *Bulletin of the Chemical Society of Japan* **1990**, *63*, 1825.
(33) Byrn, M. P.; Strouse, C. E. Porphyrin sponges. Inversion Disorder and Inversion Twinning in Lattice Clathrates Based on Five-Coordinate Metallotetraarylporphyrin Complexes, *Journal of the American Chemical Society* **1991**, *113*, 2501.
(34) Moy, S. A.; Gonzalez, J. A.; Wilson, L. J. Molecular stereochemistry of [Fe^{III}(TPP)($OCOCF_3$)], *Acta Crystallographica. Section C, Crystal Structure Communications* **1995**, *51 (Pt 8)*, 1490.
(35) Cheng, L.; Xu, N.; Powell, D. R.; Richter-Addo, G. B. (Ethanolato)[2,3,7,8,12,13,17,18-octaethylporphyrinato(2-)]iron(III), *Acta Crystallogrophica E Structure Reports Online* **2010**, *66*, m1458.
(36) Chaudhary, A.; Patra, R.; Rath, S. P. Binding of Catechols to Iron(III)-Octaethylporphyrin: An Experimental and DFT Investigation, *European Journal of Inorganic Chemistry,* **2010**, 5211.
(37) Scheidt, W. R.; Reed, C. A. Spin-State/Stereochemical Relationships in Iron Porphyrins: Implications for the Hemoproteins, *Chemical Reviews* **1981**, *81*, 543.
(38) Shaffer, C. D.; Straub, D. K. The Synthesis and Spectral Properties of Hemins Derived from Tetra(*p*-tolyl)porphyrin, *Inorganica Chimica Acta* **1989**, *158*, 167.
(39) Xu, N.; Awasabisah, D.; Powell, D. R.; Richter-Addo, G. B. 2012. in preparation.
(40) Feng, D.; Schultz, F. A. Relationship Between Structural Change and Heterogeneous Electron-Transfer Rate Constant in Iron-Tetraphenylporphyrin Complexes, *Inorganic Chemistry* **1988**, *27*, 2144.
(41) Stolzenberg, A. M.; Strauss, S. H.; Holm, R. H. Iron(II, III)-chlorin and -isobacteriochlorin complexes. Models of the Heme Prosthetic Groups in Nitrite and Sulfite Reductases: Means of Formation and Spectroscopic and Redox Properties, *Journal of the American Chemical Society* **1981**, *103*, 4763.
(42) Richard, M. J.; Shaffer, C. D.; Evilia, R. F. A Cyclic Coltammetric and Stopped-Flow Study of Five Coordinate Hemins in Noncoordinating Solvent: Evidence for Electron Transfer Through the Axial Ligand, *Electrochimica Acta* **1982**, *27*, 979.

(43) Brockway, D. J.; Murray, K. S.; Newman, P. J. An Electrochemical Study of Thiohydroxamate and Hydroxamate Complexes of Iron(III), *Journal of the Chemial Society, Dalton Trans.* **1980**, 1112.
(44) Galardon, E.; Selkti, M.; Roussel, P.; Tomas, A.; Artaud, I. Synthesis and Characterization of Mononuclear Hydroxamato and Hydroximato Complexes of Iron(III) Based on the Tris(2-pyridylmethyl)amine Ligand, *Dalton Trans.* **2008**, 6415.
(45) Kissinger, P. T.; Heineman, W. R. *Laboratory Techniques in Electroanalytical Chemistry*; 2nd ed.; Marcel Dekker: New York, 1996.
(46) Lee, W. A.; Calderwood, T. S.; Bruice, T. C. Stabilization of Higher-Valent States of Iron Porphyrin by Hydroxide and Methoxide Ligands: Electrochemical Generation of Iron(IV)-oxo Porphyrins, *Proceedings of the National Academy of Science U. S. A.* **1985**, *82*, 4301.
(47) Phillippi, M. A.; Shimomura, E. T.; Goff, H. M. Investigation of Axial Anionic Ligand and Porphyrin Substituent Effects on the Oxidation of Iron(III) Porphyrins: Porphyrin-Centered vs. Metal-Centered Oxidation, *Inorganic Chemistry* **1981**, *20*, 1322.
(48) Swistak, C.; Mu, X. H.; Kadish, K. M. Electrochemistry of Hydroxo- and Methoxo[tetrakis(2,4,6-trimethylphenyl)porphyrinato]iron in Dichloromethane. Electrogeneration of Iron(IV) and Iron(II) Porphyrins, *Inorganic Chemistry* **1987**, *26*, 4360.
(49) Mu, X. H.; Kadish, K. M. Electrochemical and Spectroelectrochemical Characterization of Intermolecular Nitrosyl Transfer between Iron and Cobalt Porphyrins, *Inorganic Chemistry* **1990**, *29*, 1031.
(50) Mu, X. H.; Kadish, K. M. Insitu Ftir and Uv-Visible Spectroelectrochemical Studies of Iron Nitrosyl Porphyrins in Nonaqueous Media, *Inorganic Chemistry* **1988**, *27*, 4720.
(51) Comiskey, J.; Farkas, E.; Krot-Lacina, K. A.; Pritchard, R. G.; McAuliffe, C. A.; Nolan, K. B. Synthesis, Structures and Speciation Studies of Ruthenium(III) Hydroxamate/Hydroximato Complexes. Crystal and Molecular Structure of Hydrated [Ru(H_2edta)(2-methoxyphenylhydroxamate)], the First Structurally Characterised Ruthenium(III)-Hydroxamate Complex, *Dalton Transactions* **2003**, 4243.
(52) Morlino, E. A.; Rodgers, M. A. J. Nitric Oxide Deligation From Nitrosyl Complexes of Two Transition Metal Porphyrins: A Photokinetic Investigation, *Journal of the American Chemical Society* **1996**, *118*, 11798.
(53) Bohle, D. S.; Debrunner, P.; Fitzgerald, J. P.; Hansert, B.; Hung, C. H.; Thomson, A. J. Electronic Origin of Variable Denitrosylation Kinetics From Isostructural $\{FeNO\}^7$ Complexes: X-ray Crystal Structure of [Fe(oetap)(NO)], *Chemical Communications* **1997**, 91.
(54) Yoshimura, T. Reaction of Nitrosylporphyrinatoiron(II) with Nitrogen Oxide, *Inorganica Chimica Acta* **1984**, *83*, 17.
(55) Novozhilova, I. V.; Coppens, P.; Lee, J.; Richter-Addo, G. B.; Bagley, K. A. Experimental and Density Functional Theoretical Investigations of Linkage Isomerism in Six-Coordinate $\{FeNO\}^6$ Iron Porphyrins with Axial Nitrosyl and Nitro Ligands, *Journal of the American Chemical Society* **2006**, *128*, 2093.

(56) Xu, N.; Powell, D. R.; Richter-Addo, G. B. Nitrosylation in a Crystal: Remarkable Movements of Iron Porphyrins Upon Binding of Nitric Oxide, *Angewandte Chemie-International Edition* **2011**, *50*, 9694.
(57) Scheidt, W. R.; Lee, Y. J.; Hatano, K. Preparation and Structural Characterization of Nitrosyl Complexes of Ferric Porphyrinates. Molecular Structure of Aquonitrosyl(meso-tetraphenylporphinato)iron(III) Perchlorate and Nitrosyl(octaethylporphinato)iron(III) Perchlorate, *Journal of the American Chemical Society* **1984**, *106*, 3191.
(58) Yi, G.-B.; Chen, L.; Khan, M. A.; Richter-Addo, G. B. Activation of Thionitrites and Isoamyl Nitrite by Group 8 Metalloporphyrins and the Subsequent Generation of Nitrosyl Thiolates and Alkoxides of Ruthenium and Osmium Porphyrins, *Inorganic Chemistry* **1997**, *36*, 3876.
(59) Wei, Z.; Ryan, M. D. Electrochemistry and Spectroelectrochemistry of Iron Porphyrins in the Presence of Nitrite, *Inorganica Chimica Acta* **2001**, *314*, 49.
(60) Ellison, M. K.; Schulz, C. E.; Scheidt, W. R. Syntheses, Characterization, and Structural Studies of Several (Nitro)(nitrosyl)iron(III) Porphyrinates: [Fe(Porph)(NO_2)(NO)], *Inorganic Chemistry* **1999**, *38*, 100.
(61) Yoshimura, T. Substituent Effects on the Electronic Absorption and MCD Spectra of Five- and Six-Coordinate Nitrosyl(tetraphenylporphyrinato)iron(II) Complexes, *Bulletin of the Chemical Society of Japan* **1990**, *63*, 3689.
(62) Fanning, J. C.; Keefer, L. K. Rapid Formation of a Potent Nitrosating Agent by Solvolysis of Ionic Nitrite in Dichloromethane, *Journal of the Chemical Society Chemical Communications* **1987**, 955.
(63) Scheidt, W. R.; Duval, H. F.; Neal, T. J.; Ellison, M. K. Intrinsic Structural Distortions in Five-Coordinate (Nitrosyl)iron(II) Porphyrinate Derivatives, *Journal of the American Chemical Society* **2000**, *122*, 4651.
(64) Kadish, K. M.; Caemelbecke, E. V.; Royal, G. In *The Porphyrin Handbook*; Kadish, K. M., Smith, K. M., Guilard, R., Eds.; Academic Press: San Diego, CA, 2000; Vol. 8.
(65) Nasri, H.; Wang, Y.; Huynh Boi, H.; Scheidt, W. R. Nitrite-bound five-Coordinate Low-Spin Iron(II) Model Complex for the Prosthetic Group of Nitrite Reductase with an Unusually Large Quadrupole Splitting. Synthesis, Moessbauer Properties, and Molecular Structure of the Complex (Nitro)(α,α,α,α-tetrakis(o-pivalamidophenyl)porphinato)iron(II), *Journal of the American Chemical Society* **1991**, *113*, 717.